In Situ Adsorption Studies at the Solid/Liquid Interface: Characterization of Biological Surfaces and Interfaces Using Sum Frequency Generation Vibrational Spectroscopy, Atomic Force Microscopy, and Quartz Crystal Microbalance

by

Diana Christine Phillips

B.S. (Western Washington University) 2001

A dissertation submitted in partial satisfaction
of the requirements for the degree of

Doctor of Philosophy

in

Chemistry

in the

GRADUATE DIVISION

of the

UNIVERSITY OF CALIFORNIA, BERKELEY

Committee in charge:

Professor Gabor A. Somorjai, Chair
Professor Heino Nitsche
Professor Song Li

Spring 2006

The dissertation of Diana Christine Phillips is approved.

Chair Date

Date

Date

University of California, Berkeley

Spring 2006

In Situ Adsorption Studies at the Solid/Liquid Interface: Characterization of Biological Surfaces and Interfaces Using Sum Frequency Generation Vibrational Spectroscopy, Atomic Force Microscopy, and Quartz Crystal Microbalance

by

Diana Christine Phillips

Abstract

In Situ Adsorption Studies at the Solid/Liquid Interface: Characterization of Biological Surfaces and Interfaces Using Sum Frequency Generation Vibrational Spectroscopy, Atomic Force Microscopy, and Quartz Crystal Microbalance

by

Diana Christine Phillips

Doctor of Philosophy in Chemistry

University of California, Berkeley

Professor Gabor A. Somorjai, Chair

Sum frequency generation (SFG) vibrational spectroscopy, atomic force microscopy (AFM), and quartz crystal microbalance (QCM) have been used to study the molecular surface structure, surface topography and mechanical properties, and quantitative adsorbed amount of biological molecules at the solid-liquid interface. The molecular-level behavior of designed peptides adsorbed on hydrophobic polystyrene and hydrophilic silica substrates has been examined as a model of protein adsorption on polymeric biomaterial surfaces. Proteins are such large and complex molecules that it is difficult to identify the features in their structure that lead to adsorption and interaction with solid surfaces. Designed peptides which possess secondary structure provide simple model systems for understanding protein adsorption. Depending on the amino acid sequence of a peptide, different secondary structures (α-helix and β-sheet) can be induced at apolar (air/liquid or air/solid) interfaces. Having a well-defined secondary structure allows experiments to be carried out under controlled

conditions, where it is possible to investigate the affects of peptide amino acid sequence and chain length, concentration, buffering effects, etc. on adsorbed peptide structure. The experiments presented in this dissertation demonstrate that SFG vibrational spectroscopy can be used to directly probe the interaction of adsorbing biomolecules with a surface or interface. The use of well designed model systems aided in isolation of the SFG signal of the adsorbing species, and showed that surface functional groups of the substrate are sensitive to surface adsorbates. The complementary techniques of AFM and QCM allowed for deconvolution of the effects of surface topography and coverage from the observed SFG spectra. Initial studies of biologically relevant surfaces are also presented: SFG spectroscopy was used to study the surface composition of common soil bacteria for use in bioremediation of nuclear waste.

Professor Gabor A. Somorjai
Dissertation Committee Chair

For my family...

Contents

List of Figures

List of Tables

Acknowledgements

I would like to thank Prof. Gabor Somorjai and Prof. Heino Nitsche for the opportunity to work with them on this project. I would not have made it this far without the mentorship and encouragement of my undergraduate research advisor Mark Bussell, and the rest of the WWU Chemistry Department.

Thanks to Ozzy Mermut for performing the AFM measurements presented in this dissertation, and for being so helpful while I was writing up. Thanks to Roger York for always pushing me, and himself, to try a little harder. Keng Chou and Keith McCrea provided excellent training on the SFG laser system. Sasha Kweskin was always willing to lend a hand in the laser lab. Somorjai group members Anthony Contreras, Mike Ferguson, Katie Bratlie, Yuri Borodko, Jeong Park, and Max Montano kept day-to-day life at LBNL interesting. I always looked forward to bringing purchase orders down the hill to Inger Coble, who could be counted on for a smile and a story.

Jennifer Prescher is acknowledged for her willingness to teach a physical chemist the art of solid phase peptide synthesis. I greatly appreciate the help of David King (HHMI) in synthesizing our difficult peptide sequences. Num-Joon Cho (Curtis Frank group at Stanford University) and Beth Irwin (Healy lab) offered many hours of their time for training on the QCM instrument.

I will always remember long nights at the cyclotron with Nitsche group members Sarah Herbison Gallaher, Lindsy Farina, Cynthia Gong, Michael Calvert, Richard Wilson, Cody Folden, and Ralf Sudowe. Julia Chamberlain is gratefully acknowledged for beginning the bacteria surface characterization studies during her undergraduate summer internship.

The following professors generously offered advice or equipment for this project: Carolyn Bertozzi, Ahamindra Jain, Kevin Healy, Susan Marqusee, Jay Keasling, Peter Vollhardt, Arup Chakraborty, Phillip Geissler, Ron Shen. I was fortunate to teach

undergraduate chemistry courses with professors Ron Cohen, Stephen Leone, Jeff Long, Martin Head-Gorden, and Alex Pines.

Life in Berkeley was shared with friends Kate, Patti, Libby, Aaron, Amanda and David, Delphine, Romelia, Nuria, Jean, Jeff, Margaret, Janell, Dave and Wendy, and Brian. Finally, I would like to thank Máté, because without his love and support this dissertation may have never been finished.

Chapter 1

Introduction

Protein adsorption at the solid/liquid interface is involved in a wide range of phenomena in both nature and industrial applications. It is of great interest to the scientific and medical communities due to its application relative to implant biocompatibility, drug delivery, and biosensors.[1; 2; 3; 4] An unfavorable example of protein adsorption is the adsorption of blood proteins onto medical devices which subsequently alter their biological and immunological responses.[5; 6] Understanding protein adsorption may provide the means to exert molecular control of surface properties of biomaterials. The mechanisms of protein adsorption in real biological systems are quite complex, so a useful starting point is the examination of model systems of well-characterized surfaces exposed to an adsorbate under controlled conditions. Proteins are composed of chains of amino acids via peptide bonds, which form secondary structural motifs including the alpha helix and beta sheet. The secondary structures associate to form tertiary domains, which assemble to form the unique three-dimensional structure of proteins (Figure 1.1). This dissertation presents studies of the molecular-level behavior of designed polypeptides adsorbed onto various model substrates with different surface hydrophobicity (for example hydrophilic silica and hydrophobic polystyrene) using sum frequency generation (SFG) vibrational spec-

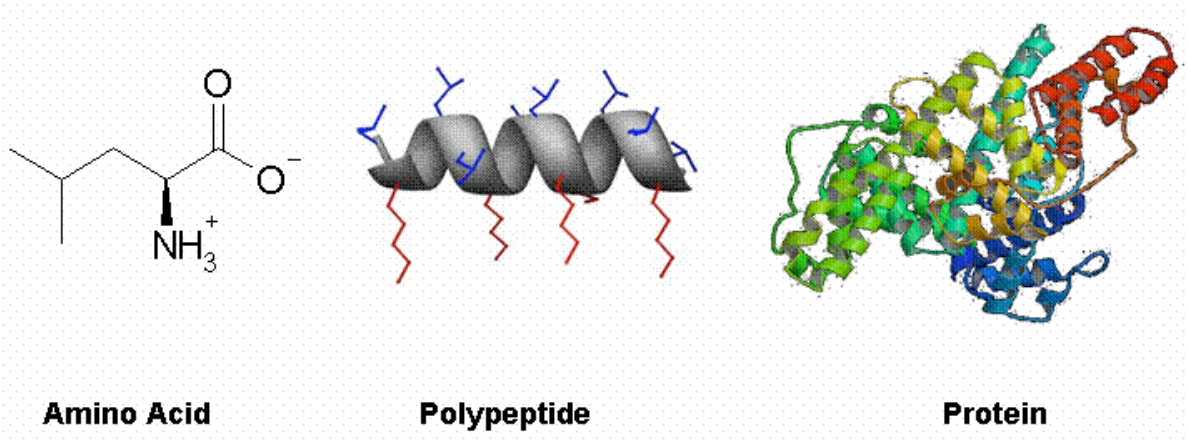

Figure 1.1. Example of the levels of structural complexity in proteins: the non-polar amino acid leucine, amphiphilic leucine-lysine α-helical peptide, and α-helical protein bovine serum albumin (BSA).

troscopy, atomic force microscopy (AFM), and quartz crystal microbalance (QCM) (Figure 1.2).

SFG vibrational spectroscopy allows in situ detection and analysis of surface molecules or structure with excellent temporal, spatial and spectral resolution.[7] In sum frequency generation spectroscopy, two input beams (typically a fixed visible and tunable infrared beam) at ω_1 and ω_2 overlap at a surface or interface to generate a surface specific sum frequency output ($\omega_{SF} = \omega_1 + \omega_2$). As an optical spectroscopy, it is applicable to all interfaces accessible by light and is generally non-destructive. SFG spectroscopy allows for the determination of surface structure of molecules at a surface or interface. The orientation of adsorbed molecules at a surface or interface is determined by their physical properties, and understanding this orientation may indicate the type of interaction occuring.

QCM is an ultra-sensitive (nanogram-range) mass sensor that monitors the real-time change in the amount of material adsorbed.[8; 9] This is achieved by exciting a piezoelectric crystal to oscillation by applying an AC voltage and monitoring the resonant frequency of the crystal over time. The resonant frequency is dependant on

the total oscillating mass, and decreases as a function of the amount of adsorbed material to the crystal (including coupled water mass). The adsorption of a biomolecule can be studied using different QCM crystal surfaces, which can help differentiate between varying affinities of adsorption in response to specific surface chemistry (i.e., hydrophobic polystyrene versus hydrophilic silica).

SFG spectroscopy and QCM are not useful for studying local characteristics of an adsorbate such as morphology (roughness and topographic heights) and lateral properties (i.e., aggregation and domain formation). Scanning AFM provides spatial resolution over the surface, including both long-range ordering and shorter-range local features of adsorbed biomolecules.[10] AFM works by raster scanning a nanoprobe across a surface and optically detecting the deflection (vertical) of the tip caused by topographical surface features. The tribological behavior and mechanical response (e.g., work of adhesion, elastic modulus, viscoelastic characteristic) of the adsorbed material can also be characterized and the friction coefficient of the adsorbate determined by mapping the lateral deflection induced on a scanning tip.[11]

Using this multi-technique approach, we can successfully answer three fundamental questions regarding in situ biomolecular adsorption: a) what is the molecular bonding/structure of the adsorbate on the surface (SFG), b) how much biomaterial adsorbs over a given time and relative adsorption affinity (QCM), and c) how does the adsorbed biomaterial appear in the lateral and vertical dimensions (AFM)?

Our current studies show that much can be learned from applying SFG, AFM and QCM to biological problems such as protein adsorption and biomaterial characterization. In order to engineer better implantable materials, a better understanding of the interaction of proteins with artificial materials is required. Proteins undergo both orientational and comformational changes upon adsorption onto a solid surface. The mechanisms of adsorption include hydrophobic and charge interactions which are

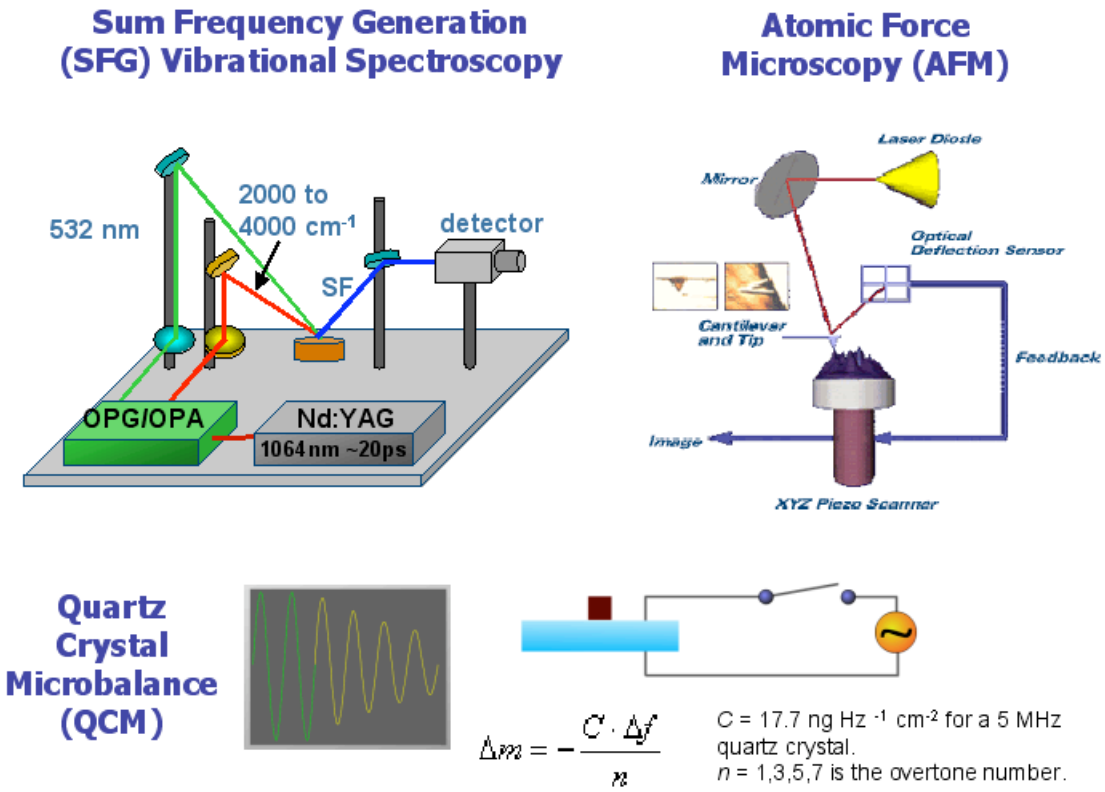

Figure 1.2. We have studied biomolecule adsorption at the solid/liquid interface using the techniques of SFG spectroscopy (surface monolayer composition and ordering), AFM (surface topography and mechanical properties), and QCM (surface coverage and adsorbed mass).

difficult to decouple in observed SFG spectra. With the goal of understanding protein adsorption, we begin with a detailed and systematic study of peptide adsorption on model and actual biomaterials, which we hope to use in interpreting more complex protein adsorption studies in the future. This work will lead to a better understanding of protein adsorption, and allow for the development of more effective biomaterials.

Chapter 2 describes the theory and application of AFM, QCM, and SFG for in situ study of adsorption at biological surfaces and interfaces. These techniques are used to study the adsorption of a model amphiphilic peptide on model hydrophobic and hydrophilic surfaces, discussed in Chapter 3. Depending on the amino acid

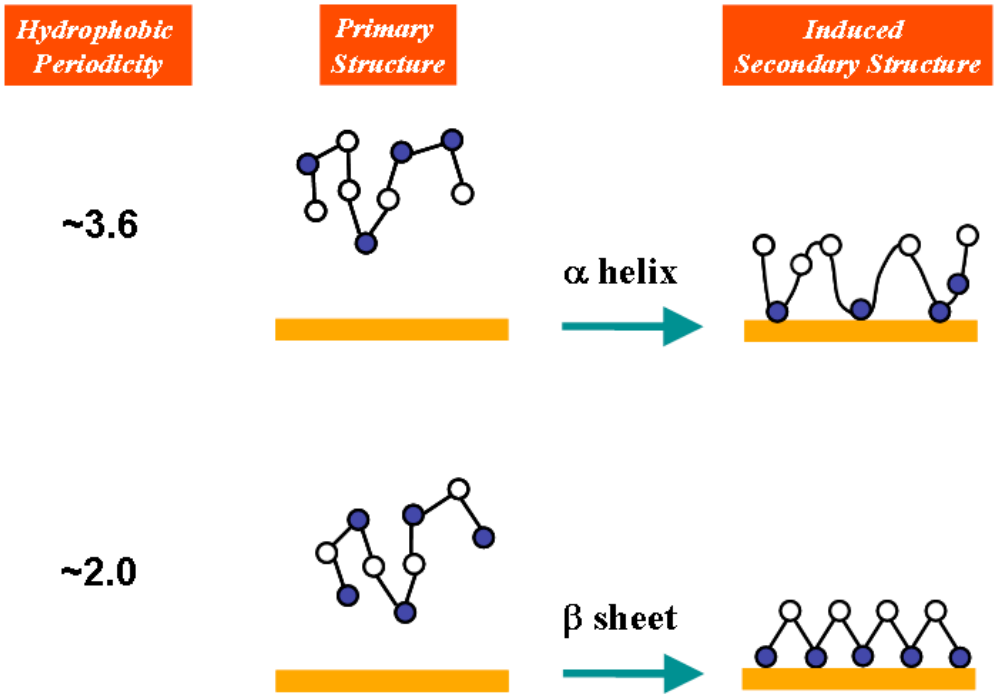

Figure 1.3. Hydrophobic periodicity effects on peptide secondary structure, redrawn from reference [12].

sequence of a peptide, different secondary structures (alpha helix and beta sheet) can be induced at apolar (air/liquid or air/solid) interfaces (Figure 1.3).[12] Peptides with this level of complexity are ideal for studies using SFG spectroscopy. The adsorption of the peptide is sensitive to surface hydrophobicity, which affects the structure, morphology and mass adsorbed. The combination of SFG, AFM and QCM can indicate the mechanism of adsorption (hydrophobic versus charge interactions), as well as distinguish between monolayer and multilayer deposition.

Chapter 4 discusses adsorption studies of a series of model peptides on model surfaces. We show that SFG spectroscopy is useful for investigating model systems under controlled conditions, where it is possible to isolate the effects of variables such as surface hydrophobicity, peptide chain length and sequence, solution ionic strength, and peptide concentration on adsorption. The amino acids of these peptides

were found to act as individual chromophores, and produce unique SFG signatures when adsorbed on hydrophobic polystyrene surfaces. On silica, only peptides which possess a predominant secondary structure in solution generate peptide specific SFG modes upon adsorption. This indicates solution secondary structure leads to specific adsorption at the silica surface.

Chapter 5 describes surface characterization studies of living bacteria species. Soil microbes are known to interact with environmental pollutants such as heavy metal and radionuclies through a variety of surface mediated interactions. SFG spectroscopy was used to study the surface of *Deinococcus radiodurans*, *Bacillus sphaericus*, and *Shewanella putrefaciens* in the CH stretching region of the infrared. The observed SFG spectra are unique for each bacteria species, due to differences in their surface protein layers. These initial experiments demonstrate the utility of SFG spectroscopy for studying complicated biological systems.

Bibliography

[1] Kasemo, B. *Surf. Sci.*, **2002**, *500*, 656.

[2] Ratner, B. D. *Molecular Recognition*, **1996**, *9*, 617.

[3] Gopel, W. *Biosensors and Bioelectronics*, **1998**, *13*, 723.

[4] Horbett, T. A.; Brash, J. L. *Proteins at Interfaces II: Fundamentals and Applications*; American Chemical Society: Washington, DC, **1995**.

[5] Kasemo, B. *Curr. Opin. Solid State Mater. Sci.*, **1998**, *3*, 451.

[6] Castner, D. G.; Ratner, B. D. *Surf. Sci.*, **2002**, *500*, 28.

[7] Shen, Y. R. *Pure and Applied Chemistry* **2001**, *10*, 1589.

[8] Marx, K. A. *Biomacromolecules*, **2003**, *4*, 1099.

[9] Hook, F.; Rodahl, M.; Brzezinski, P.; Kasemo, B. *Langmuir* **1998**, *14*, 729.

[10] Fotiadis, D.; Scheuring, S.; Muller, S. A.; Engel, A.; Muller, D. J. *Micron*, **2002**, *33*, 385.

[11] Hugel, T.; Seitz, M. *Macromol. Rapid. Commun.*, **2001**, *22*, 989.

[12] DeGrado, W. F.; Wasserman, Z. R.; Lear, J. D. *Science* **1989**, *243*, 622.

Chapter 2

Application of AFM, QCM, and SFG Vibrational Spectroscopy to In Situ Adsorption Studies of Biological Surfaces and Interfaces

Modern surface chemistry was developed in the 1960s, when techniques that could detect the small number of surface atoms relative to bulk atoms were discovered.[1] These surface sensitive techniques were predominantly electron-based spectroscopies, such as low energy electron diffraction (LEED) and x-ray photoelectron spectroscopy (XPS). Experiments that probe with electrons, atoms or ions require ultra-high vacuum (UHV) and reduced pressures at the interface are not amenable to investigation of biological systems in their native environment: aqueous phase and ambient temperatures and pressures. The development of scanning probe techniques, such as scanning tunneling microscopy (STM) and atomic force microscopy (AFM), in the 1980s lead to a renewed interest in the field of surface chemistry.[2] AFM can be

used to image and manipulate biological systems in situ on the nanometer scale. Another surface sensitive spectroscopy developed during the 1980s is the non-linear optical technique of sum frequency generation (SFG) spectroscopy.[3; 4] As an optical technique SFG spectroscopy probes vibrational modes of molecules at a surface or interface, and yields information on molecular structure and composition. Both the techniques of AFM and SFG spectroscopy are suitable for studying biological surfaces and interfaces under relevant conditions. In addition to AFM and SFG, we use a quartz crystal microbalance (QCM) to monitor both mass and viscoelestic properties of biological adsorbates in real time.

2.1 Contact-Mode Atomic Force Microscopy

2.1.1 Theoretical Background

AFM measures the van der Waals forces between a raster scanned tip and the surface, and yields three-dimensional topographical and surface mechanical information at the molecular scale.[2; 5] Contact-mode AFM measures short range repulsive forces, while non-contact mode measures longer range attractive forces. All of the AFM measurements reported in this dissertation were obtained in contact-mode operation. AFM utilizes a sharp tip at the end of a cantilever, which bends in response to the force between the tip and the sample. The cantilever motion can be described using Hooke's Law for small displacements.[6] The motion of the cantilever is controlled by piezoelectric actuators, which adjust the tip-to-sample distance to keep the force between the surface and tip constant. The deflection of the tip is measured using a helium-neon (HeNe) laser, which is reflected off the cantilever onto a position sensitive photo-detector (shown schematically in Figure 2.1). Vertical motion of the tip is registered by comparing the voltages measured in the upper and lower quadrants

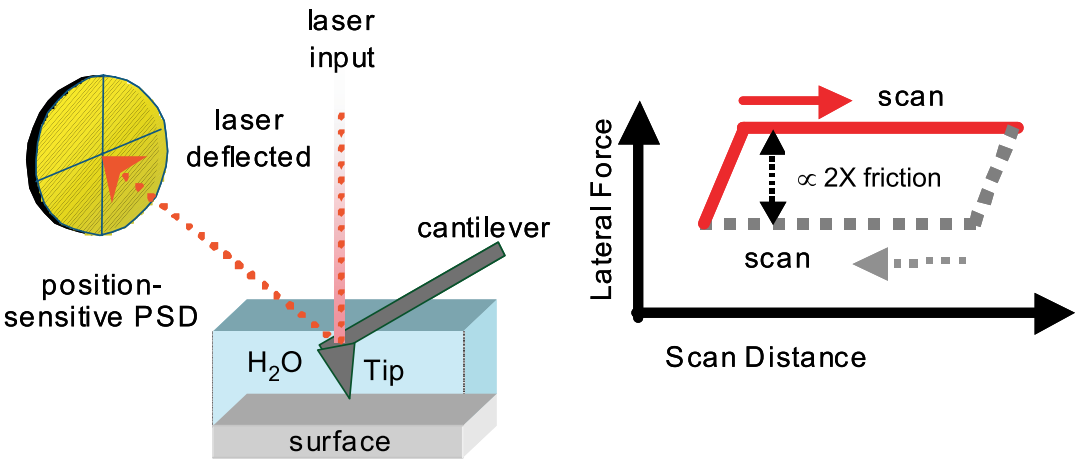

Figure 2.1. AFM experimental schematic. The diagram on the left shows schematically how the deflection of the tip is measured using a photodiode. The friction of the surface can be measured by plotting the lateral force on the tip versus the applied normal load.

of the photodiode. The voltages measured in the left and right quadrants indicate the amount of torque on the cantilever. When the tip encounters surface features during scanning, the piezos are raised and lowered through a feedback loop to maintain a constant tip deflection (tip-to-sample distance, not height), which maintains a constant load. A three dimensional topographic image is obtained by measuring the tracking piezo motion (which moves in the z direction for maintaining constant force, and the x and y directions for scanning the sample). Mechanical properties such as friction are determined by measuring the force on the tip during a line-scan. The friction measurement is a convolution of both friction and topographical information. It is necessary to compare both the topograph and friction map in order to avoid artifacts in the friction measurement.

2.1.2 Experimental Set-up

AFM scanning probe images shown in this thesis are obtained using a Molecular Imaging instrument with a 30-μm scan head (Pico SPM). Scanning is performed in

contact mode and at low loads (<5 nN) using gold-coated silicon nitride Si_3N_4 tips with radius, r = 15 nm, and a nominal spring constant, k = 0.2 N·m^{-1} (Veeco Probes). The root-mean-square (rms) surface roughness was determined for a 2.5 μm × 2.5 μm surface. Images of the bare surfaces were acquired in solution prior to addition of the peptide or protein sample. Friction data was obtained at the peptide/buffer solution interface by laterally scanning a 200 nm × 200 nm area at 2 Hz (overtop the adsorbed peptide) at various normal force loads (0-17 nN). The force-distance response curve on a silica substrate was calibrated using the spring constant of the tip to determine the applied normal loads. Friction experiments were obtained using a sample concentration high enough to ensure sufficient coverage of the surface and minimize convolution of substrate effects. A relative measure of the lateral force exhibited on the tip (measured in mV) at specified normal loads was calculated from the average difference of the trace versus retrace image (Figure 2.1). The maximum load applied to each surface was determined by observation of load-induced permanent deformations to the surface. The relative friction was obtained from the slope of the plot of lateral force (F_L) versus normal load (F_N).

2.1.3 Sample AFM Data

AFM topographical images are calibrated using a grating with known feature heights. The topographical data for a 25 nm grating is shown, along with the cross sectional heights, in Figure 2.2. Figure 2.3 shows AFM topographical and friction images for the polymer poly(2-hydroxyethyl methacrylate), or p(HEMA), and for the blood serum protein, bovine serum albumin (BSA), adsorbed on p(HEMA). This polymer is used commercially as the base material for soft contact lenses. AFM has been used to study the surface mechanical properties of p(HEMA) before and after protein adsorption.[7] The topographical and friction map of bare p(HEMA) show a

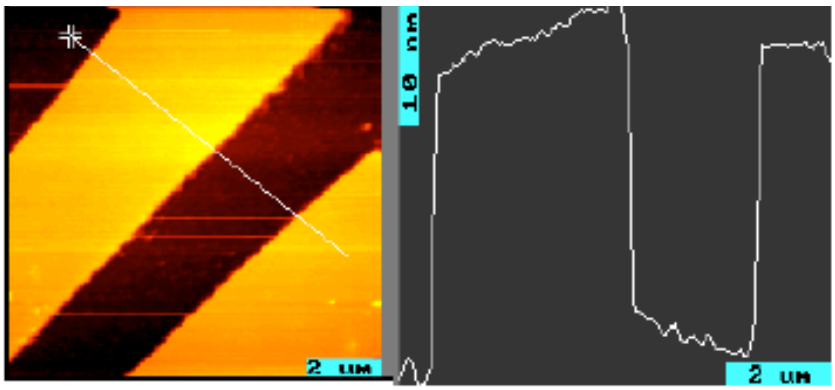

Figure 2.2. AFM topography and cross sectional data for a 25 nm grating, which is used for calibration.

relatively smooth, soft surface. Adsorption of BSA significantly increases the friction of the surface.

2.2 Quartz Crystal Microbalance

2.2.1 Theoretical Background

As initially demonstrated by Sauerbrey, the QCM is a highly sensitive mass sensor capable of measuring nanogram quantities of adsorbed material on surfaces.[11] The mechanism involves exciting a piezoelectric crystal (through deposited metal electrodes) with a RF voltage near the crystal's resonant frequency and driving it to a shear oscillation.[11; 12] After excitation, the voltage is switched off and the decay in the voltage over the crystal is observed as an exponentially damped sinusoidal wave. The "wet" mass added (Δm) induces a linear resonant frequency shift (Δf) according to Eq 1, provided that the adsorbed mass in a liquid environment is evenly distributed, produces a sufficiently rigid and thin film (i.e. elastic masses are adsorbed). In Eq 1, n denotes the overtone number and C is the mass sensitivity

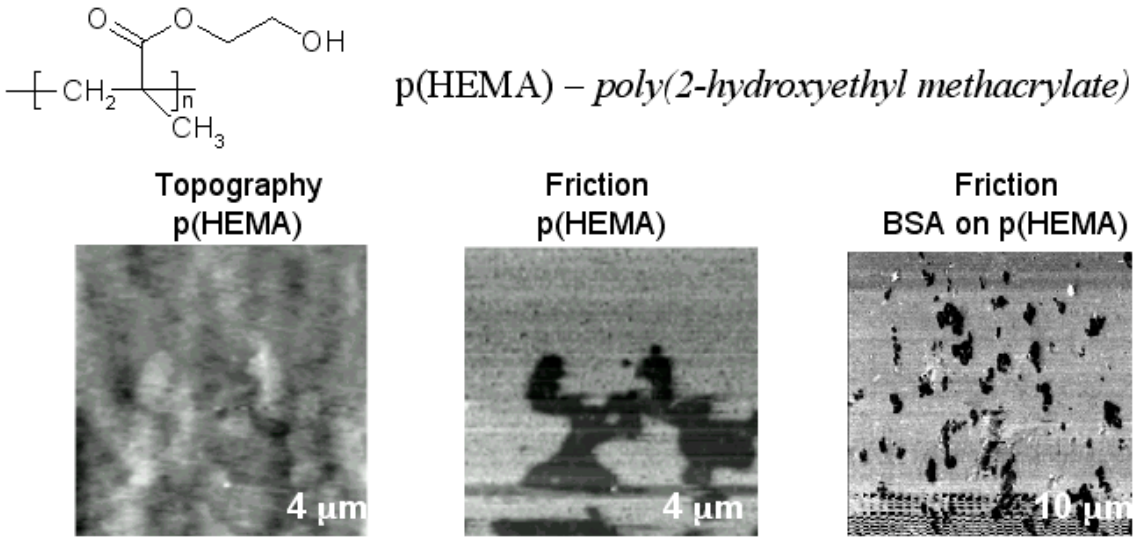

Figure 2.3. AFM topography and friction data for bare p(HEMA) polymer (structure shown above the topograph). When bovine serum albumin (BSA) protein is adsorbed on p(HEMA), the friction increases.

constant for $\Delta f = 1$ Hz (17.7 ng·cm^{-2} using a 5 MHz crystal).

$$\Delta m = \frac{-C\Delta f}{n} \tag{2.1}$$

The QCM-D technique is very useful in applications involving biomolecule adsorption, due to its highly sensitive detection of mass at the surface-solution interface and its capability to characterize the dissipative energy or viscoelastic behavior of the mass deposited.[12; 13; 14; 15] In QCM-D, the variation in dissipation energy (ΔD) is measured concurrently with the frequency change and reflects the viscoelastic properties of the adlayer. The energy dissipation factor is defined as the ratio between the energy dissipated per oscillation cycle and the net stored energy in the oscillating system. For a perfectly elastic adsorbate, the change in energy dissipation is negligible. In systems where the adsorbate does not behave as an elastic mass (as in the case of many biomacromolecules)[16; 17] significant dissipative losses occur due to internal and/or interfacial friction. This limits the validity of the Sauerbrey relation.[15]

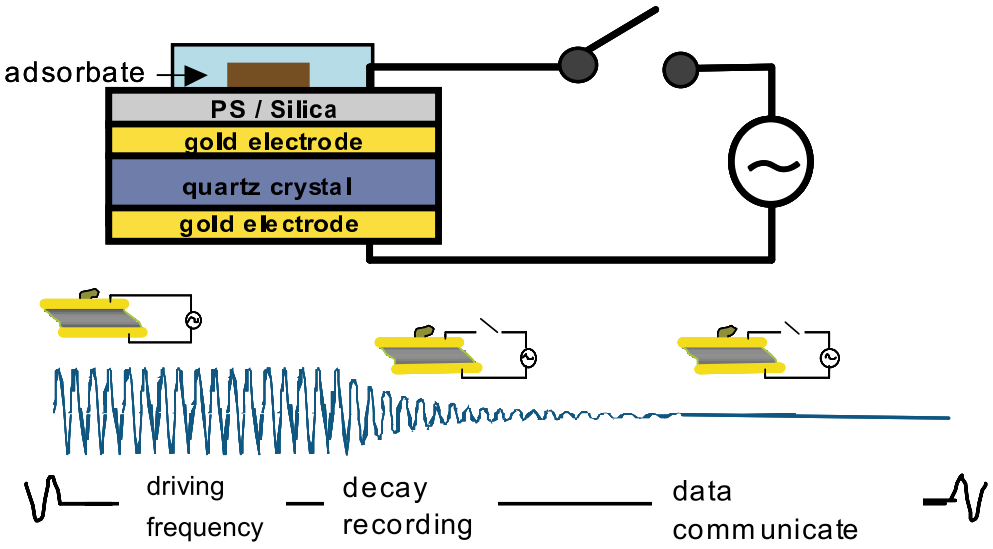

Figure 2.4. In QCM-D, an AC voltage is pulsed across a piezoelectric quartz crystal at the crystals resonant frequency and at several overtones, driving the crystal to oscillate in shear mode at the resonant or overtone frequency. The shear wave at each frequency is allowed to dampen, and the inverse of the decay time constant is recorded simultaneously with Δf and ΔD. The QCM-D technique is typically sensitive to surface coverage in the range of ng/cm^2.

2.2.2 Experimental Set-up

We use a Q-sense D300 model QCM-D for all QCM measurements presented in this thesis, shown schematically in Figure 2.4. SiO_2-coated sensor crystals (Q-Sense QSX 303, AT-cut, 5 MHz, active surface area = 0.2 cm^2) are used as a hydrophilic substrate, or are coated with polystyrene for use as a hydrophobic substrate. The sensor crystal is initially stabilized in pH 7.4 phosphate buffered saline solution. A volume of ~0.5 mL of temperature-stabilized sample liquid is delivered to the chamber containing the sensor crystal (internal volume, 80 μL) to ensure a complete exchange of the liquid. Signal distortion (peaks of $f < 5$ Hz and $D < 0.6 \cdot 10^{-6}$) is observed briefly upon sample injection. Measurements of f and D are acquired at several harmonics (15, 25, and 35 MHz) simultaneously. All measurements were performed

at a temperature of 24-25 °C, to within 0.5 °C. The QCM liquid cell was thoroughly cleaned with Hellmanex between measurements.

2.2.3 Sample QCM data

Sample QCM-D data (courtesy of Q-Sense) of BSA protein adsorbed on silica is shown in Figure 2.5. Adsorption of BSA leads to a large Δf, with monotonic adsorption kinetics. BSA strongly adsorbs to the surface, as shown by the small frequency change observed upon rinsing. QCM measurement of 1 mg/mL leucine amino acid adsorbed onto hydrophobic PS indicates negligible adsorption from buffer. Similarly, the inset in Figure 2.6 shows negligible adsorption of leucine on the hydrophilic silica from solution. The negligible decrease in frequency ($\leq$ 1 Hz) observed upon adsorption of leucine from buffer solution on both the PS and SiO_2 surface indicates very little adsorption of weakly bound amino acid. Previous studies of amino acids do not have strong affinity for hydrophobic and hydrophilic surfaces at pH 7.4, since there is little free energy gain from the adsorption on a surface.[18]

2.3 Sum Frequency Generation (SFG) Vibrational Spectroscopy

2.3.1 Theoretical Background

The theory of SFG spectroscopy was first proposed by Bloembergen,[19] and the technique was initially developed by the Shen group of UC Berkeley.[4] Several excellent reviews on the theory and analysis of SFG spectra have been written.[21; 22] The theory of the SFG process can be described using quantum perturbation theory. In the presence of a strong electric field (i.e. laser light), a non-linear response in the

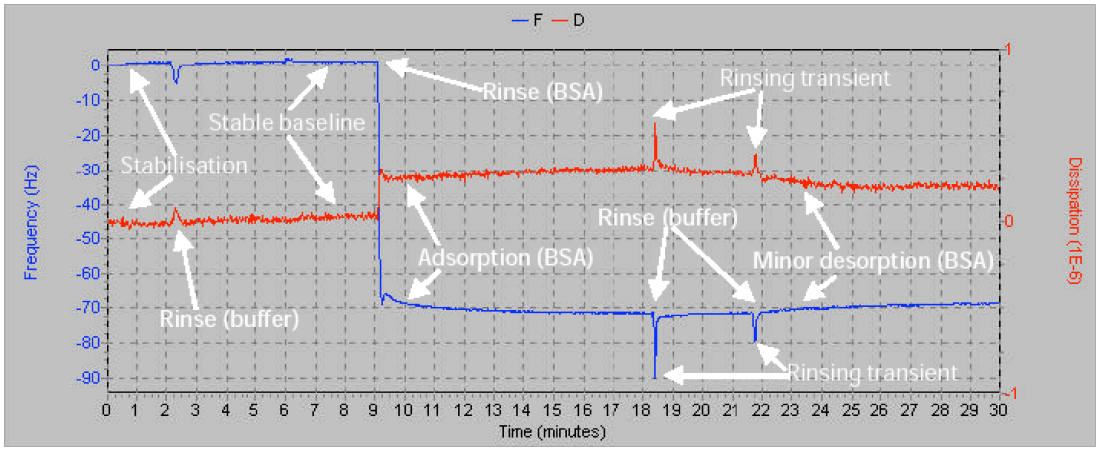

Figure 2.5. QCM-D data of BSA adsorbed on silica showing both the change in frequency and energy dissipation, Δf and ΔD, upon adsorption. Data from Q-Sense.

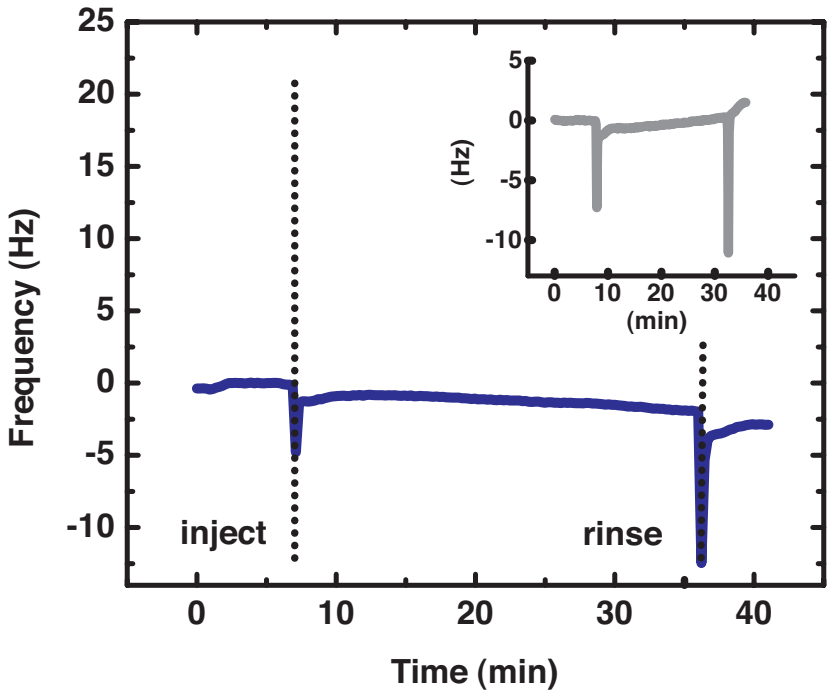

Figure 2.6. QCM data of Leucine amino acid on polystyrene (blue) and silica (inset, grey). The spikes in the data are from pressure changes in the cell upon injection and rinsing. There is very little adsorption of Leucine amino acid to both polystyrene and silica surfaces at pH 7.4.

dipole moment of a medium is observed. The polarization of a medium, $\mathbf{P}$, is defined as the dipole per unit volume, $\mathbf{P} = \mu/V$, and can be written as:

$$\mathbf{P}(\omega) = \frac{\mu^{(0)}}{V} + \frac{\alpha \mathbf{E}(\omega)}{V} = \mathbf{P}^{(0)}(\omega) + \varepsilon_0 \chi^{(1)} \mathbf{E}(\omega) \tag{2.2}$$

where $\mu^{(0)}$ is the static dipole, α is the polarizability, $\mathbf{E}(\omega)$ is the electric field of the radiation, and $\chi^{(1)}$ is the linear susceptibility of the media. The polarization can be expanded as follows:

$$\mathbf{P}(\omega, 2\omega, ...) = \mathbf{P}^{(0)} + \mathbf{P}^{(1)} + \mathbf{P}^{(2)} + ... = 0 + \varepsilon_0 \chi^{(1)} \mathbf{E}(\omega) + \varepsilon_0 \chi^{(2)} \mathbf{E}(\omega)\mathbf{E}(\omega) + ... \tag{2.3}$$

where $\chi^{(2)}$ is the surface non-linear (second-order) susceptibility, a third rank tensor. We are specifically interested in $\mathbf{P}^{(2)}$, which is responsible for SFG:

$$\mathbf{P}^{(2)} = \begin{bmatrix} P_x \\ P_y \\ P_z \end{bmatrix} = \varepsilon_0 \begin{bmatrix} \chi_{xxx} & \cdot & \cdot \\ \cdot & \chi_{yyy} & \cdot \\ \cdot & \cdot & \chi_{zzz} \end{bmatrix} \begin{bmatrix} E_x^1 \\ E_y^1 \\ E_z^1 \end{bmatrix} \begin{bmatrix} E_x^2 \\ E_y^2 \\ E_z^2 \end{bmatrix} \tag{2.4}$$

In sum frequency generation spectroscopy, two pulsed laser beams, one of fixed frequency ω_{vis} (532 nm) and one of tunable frequency ω_{IR}, are overlapped spatially and temporally at an interface. Light at the sum frequency ω_{SFG} is collected in the reflected direction. The intensity of this light (given by $|\mathbf{P}^{(2)}|^2$) is proportional to the absolute square of the effective surface non-linear susceptibility, $\chi^{(2)}_{eff}$:

$$I(\omega_{SFG}) \propto |\chi^{(2)}_{eff}|^2 I(\omega_{vis}) I(\omega_{IR}) \tag{2.5}$$

The effective surface non-linear susceptibility is related to $\chi^{(2)}$, the surface non-linear susceptibility through the tensorial Fresnel coefficients:[23]

$$\chi^{(2)}_{eff} = [\mathbf{L}(\omega_{SFG}) \cdot \hat{e}_{SFG}] \cdot \boldsymbol{\chi}^{(2)} : [\mathbf{L}(\omega_{vis}) \cdot \hat{e}_{vis}][\mathbf{L}(\omega_{IR}) \cdot \hat{e}_{IR}] \tag{2.6}$$

where $\hat{e}_i$ is a unit polarization vector of the optical field at ω_i, and $\mathbf{L}(\omega_i)$ is the tensorial Fresnel factor.

The second order non-linear susceptibility has two components, a non-resonant term and, when the infrared beam is at a frequency which coincides with a frequency of a molecular vibration, a resonant term. This is expressed under the dipole approximation as:[23]

$$\boldsymbol{\chi}^{(2)} = \boldsymbol{\chi}^{(2)}_{NR} + \boldsymbol{\chi}^{(2)}_{R} = \boldsymbol{\chi}^{(2)}_{NR} + N_s \langle \boldsymbol{\alpha}^{(2)}_{R} \rangle_f = \boldsymbol{\chi}^{(2)}_{NR} + N_s \int \boldsymbol{\alpha}^{(2)}_{R} f(\Omega) d\Omega \tag{2.7}$$

where $\boldsymbol{\chi}^{(2)}_{NR}$ comes from non-resonant excitations, N_s is the surface density of molecules, the symbol $\langle \boldsymbol{\alpha}^{(2)}_{R} \rangle_f$ represents an orientational average over an orition distribution function $f(\Omega)$, $\boldsymbol{\alpha}^{(2)}_{R}$ is the resonant non-linear hyperpolarizability (a tensor of rank 3), and Ω denotes a set of orientational angles that describes a transformation between the laboratory and molecular coordinate system[23; 24; 25]. The resonant nonlinear hyperpolarizability is composed of Lorentzian resonant terms:

$$\boldsymbol{\alpha}^{(2)}_{R}(\omega_{IR}) = \sum_q \frac{\mathbf{a}_q}{\omega_{IR} - \omega_q + i\Gamma_q} \tag{2.8}$$

where $\mathbf{a}_q$ is the amplitude of the qth resonance, Γ_q is the line width (or damping factor) of the qth resonance, ω_{IR} is the IR frequency, ω_q is the frequency of the qth molecular vibration. For azimuthally isotropic surfaces ($x = y, x = -x, x = -y, z \neq -z$), there are seven nonzero elements of $\boldsymbol{\chi}^{(2)}$:

$\boldsymbol{\chi}^{(2)}_{zzz}$,

$\boldsymbol{\chi}^{(2)}_{xxz} = \boldsymbol{\chi}^{(2)}_{yyz}$,

$\boldsymbol{\chi}^{(2)}_{xzx} = \boldsymbol{\chi}^{(2)}_{yzy} = \boldsymbol{\chi}^{(2)}_{zxx} = \boldsymbol{\chi}^{(2)}_{zyy}$,

with the surface defined as the $\hat{x}-\hat{y}$ plane and $\hat{z}$ along the surface normal. SFG spectra presented in this dissertation were collected primarily using $s_{sfg}s_{vis}p_{ir}$ polarization combination (*ssp*), which probes the *yyz* component of $\boldsymbol{\chi}^{(2)}$. Additional spectra were collected using $s_{sfg}p_{vis}s_{ir}$ polarization (*sps*), which probes the *yzy* component of $\boldsymbol{\chi}^{(2)}$.

In the SFG experiment, the tunable beam is scanned across the IR. When ω_{IR} comes into resonance with ω_q the resonant term and SFG signal intensity is enhanced.

The amplitude of the qth resonance term, $\mathbf{a}_q$, is related to the infrared dipole moment and the Raman polarizability, $\partial\boldsymbol{\mu}/\partial Q_q$ and $\partial\boldsymbol{\alpha}_q^{(1)}/\partial Q_q$, respectively:

$$\mathbf{a}_{\mathrm{q,ijk}} = -\frac{N_s}{\varepsilon_0}\sum_{i'j'k'}\frac{1}{2\omega_q}\frac{\partial\boldsymbol{\alpha}_{i'j'}}{\partial Q_q}\frac{\partial\boldsymbol{\mu}_{k'}}{\partial Q_q}\langle(\hat{i}\cdot\hat{i}')(\hat{j}\cdot\hat{j}')(\hat{k}\cdot\hat{k}')\rangle \tag{2.9}$$

where N_s is the surface density of molecules, Q_q is the classical normal coordinate of the qth vibrational mode, and $\hat{i},\hat{j},\hat{k}$ are the laboratory coordinates which are transformed into $\hat{i}',\hat{j}',\hat{k}'$, the molecular coordinates (averaged over the molecular orientations).[23; 26] According to Eqs 2.9, a vibrational resonance is SFG active when it is both IR active and Raman active.[27; 28] The integral in equation 2.7 demonstrates how the orientation distribution of a molecule can change its SFG spectra. For an adsorbate with many IR and Raman active modes, the way in which the adsorbate bonds with the interface can change the orientation distribution and hence the intensity of the modes that appear in the SFG spectra. This is due to the fact that at a given interface, some parts of the molecule may have different geometrical orientations due to specific interactions with the surface.[29; 30] As a result, specific surface interactions can cause some modes to produce SFG signal at certain interfaces, while other modes may be SFG active at different interfaces.

2.3.2 Experimental Set-up

SFG spectra were obtained using two different laser systems: a 1064 nm mode-locked Nd:YAG laser (Ekspla, Lithuania) with a pulse width of 20 ps, operating at a 10 Hz repetition rate; and a PL2143A Nd:YAG laser with a 20 ps pulse width and 20 Hz repetition rate (Leopard D-20, Continuum, Santa Clara, CA). On both laser systems, the fundamental radiation is sent to an optical parametric generator/amplifier (OPG/OPA) stage (LaserVision, Bellevue, WA) where tunable infrared radiation is produced in addition to frequency-doubled radiation at 532 nm. The OPG/OPA consists of two parts. The first is an angle-tuned potassium titanyl phosphate (KTP)

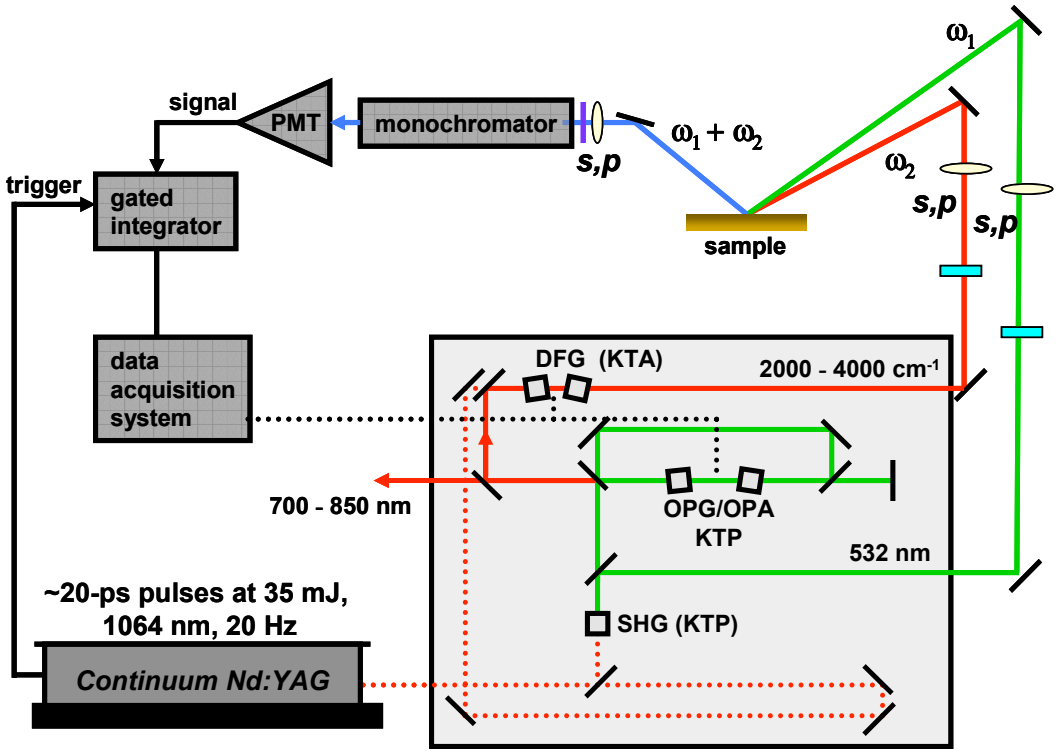

Figure 2.7. Schematic of the SFG laser system. The 1064 nm laser pumps and OPA/OPG system, where the fndamental is frequency doubled to generate a 532 nm visible beam, and to generate tunable IR (2000 - 4000 cm^{-1}) through frequency mixing. The beams are then aligned temporally and spatially at the sample to produce the SFG signal.

stage pumped with 532 nm light to generate near infrared radiation between 1.35-1.85 μm. This output is then mixed with the 1064 nm fundamental in an angle-tunable potassium titanyl arsenate (KTA) stage to produce a tunable infrared beam from 2000-4000 cm^{-1} (7 cm^{-1} FWHM). As shown schematically in Figure 2.7, the tunable infrared beam is combined with the 532 nm radiation at the sample interface at incident angles near 62° and 58°, respectively, with respect to the surface normal.

SFG photons are collected in the reflected geometry. When analyzing liquid samples in this thesis, the beams are reflected through transparent silica substrate in order

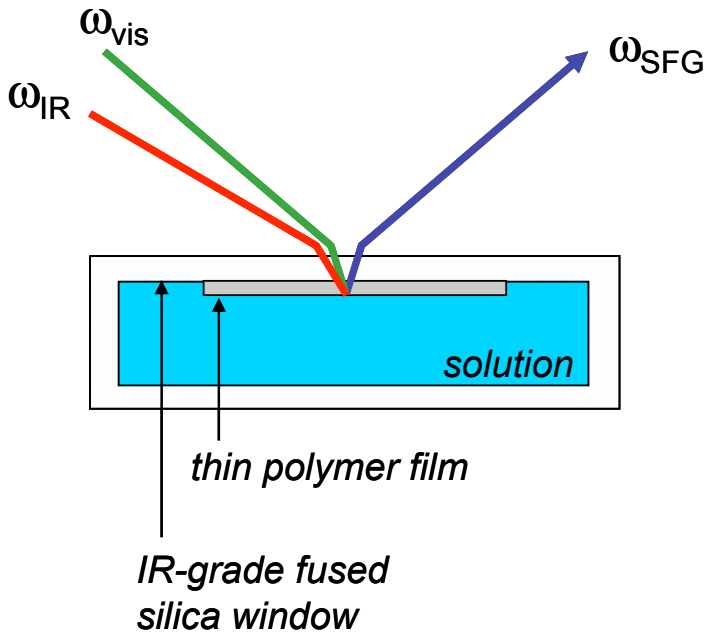

Figure 2.8. Schematic of the SFG sample set-up in reflection geometry for studies at the solid/liquid interface.

to measure the solid/liquid interface (Figure 2.8). Reflecting through the sample liquid itself is not an option, due to attenuation of the infrared beam by strong water absorbance in the infrared. The SFG signal generated from the sample is collected by a photomultiplier tube, sent to a gated integrator, and stored digitally. The measurement of the SFG signal is calibrated by placing a thin film of polystyrene in the path of the infrared beam, and measuring the attenuation of the strong non-resonant SFG signal from a gold surface. Based on the known position of the polystyrene peaks, the monochromator and OPG system can be calibrated. Figure 2.9 shows the calibration spectrum.

2.3.3 Sample SFG Spectra

SFG spectroscopy can be used to selectively probe the structure and composition of surface adsorbates or the surface itself. Figure 2.10 shows the SFG spectrum of

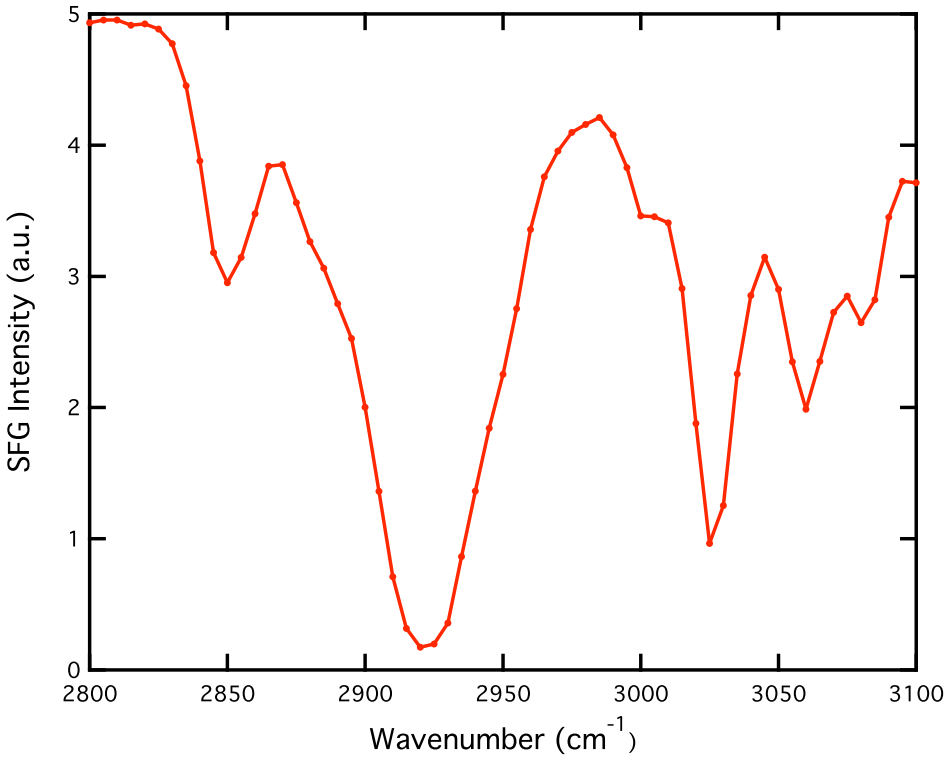

Figure 2.9. SFG calibration scan: non-resonant SFG signal from a gold surface, with a polystyrene film placed the the IR beam path. The position of the peak at 2920 cm^{-1} is used to calibrate the SFG detection system.

polystyrene, and how the vibrational modes of the phenyl rings in the polystyrene surface are affected by protein adsorption. The SFG spectrum in Figure 2.10 is of partially deuterated polystyrene, PS-d_3 (backbone protons are deuterated). The peaks in the 3000-3100 cm^{-1} range are from CH stretch modes of the phenyl ring, as illustrated in the top figure. This is confirmed by experiments using fully deuterated polystyrene (PS-d_8), where these modes are shifted out of this spectral region. Without adsorbed proteins, a large peak at 3073 cm^{-1} and a shoulder around 3053 cm^{-1} are observed, and are assigned to the ν_2 and ν_{7a} modes, respectively. The SFG spectrum following adsorption of bovine serum albumin (BSA) protein from pH 7.4 buffer is also shown. Their are new CH resonances around 2860 cm^{-1} and 2930 cm^{-1} due to the protein, while the polystyrene phenyl mode is still present but has been significantly atten-

uated. Earlier work by the Somorjai group has found that the SFG intensity of the phenyl CH modes slowly attenuate as more protein molecules are adsorbed.[31] This result indicates that the structure and orientation of the underlying phenyl ring in the polystyrene substrate is affected by protein deposition, presumably due to the interaction between phenyl rings and adsorbed protein molecules. It demonstrates that SFG directly probes the adsorbate-substrate interaction. In this dissertation, we have focused on characterizing the surface structure of the adsorbing molecules, and have used fully deuterated polystyrene as our hydrophobic substrate.

We have studied the adsorption of several amino acids, including amino acids with hydrophobic side chains (leucine, alanine, phenylalanine) and hydrophilic side chains (arginine, lysine). The amino acids were adsorbed from phosphate buffered saline (PBS) solution at pH 7.4. Upon initial adsorption of an amino acid solution to hydrophobic polystyrene, we do not see SFG signal. However, following exposure of the surface to the air/solution interface, we observe SFG signal from amino acids with hydrophobic side chains (leucine, alanine, etc.), as demonstrated by the SFG spectrum of dried L-leucine amino acid on deuterated polystyrene, obtained in *ssp* polarization, in Figure 2.11. Symmetric and asymmetric CH_3 stretches are observed at 2872 cm^{-1} and 2958 cm^{-1}, respectively, from the leucine side-chain. Amino acids are known to order at air/water interface with side chains sticking out of the bulk. It is possible that the observed SFG signal is due to a Langmuir-Blodgett type deposition to the substrate when placed in contact with the solution following exposure to air.

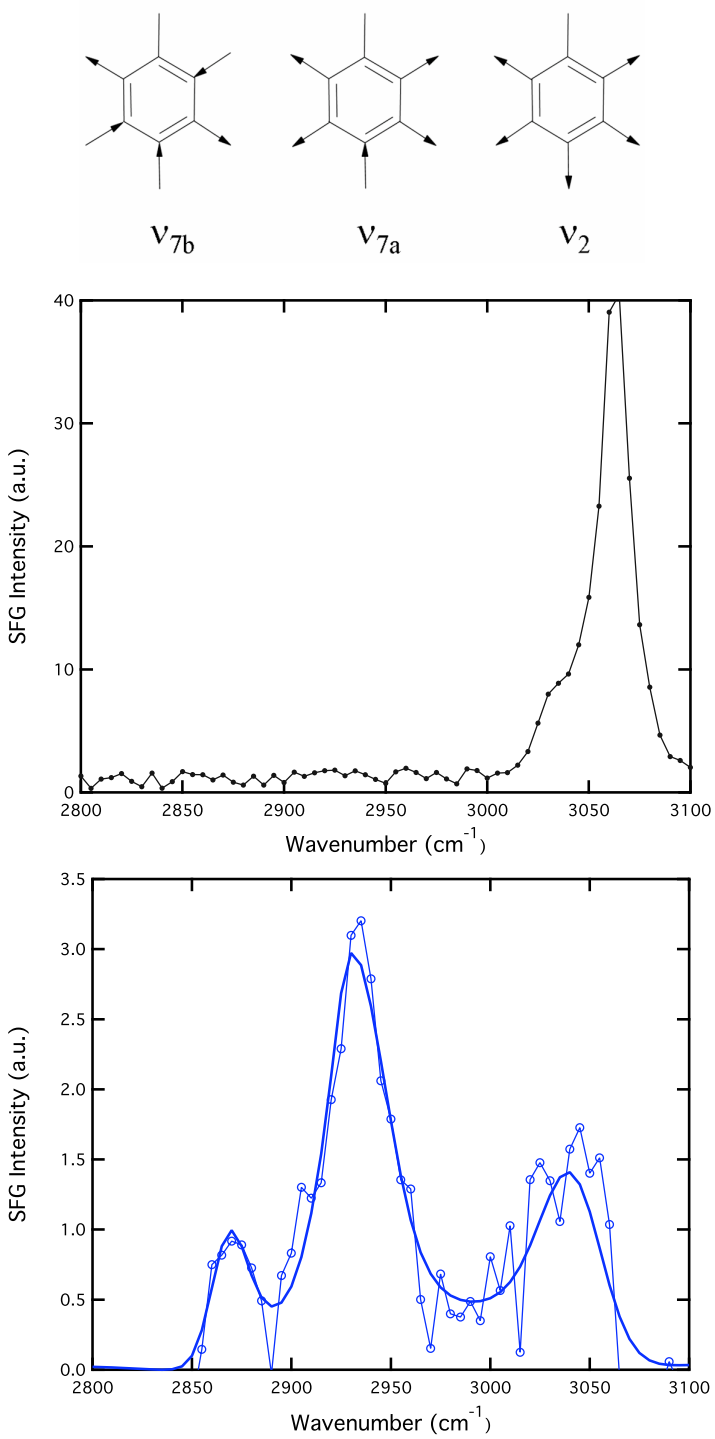

Figure 2.10. SFG spectrum of partially deuterated polystyrene, PS-d_3, top. SFG spectrum of bovine serum albumin (BSA) on PS-d_3, bottom.

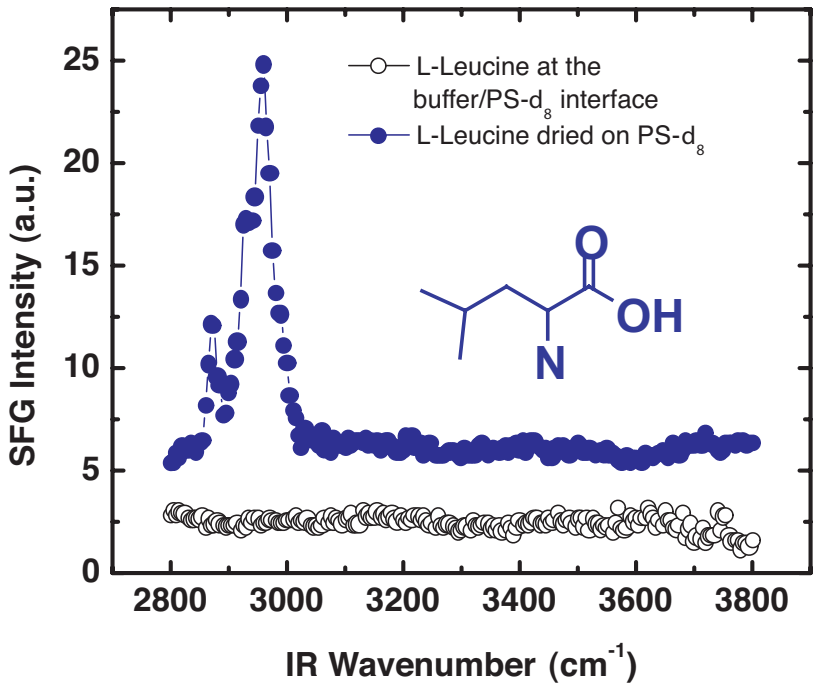

Figure 2.11. SFG spectrum of dried Leucine amino acid on fully deuterated polystyrene, PS-d_8. Resonances at 2868 and 2954 cm^{-1} are assigned to symmetric and asymmetric methyl stretching modes, respectively.

Bibliography

[1] Somorjai, G. A. *Introduction To Surface Chemistry And Catalysis*, Chapter 1; John Wiley & Sons, Inc.: New York, NY, **1994**.

[2] Binnig, G.; Quate, C. F.; Gerber, C. *Phys. Rev. Lett.*, **1986**, *56*, 930.

[3] Shen Y. R. *The Principles of Nonlinear Optics*; Wiley: New York, 1984.

[4] Shen, Y. R. *Nature*, **1989**, *337*, 519.

[5] Sheiki, S. S. *Adv. Poly. Sci.*, **2000**, *151*, 61.

[6] Fotiadis, D.; Scheuring, S.; Muller, S. A.; Engel, A.; Muller, D. J. *Micron*, **2002**, *33*, 385.

[7] Koffas, T. S.; Amitay-Sadovsky, E.; Kim, J.; Somorjai, G. A. *J. Biomater. Sci. Polymer Edn.*, **2004**, *15*, 475.

[8] Lee, N. H.; Christensen, L. M.; Frank, C. W. *Langmuir*, **2003**, *19*, 3525.

[9] Opdahl, A.; Hoffer, S.; Mailhot, B.; Somorjai, G. A. *Chem. Rec.*, **2001**, *1*, 101.

[10] Opdahl, A.; Somorjai, G. A. *ACS Symposium Series: Application of Scanned Probe Microscopy to Polymers*, American Chemical Society: Washington, DC, **2005**, *897*, Chapter 9, 112.

[11] Sauerbrey, G. Z. *Phys.*, **1959**, *155*, 206.

[12] Czanderna, A. W.; Lu, C. in *Applications of Piezoelectric Quartz Crystal Microbalances* edited by Lu, C. and Czanderna, A. W. (Elsevier, Amsterdam, **1984**), Vol. 7, p. 1.

[13] Krim, J.; Chiarello, R. J. *Vac. Sci. Technol. B.*, **1991**, *9*, 1343.

[14] Widom, A.; Krim, J. *Phys. Rev. B.*, **1986**, *34*, 1403.

[15] Marx, K. A. *Biomacromolecules*, **2003**, *4*, 1099.

[16] Hook, F.; Rodahl, M.; Brzezinski, P.; Kasemo, B. *Langmuir* **1998**, *14*, 729.

[17] Hook, F.; Kasemo, B.; Nylander, T.; Fant, C.; Sott, K.; Elwing, H. *Anal. Chem.* **2001**, *73*, 5796.

[18] Basiuk, V. A.; Gromovoy, T. U.; KhilChevskaya, E. G. *Origins Life Evol. Biosphere*, **1995**, *25*, 375.

[19] Bloembergen, N.; Chang, R. K.; Jha, S. S.; Lee, C. H. *Phys. Rev.*, **1968**, *174*, 813.

[20] Shen, Y. R. *IEEE Journal on Selected Topics in Quantum Electronics*, **2000**, *6*, 1375.

[21] Lambert, A. G.; Davies, P. B.; Neivandt, D. J. *App. Spectrosc. Rev.*, **2005**, *40*, 103.

[22] Wang, H. F.; Gan, W.; Lu, R.; Rao, Y. ; Wu, B. H. *Int. Rev. Phys. Chem.*, **2005**, *24*, 191.

[23] Wei, X.; Hong, S. C.; Zhuang, X.; Goto, T.; Shen, Y. R. *Phys. Rev. E.*, **2000**, *62*, 5160.

[24] Hirose, C.; Akamatsu, N.; Domen, K. *Appl. Spectrosc.*, **1992**, *46*, 1051.

[25] Zhuang, X.; Miranda, P. B.; Kim, D.; Shen, Y. R. *Phys. Rev. B.*, **1999**, *59*, 12632.

[26] Superfine, R.; Huang, J. Y.; Shen, Y. R. *Chem. Phys. Lett.*, **1990**, *172*, 303.

[27] Doyle, A. W.; Fick, J.; Himmelhaus, M.; Eck, W.; Graziani, I.; Prudovsky, I.; Grunze, M.; Maciag, T.; Neivandt, D. J. *Langmuir* **2004**, *20*, 8961.

[28] Wang, J.; Buck, S.; Chen, Z. *J. Phys. Chem. B.* **2002**, *106*, 11666.

[29] Baldelli, S.; Mailhot, G.; Ross, P. N.; Somorjai, G. A. *J. Am. Chem. Soc.*, **2001**, *123*, 7697.

[30] Baldelli, S.; Mailhot, G.; Ross, P.; Shen, Y. R.; Somorjai, G. A. *J. Phys. Chem. B.*, **2001**, *105*, 654.

[31] Kim, J.; Somorjai, G. *J. Am. Chem. Soc.*, **2003**, *125*, 3150.

Chapter 3

Adsorption Studies of a Model Amphiphilic Peptide on Hydrophobic and Hydrophilic Surfaces

Reproduced with permission from *J. Am. Chem. Soc.*, **2006**, *128*, 3598.

3.1 Abstract

The adsorption of a 14-amino acid amphiphilic peptide, LK_{14}, composed of leucine (L, nonpolar) and lysine (K, charged), on hydrophobic polystyrene (PS) and hydrophilic silica (SiO_2) was investigated in situ by Quartz Crystal Microbalance (QCM), Atomic Force Microscopy (AFM), and Sum Frequency Generation (SFG) Vibrational Spectroscopy. The LK_{14} peptide, adsorbed from a pH 7.4 phosphate buffered saline (PBS) solution, displayed very different coverage, surface roughness

and friction, topography, and surface-induced orientation when adsorbed onto PS vs. SiO_2 surfaces. Real-time QCM adsorption data revealed that the peptide adsorbed onto hydrophobic PS through a fast (t < 2 min) process, while a much slower (t > 30 min) multi-step adsorption and rearrangement occurred on the hydrophilic SiO_2. AFM measurements showed different surface morphologies and friction coefficients for LK_{14} adsorbed on the two surfaces. Surface-specific SFG spectra indicate very different ordering of the adsorbed peptide on hydrophobic PS as compared to hydrophilic SiO_2. At the LK_{14} solution/PS interface, CH resonances corresponding to the hydrophobic leucine side chains are evident. Only NH modes are observed at the peptide solution/SiO_2 interface, indicating a different average molecular orientation on this hydrophilic surface. The surface-dependant difference in the molecular-scale peptide interaction at the solution/hydrophobic solid vs. solution/hydrophilic solid interfaces (measured by SFG) demonstates significantly different macromolecular-level adsorption properties on the two surfaces (determined by AFM and QCM).

3.2 Introduction

A fundamental understanding of the surface-induced adsorption behavior of biologically relevant peptides and their molecular conformation at polar and nonpolar interfaces is essential for the development of surface-modified biomaterials which are applicable to biofouling, biodiagnostics, proteomics, immunosensors, and tissue engineering.[1] The controlled immobilization of bioactive peptides onto various artificial bioplatforms (for example, via the hydrophobic effect) is the foundation for such technologies.[2; 3; 4] The behavior of synthetic short-chain amphiphilic peptides at solid interfaces is of particular interest, because they possess uniquely variable hydrophobic/hydrophilic domains. By controlling the amino acid sequence and relative content of these domains, one can promote specific interfacial interactions.[5; 6]

Achieving interface-directed orientation and conformational control of such peptides can be useful in the design of specific surface adaptors, in which selective functional sequences are displayed for recognition or reception.[7; 8]

As demonstrated by DeGrado and Lear, the distribution of hydrophobic and hydrophilic amino acid residues of a short peptide (less than 20 amino acids) can be tailored to match the repeat periodicity of a desired secondary structure which can be induced by the anisotropy of an nonpolar interface or by self-aggregation to form peptide micelles.[5; 6; 9] For example, lysine (K, charged) and leucine (L, nonpolar) amino acid residues sequenced with a hydrophobic periodicity of 3.6 and 2 residues/turn tend towards α-helical and β-sheet conformations, respectively, at the air/water interface. This occurs from maximizing the interactions of hydrophobic residues with a nonpolar interface. The residue composition (i.e. leucine/lysine molar ratio), charge periodicity and nominal chain length serve as fundamental variables for directing peptide assembly into a desired amphiphilic secondary structure.[5; 10; 11; 12] Previous studies of short-chain amphiphilic peptides have revealed that structural transitions can occur at an air/water interface (i.e. α-helix to random coil to β-sheet), which are highly time- and concentration-dependant.[13; 14]

The conformational behavior of amphiphilic peptides in solution and at the air/water interface has previously been studied; however, there is little experimental data available on peptide adsorption at solid surfaces.[5; 13; 15; 16; 17; 18] This is attributed to the limited number of surface-specific techniques available for conformational analysis, which explicitly provide the necessary molecular-scale information (i.e. solid-state Nuclear Magnetic Resonance, and surface-enhanced Raman spectroscopy).[19; 20; 21] Even fewer techniques are amenable to interrogating peptide behavior at the solid/liquid interface, a buried interface, which is most applicable to biological systems.[22] Recent studies have demonstrated that imaging microscopy techniques, such as Atomic Force Microscopy (AFM), can be valuable for studying

the relation between molecular conformations of polypeptides and the morphology of adsorbed films on hydrophilic and hydrophobic surfaces.[23] However, it is difficult to quantify the amount of polypeptide adsorbed at an interface via imaging methods. The Quartz Crystal Microbalance-Dissipation (QCM-D) instrument is a highly sensitive surface mass detector (i.e. nanogram range) which is also capable of viscoelastic characterization (via energy dissipation measurements) of bound masses. While this analytic mass and viscoelasticity sensor is amenable to studies at the biological solution/solid interface, it lacks molecular specificity as does AFM. Sum Frequency Generation (SFG) is a vibrational spectroscopy is a powerful technique for extracting molecular-level information of biomolecules at interfaces, including protein and peptide adsorption at the solid/air interface,[24; 25] air/water interface,[26] and more recently at the biologically relevant solid/liquid interface.[27; 28; 29; 30] The nonlinear SFG process is an intrinsically surface specific–under the dipole approximation, SFG is forbidden in media that possess inversion symmetry.[31] Inversion symmetry is necessarily broken at surfaces and interfaces, but rarely broken in bulk media. Although SFG spectroscopy has been successful in determining relative spatial ordering of proteins at bio-interfaces, identifying specific amino acid interactions with the surface has proven to be difficult due to the large number of surface-interacting residues.[28; 29; 32] Many questions remain regarding the driving forces and mechanism of adsorption of specific peptides sequences, which are suitable for investigation with surface-specific techniques.

In the present work we investigate the adsorption behavior of a model amphiphilic peptide, with sequence Ac(LKKLLKLLKKLLKL)NH_2 (LK_{14}), on hydrophobic polystyrene (PS) and hydrophilic silica (SiO_2) surfaces using three, in situ, surface-sensitive techniques. The peptide sequence was synthesized with a hydrophobic residue periodicity to induce an α-helical conformation at a nonpolar surface or interface. The formation of an α-helix in solution (confirmed using CD spec-

troscopy) by this amphiphilic peptide separates the leucine (hydrophobic) and lysine (hydrophilic) side-chains, as illustrated in Figure 3.1, allowing for investigation of the hydrophobic vs. electrostatic bonding interactions upon adsorption.[5]

Adsorption measurements using the quartz crystal microbalance-dissipation (QCM-D) technique provided information regarding the peptide adsorption affinity for the hydrophobic vs. hydrophilic surface, and offer a direct comparison of the time-scale for adsorption of the peptide layer. The frequency and energy dissipation changes are related to the wet adsorbed mass and the elastic/viscoelastic nature of the adsorbed film, respectively. Atomic force microscopy (AFM) was used to image the time-dependant morphology of the adsorbed peptide film, as well as to compare the friction behavior of the adsorbed peptide on the two surfaces. SFG vibrational spectroscopy was used to obtain surface-specific and molecular-level information about the relative ordering of surface-active amino acid residues at the solid/liquid (hydrophobic and hydrophilic) interface. By characterizing the adsorbed morphology, friction, mass, dissipative energy, and average molecular orientation of the peptide on the two surfaces, we determined that the surface hydrophobicity dictates the surface interactions and adsorbed properties of the amphiphilic LK_{14}.

3.3 Experimental

3.3.1 LK_{14} Peptide Synthesis

LK_{14} peptide with sequence Ac(LKKLLKLLKKLLKL)NH_2 was synthesized using an Advanced ChemTech (ACT) 396 automated synthesizer using standard 9-fluorenylmethyloxycarbonyl (FMOC) protocols, as described in Appendix A.[33] Rink amide 4-methylbenzhydrylamine resin (Novabiochem) was prepared by swelling in 1-Methyl-2-pyrrolidinone, then mixing with a FMOC protected amino acid (Advanced

ChemTech). The carboxylic acid group of the protected amino acid was activated prior to coupling to the resin by mixing with 1-Hydroxybenzotriazole. The mixture was agitated (12 h) to ensure complete coupling of the first amino acid. The starter resin was then placed in the ACT instrument for completion of the synthesis. Acetylation of the N-terminus was accomplished by adding acetic anhydride to the resin-bound peptide. The peptide was cleaved from the resin in a solution of 95% trifluoroacetic acid and 5% water, precipitated from solution, lyophilized to dryness. The peptide was purified using reversed-phase high pressure liquid chromatography. The composition of the peptide was characterized and electrospray ionization mass spectrometry (ESI-MS). ESI-MS showed M^{+2} and M^{+3} peaks corresponding to a mass of 1692.3 amu for the non-acetylated peptide. Lyophilized peptide samples were stored in a freezer (-15 °C), and a stock solution of 1 mM peptide in pH 7.4 phosphate buffered saline (PBS; 0.01 M phosphate buffered saline, 0.14 M NaCl, 0.0027 M KCl) solution was used for QCM, AFM and SFG analysis. Ultrapure water (Millipore, Milli-Q 18 MΩ·cm) was used to prepare all solutions. For comparison across all techniques, all experiments were performed at low peptide concentration (0.1 mg/mL) unless otherwise stated.

3.3.2 Circular Dichroism Spectroscopic Measurements

Peptides with this sequence (LK_{14}) have been shown to form tetrameric α-helical aggregates under the above solution conditions with hydrophobic leucine residues segregated to the core.[5] Circular Dichroism spectroscopy was used to confirm the solution structure of this peptide. CD spectroscopy is a non-destructive technique for secondary structure determination of biomolecules in solution. CD measures the difference in absorption of right- and left-handed circularly polarized light. CD spectra are obtained between 190 nm and 250 nm where peptide backbone amide transitions

occur. CD spectra were obtained using a AVIV 62XX instrument using x mM solution in a 1-cm strain-free (Aviv) cuvette. The CD spectrum of LK_{14} is shown in Figure 3.1.

3.3.3 QCM Measurements

A QCM-D instrument (Q-Sense D300, Gothenburg, Sweden) was used to measure the wet mass of adsorbed peptides on silica and polystyrene surfaces, as described in Chapter 2 of this thesis. Briefly, the "wet" mass added (Δm) induces a linear resonant frequency shift (Δf) according to Eq 3.1 if the following conditions are met: the adsorbed mass in a liquid environment is evenly distributed and produces a sufficiently rigid and thin film (i.e. elastic masses are adsorbed). In Eq 1, n denotes the overtone number and C is the mass sensitivity constant for $\Delta f = 1$ Hz (17.7 ng·cm^{-2} using a 5 MHz crystal).

$$\Delta m = \frac{-C\Delta f}{n} \tag{3.1}$$

SiO_2-coated sensor crystals (Q-Sense QSX 303, AT-cut, 5 MHz, active surface area = 0.2 cm^2) were cleaned in NOCHROMIX solution (24 h) and oxygen plasma treated (2 min) prior to use. A 100 nm layer of polystyrene was spin-coated on the cleaned crystals to prepare the hydrophobic surface. The shift in resonance frequency (Δf) and dissipation (ΔD) was measured simultaneously at the fundamental (n = 1) and overtone (n = 3, 5, 7) frequencies. All solutions were thermally equilibrated in the T-loop of the QCM (0.5 mL at 25 °C), and the sensor crystal was thermally equilibrated in PBS solution prior to injection of the peptide solution. The period required to achieve a stable signal ($\Delta f \leq 3$ Hz) in the resonant frequency was 5 and 25 min for the SiO_2 and the PS surfaces, respectively. The entire system was thoroughly cleaned with sodium dodecyl sulfate detergent (1 h), and flushed with water and

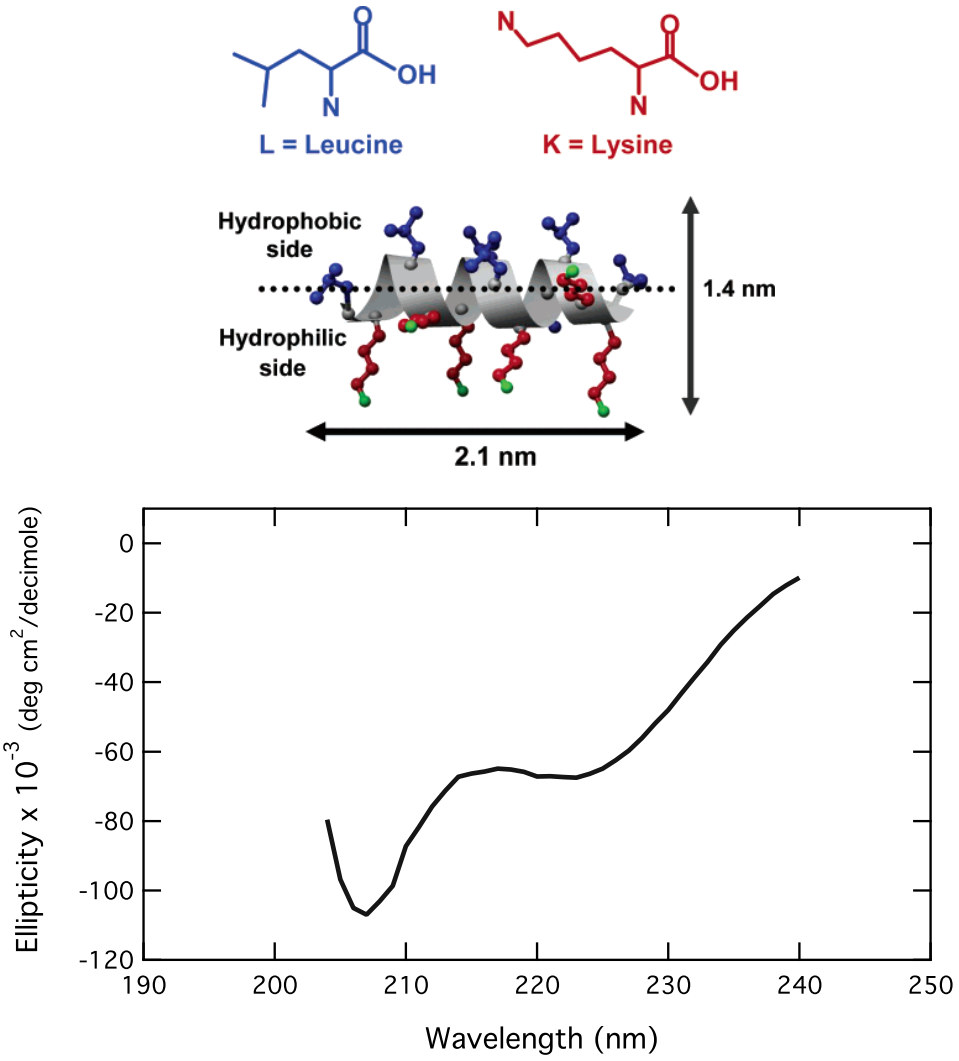

Figure 3.1. Ideal dimensions of the α-helical LK_{14} peptide in solution. Width across the helical barrel and total width including the side chains were calculated using ideal helical bond angles and van der Waals radii. The peptide forms α-helical tetramers under the solution conditions employed in the experiment. The CD spectrum of LK_{14} confirms the helical structure in solution.

ethanol (10 cycles) between sample measurements. Duplicate measurements were obtained for both the hydrophilic and hydrophobic surfaces.

3.3.4 AFM Measurements

AFM scanning probe images were obtained using a Molecular Imaging instrument with a 30-μm scan head (Pico SPM) to collect topographic and friction images of a $\sim$ 500 square micron area, as described in Chapter 2. Images of the bare SiO_2 and PS surfaces were acquired in pH 7.4 PBS. Friction data was obtained at the peptide/buffer solution interface by laterally scanning a 200 nm $\times$ 200 nm area at 2 Hz (overtop the adsorbed peptide) at various normal force loads (0-17 nN). The force-distance response curve on a silica substrate was calibrated using the spring constant of the tip to determine the applied normal loads. Friction experiments were obtained using a peptide concentration of 1 mg/mL to ensure sufficient coverage of the surface and minimize convolution of substrate effects.

3.3.5 SFG Spectroscopic Measurements

SFG spectra were obtained with a mode-locked Nd:YAG laser (Ekspla, Lithuania), using the set-up described in Chapter 2 and shown schematically in Figure 2.5 and Figure 3.2. The tunable infrared beam is combined with the 532 nm radiation at the sample interface at incident angles of 62° and 58°, respectively, with respect to the surface normal. For each scan, data is collected with 10 shots/data point in 5 cm^{-1} increments in the 2800-3600 cm^{-1} range. For a given condition, SFG measurements were repeated at least six times to increase the signal-to-noise ratio and the collected data were averaged to produce the final spectra presented in this paper. All spectra shown here were collected with the *ssp* (sum, visible, infrared, respectively) polarization combination.

The intensity of the SFG signal is fit to the equation:

$$\mathbf{I_{SFG}} \propto |\boldsymbol{\chi}^{\mathbf{(2)}}_{\mathbf{NR}} \mathbf{e}^{i\phi_{\mathbf{NR}}} + \sum_{\mathbf{q}} \frac{\mathbf{a_q}}{\omega_{\mathbf{IR}} - \omega_{\mathbf{q}} + i\boldsymbol{\Gamma}_{\mathbf{q}}} \mathbf{e}^{i\gamma_{\mathbf{q}}}|^{\mathbf{2}} \tag{3.2}$$

where $\mathbf{a}_q$ is the amplitude of the qth resonance, Γ_q is the line width (or damping factor) of the qth resonance, ω_{IR} is the IR frequency, ω_q is the frequency of the qth molecular vibration, $e^{i\gamma_q}$ is the phase of the mode, and $e^{i\phi_{NR}}$ is the phase of the non-resonant background. When ω_{IR} is scanned across the IR and comes into resonance with ω_q, the resonant term and SFG signal intensity is enhanced. The amplitude of the qth resonance term, $\mathbf{a}_q$, is described as:

$$\mathbf{a}_{\mathrm{q}} \propto \frac{\partial \vec{\boldsymbol{\mu}}}{\partial Q_q} \otimes \frac{\partial \boldsymbol{\alpha}^{(1)}_q}{\partial Q_q} \tag{3.3}$$

where $\partial\vec{\boldsymbol{\mu}}/\partial Q_q$ and $\partial\boldsymbol{\alpha}^{(1)}_q/\partial Q_q$ are the infrared dipole and Raman polarizability derivatives with respect to Q_q, the classical normal coordinate of the qth vibrational mode.[44; 47] This equation demonstrates that a vibrational resonance is SFG active when it is both IR and Raman active.[48; 49]

3.3.6 Sample Preparation

Fused silica windows (Esco Products) were cleaned by soaking in a saturated NOCHROMIX (Godax Laboratories) oxidizing solution and rinsing with deionized water. Polystyrene thin films (200 nm) were prepared by spin-casting (Specialty Coating Systems, P-6000 Spin Coater) a 3 wt% solution of deuterated polystyrene (PS-d_8, MW $\sim$ 300 000, Polymer Source, Inc.) in toluene onto the fused silica windows and annealing at 110 °C (12 h). Background QCM, AFM and SFG measurements were obtained on clean PS and SiO_2 surfaces in PBS solution prior to addition of the peptide solution. Contact with air was minimized by introducing the peptide solution

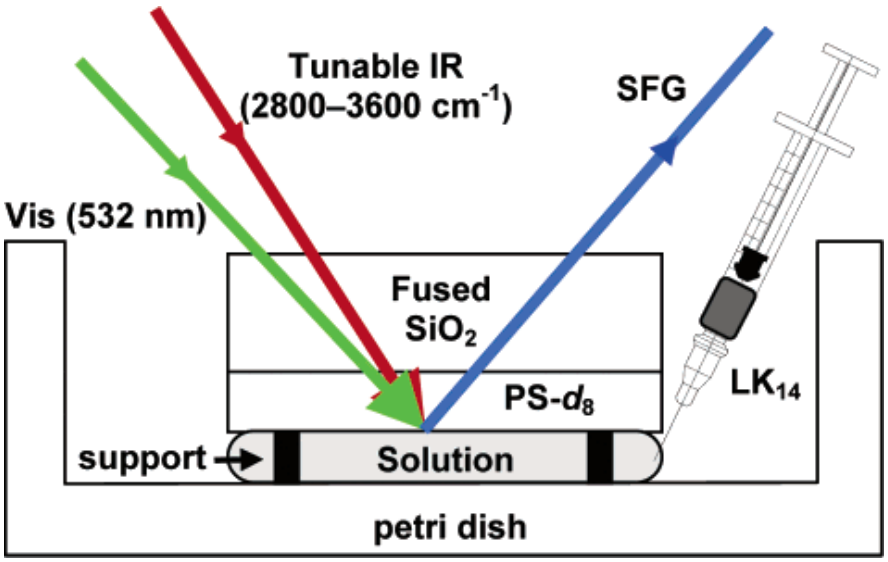

Figure 3.2. Schematic of the SFG experimental set-up. The hydrophobic PS-d_8/aqueous PBS interface is created by spin-coating PS-d_8 (300 nm) onto SiO_2 windows and exposing it first to PBS solution, followed by injection of the LK_{14} solution. The hydrophilic SiO_2/aqueous interface is similarly prepared by direct exposure to the solution (no PS-d_8 spin coated).

directly to the buffer/solid interface (Figure 3.2). For example, the solid substrate placed on top of a reservoir of peptide solution exposed to the air/water interface produced different SFG spectra (similar to dried peptide film spectra) possibly indicating the formation of a Langmuir-Blodgett peptide film at the air/water interface.

3.4 Results

3.4.1 QCM Measurements of LK_{14} Adsorption on PS versus SiO_2

Using a QCM-D we monitored the adsorption process of the LK_{14} peptide (0.1 mg/mL) in situ on both hydrophobic and hydrophilic surfaces. Figures 3.3a and 3.3b show the change in frequency and dissipation (at $n = 3$ overtone) as the peptide is

adsorbed onto the PS and SiO_2 surface, respectively. The arrows mark the starting point of the measurement when the peptide solution is exposed to the surface (t = 0 = $\Delta f = \Delta D$). The vertical dashed lines indicate the end of the experiment when the surface is flushed with buffer solution. The spikes in frequency and dissipation upon peptide injection and rinsing with buffer are due to transient variations in pressure and temperature as new solutions are introduced.

On PS, the adsorption appears characteristic of a single-step, first-order process.[52] The adsorption occurs in ∼2 min with a shift in frequency and dissipation of Δf = -7.4 Hz and $\Delta D = 0.26 \times 10^{-6}$, respectively. Upon washing the LK_{14}/PS surface with buffer at t = 20 min, only minor desorption ($\Delta f < 0.5$ Hz) was observed.

Multi-step (nonmonotonic) adsorption behavior is observed in both Δf and ΔD for LK_{14} on SiO_2. The total frequency shift of -15.4 Hz is accompanied by an increase in the total dissipation, Δf = 1.5-2.0($\times$ 10^{-6}). Unlike the hydrophobic surface, washing LK_{14}/SiO_2 with PBS causes a positive frequency shift of 1.6 Hz (t = 70 min). A large drop in frequency (Δf_1 = -9 Hz) is initially observed up to t = 5 min, subsequently followed by smaller, nonequivalent steps ($\Delta f_{2,3,4} \approx$ -1 Hz) up to t = 35 min.

3.4.2 AFM Measurements of LK_{14} Adsorption on PS versus SiO_2

AFM images of the adsorbed peptide on the hydrophobic and hydrophilic surfaces were obtained in situ at two concentrations (1 mg/mL and 0.1 mg/mL). The adsorbed morphology of LK_{14} on the polystyrene surface at low concentration of peptide is shown in Figure 3.4.

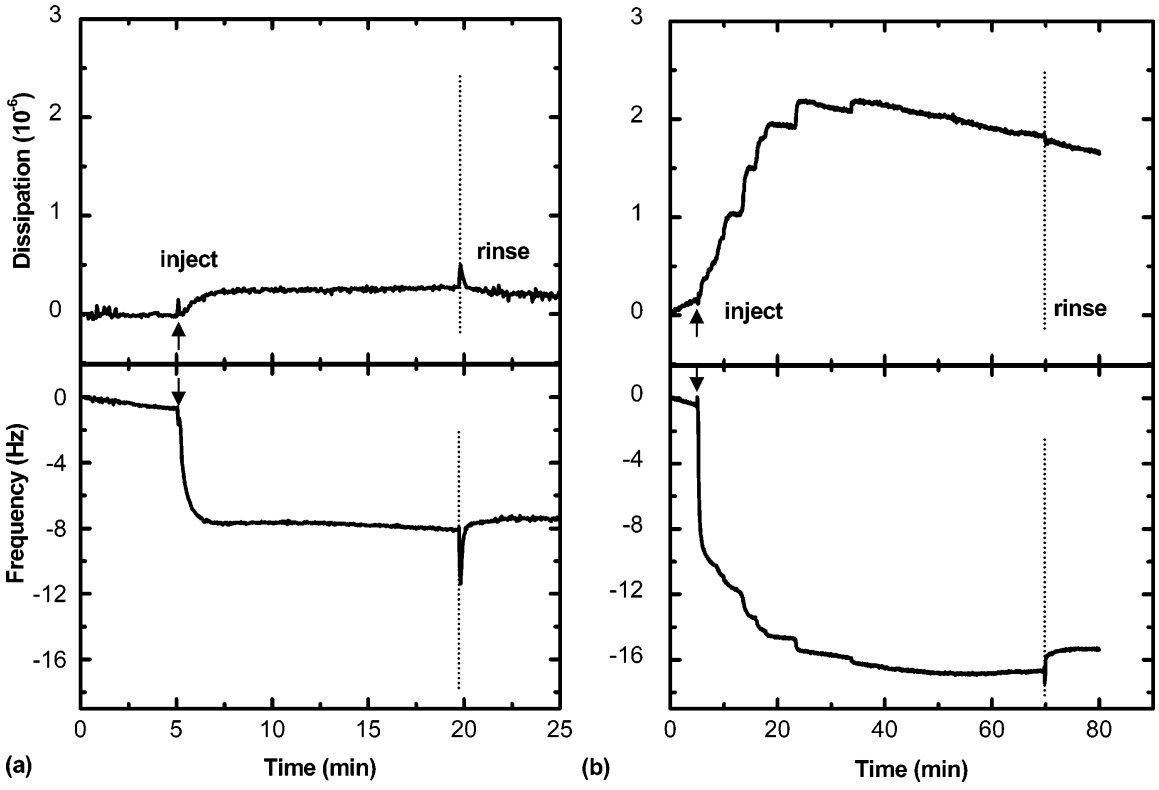

Figure 3.3. QCM data showing real-time changes in energy dissipation (top) and frequency (bottom) resulting from LK_{14} adsorption onto: (a) PS and (b) SiO_2. On PS, a typical single-step exponential adsorption is observed in <2 min, while on SiO_2 a multi-step process occurs over 35 min.

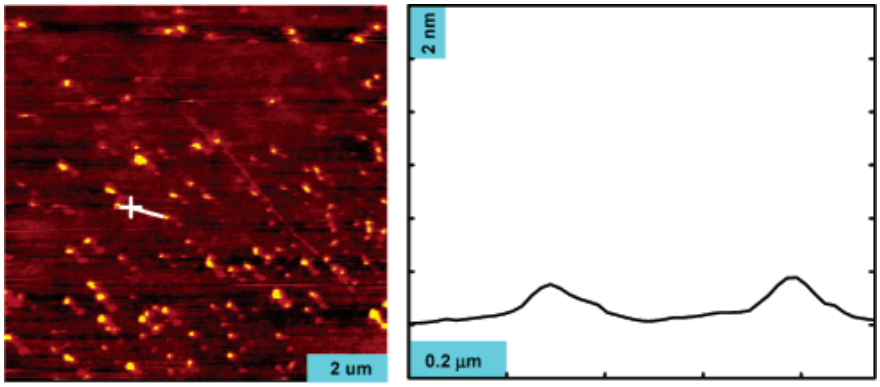

Figure 3.4. AFM image and topograph of 0.1 mg/mL LK_{14} adsorbed onto PS showing 1.5 nm heights imaged after 5 min. Similar topographic heights are observed at longer time-scales.

AFM analysis of LK_{14} adsorbed on polystyrene at higher concentrations is not presented due to the absence of observable features, presumably from increased coverage resulting in a smooth monolayer. Adsorption at low concentration resulted in an increase in rms roughness from 0.4 ± 0.1 nm (featureless bare PS) to 0.8 ± 0.2 nm (LK_{14}/PS, round features ∼200 nm wide). The AFM cross section profile shows topographical features as small as 1.5 nm in height.

Figure 3.5a shows the morphology of low concentration LK_{14} adsorbed onto SiO_2 at t< 5 min. In comparison to the bare silica surface (rms surface roughness of 0.2 ± 0.1 nm), adsorption of the peptide induced a 4-fold increase in the roughness to 0.7 ± 0.1 nm within minutes of exposure to SiO_2. Initially, the peptide forms monodisperse spherical aggregates, with lateral dimensions between 150 and 300 nm and feature heights of distinctly 2.5 or 5.0 nm. Between 5-10 min of adsorption, we observed significant lateral aggregation and an increase in the density of surface features, as evident by the 7-fold rise in roughness to 1.2 ± 0.3 nm (Figure 3.5b). At t = 5-10 min the surface-bound LK_{14} displays larger lateral size distribution with features ranging from 0.200-1.0 μm in width. However, this lateral growth is not accompanied by a change in feature height as shown in Figure 3.5b (i.e. topographic heights of 2.5

nm and predominantly 5.0 nm remain constant). An image obtained after 30 min of adsorption yields a surface roughness of 1.3 ± 0.1 nm (Figure 3.5c). Topographical analysis indicates a gradual morphological transition on SiO_2 from small, spherical islands (∼200 nm wide) to much larger, laterally aggregated domains (up to 1.5 μm) over a 30 min period.

Adsorption from a 10-fold higher concentration of peptide (1 mg/mL) produces a very different topography on SiO_2, as shown in Figure 3.5d. In this case, we immediately observe a large quantity of densely packed LK_{14} with feature heights of >10 nm. The massive deposition of peptide is accompanied by a 12-fold increase in the roughness (from 0.18 ± 0.1 nm to 2.3 ± 0.2 nm). At high concentrations, no time-dependant perturbation of the height or feature width is seen via AFM. Using AFM lateral force detection, we also obtained the friction force exhibited by the adsorbed LK_{14} (1 mg/mL) on both the hydrophobic and hydrophilic surface (Figure 3.6). The maximum normal load capacity on the LK_{14}/PS and LK_{14}/SiO_2 systems was 2 nN and 17 nN, respectively. In the case of LK_{14} adsorbed onto SiO_2, the surface friction doubled in comparison to the bare surface as indicated by the slopes of the lateral force plots. The LK_{14} adsorption onto PS did not produce a significant change in the friction force and slightly decreased by a factor of 1:0.8 (bare PS: LK_{14} on PS).

3.4.3 SFG Spectroscopic Measurements of LK_{14} Adsorption on PS-d_8 versus SiO_2

We conducted SFG experiments on deuterated polystyrene (PS-d_8) and SiO_2 before and after adsorption of a 0.1 mg/mL LK_{14} peptide solution to examine the effect of the interface hydrophobicity on adsorption. These substrates are suitable for the SFG study because neither generate SFG features in the spectral region under study (2800-3600 cm^{-1}). The SFG spectra of amphiphilic LK_{14} adsorbed on a hydropho-

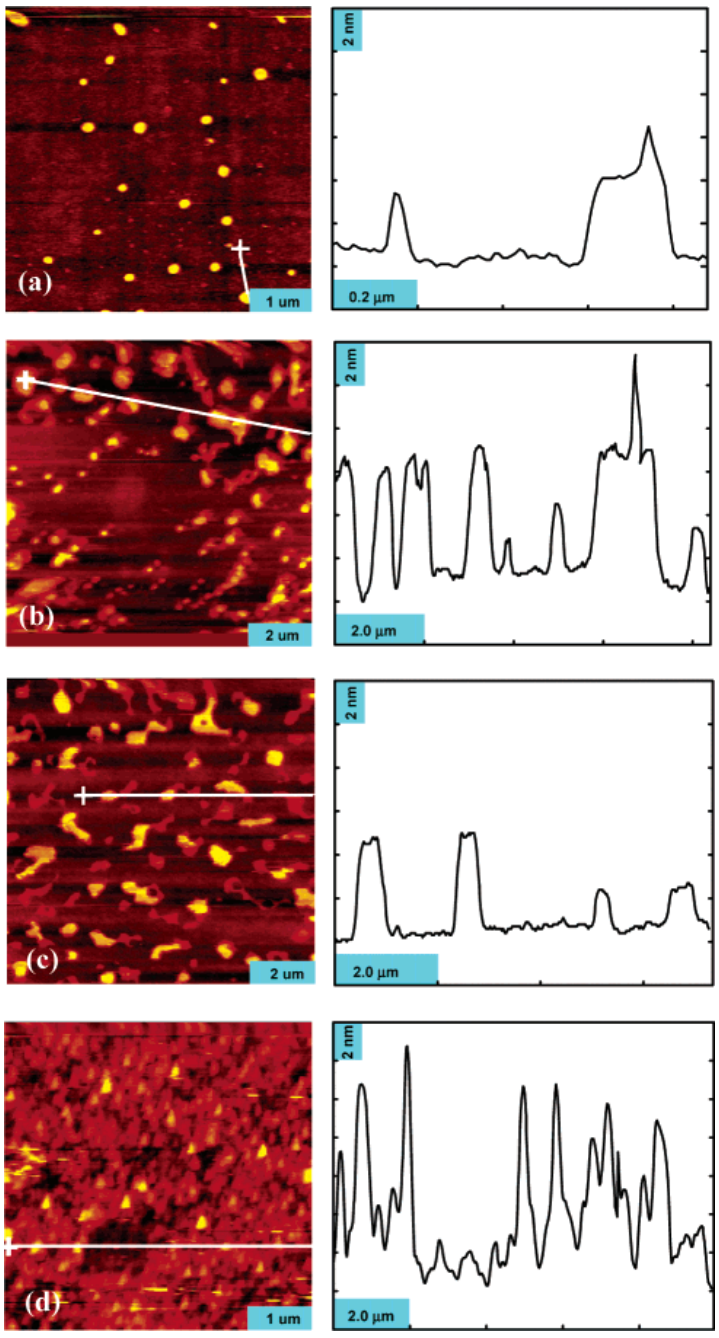

Figure 3.5. AFM images and topographs of 0.1 mg/mL LK_{14} adsorbed onto SiO_2 (showing distinctly 2.5 nm and 5.0 nm heights) imaged at: (a) <5 min, (b) 5-10 min, (c) >30 min. Image of LK_{14} adsorbed at a higher solution concentration (1 mg/mL) is displayed in (d). The depressed region on the film (dark square) is the result of scanning at a normal force >17 nN, and inducing damage to the film.

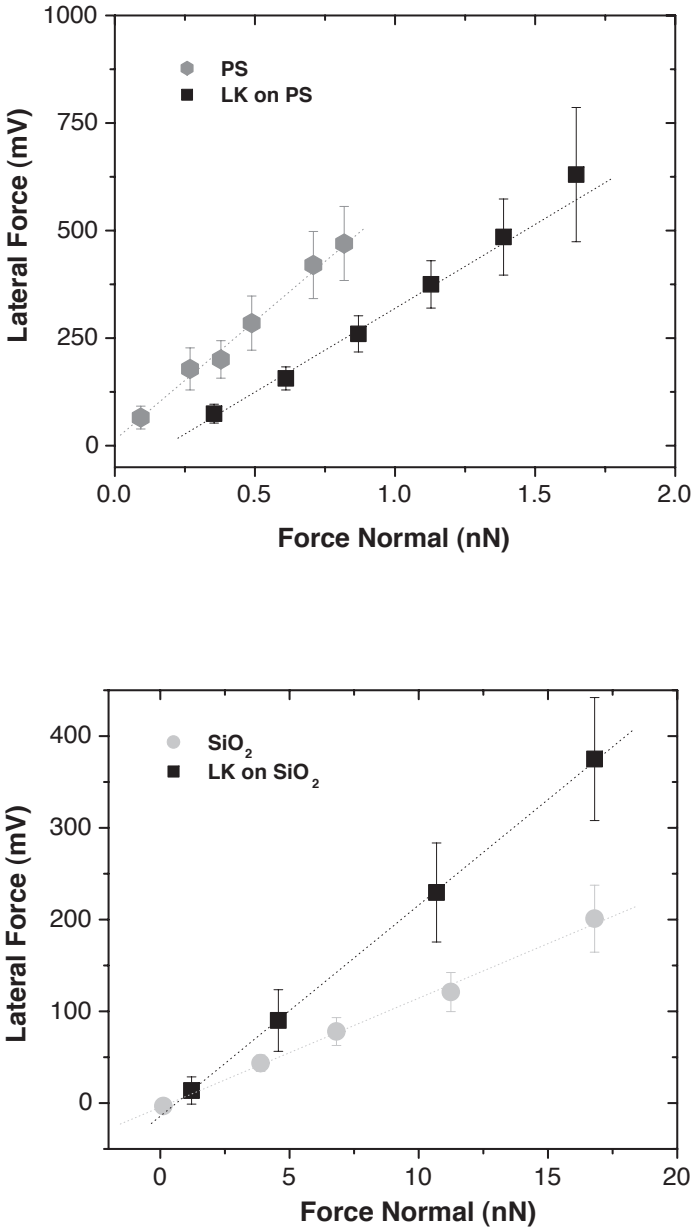

Figure 3.6. AFM relative friction behavior (obtained by the slope of $F_L : F_N$) of LK_{14} (1 mg/mL) adsorbed onto (a) PS, and (b) SiO_2. A small decrease in friction occurs upon LK_{14} adsorption onto PS as indicated by the ratio of the slopes of the bare surface to LK_{14}/PS (1: 0.8). Friction is doubled after LK_{14} adsorption on SiO_2.

bic (Figure 3.7) and hydrophilic (Figure 3.8) surface indicate that the nature of the adsorption is strongly dependent on the surface hydrophobicity.

The solid lines in Figures 3.7 and 3.8 are the least square fits of the raw SFG data to Eq 3.2. Background SFG spectra of PBS on the bare surfaces are plotted in black in Figures 3.7 and 3.8. On the hydrophobic PS-d_8 we observe OH stretching modes (3092 cm^{-1}) (before and after peptide adsorption) which are assigned to structured water molecules. Upon peptide adsorption, CH stretching modes appear and are assigned to CH_3 symmetric (2869 cm^{-1}), Fermi resonance of methyl symmetric stretch (2935 cm^{-1}). The mode at 2895 cm^{-1} is assigned to either CH or a methylene Fermi resonance, in agreement with previous studies of the leucine amino acid.[53; 54]

On the hydrophilic SiO_2/water interface, we observe peaks from OH modes at $\sim$3200 cm^{-1} and $\sim$3400 cm^{-1} from the hydrogen bonded water. Upon injecting LK_{14} into the PBS solution, the OH modes decrease in intensity and a NH stretching mode appears (Figure 3.8). As later discussed, the assignment of the NH mode is not trivial since the LK_{14} peptide contains NH^{+3} moieties on the lysine side chains and the N-terminus of the peptide backbone, as well as NH moieties in the peptide backbone (designated Amide A). The amplitude of the small peak observed around 2870 cm^{-1} is on the order of the noise and is therefore not fit. The differences in the peak intensities of the CH and NH modes are due to differences in the various contributions to the SFG signal (i.e. Raman polarizability, IR dipole transition amplitude, number of oscillators/surface concentration, and average molecular orientation).

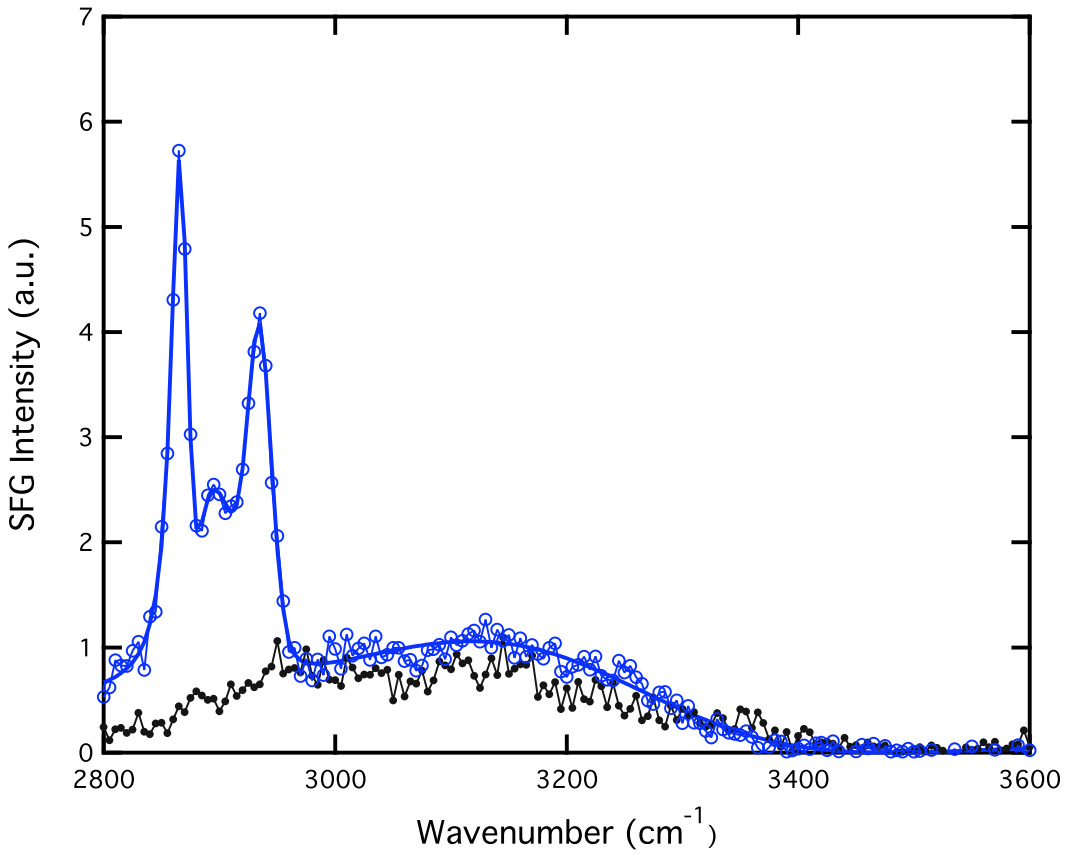

Figure 3.7. SFG spectrum of PBS solution (black) and LK_{14} (blue) adsorbed onto PS-d_8. The broad peak centered at 3092 cm^{-1} is assigned to structured water molecules. Peaks at 2869 cm^{-1} (CH_3 symmetric), 2895 cm^{-1} (CH or CH_2 Fermi resonance), and 2935 cm^{-1} (CH_3 Fermi resonance) are observed.

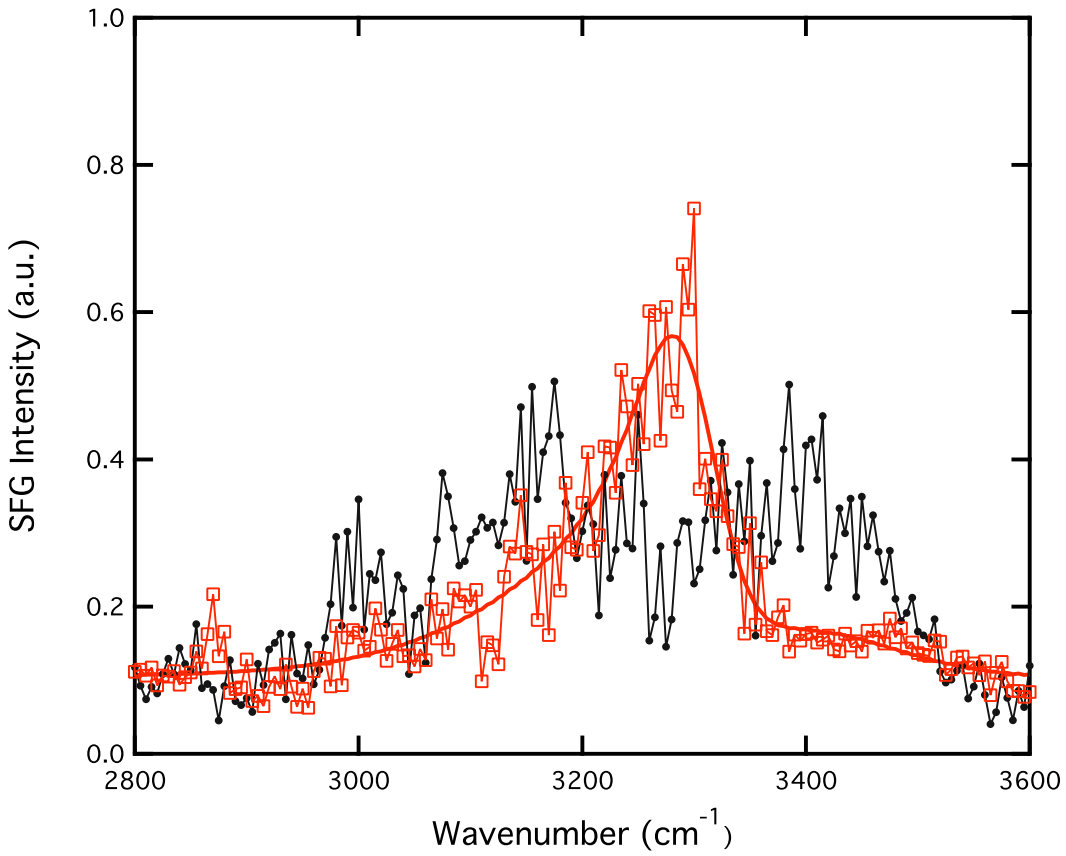

Figure 3.8. SFG spectrum of PBS solution (black) and LK_{14} (red) adsorbed onto SiO_2. The dominant peak at 3294 cm^{-1} is assigned to an NH stretching mode, and a weak OH peak is observed at $\sim$3190 cm^{-1}.

3.5 Discussion

3.5.1 Quartz Crystal Microbalance Studies of LK_{14} Adsorption on Hydrophobic and Hydrophilic Surfaces

On PS, the net Δf = -7.4 Hz corresponds to LK_{14} adsorption with a hydrated mass of 130 ng·cm^{-2}. The monolayer of peptide is stable, with negligible desorption upon washing the LK_{14}/PS surface with buffer ($\Delta f_{wash} \approx 0$). The adsorption occurs in a single step process and reaches steady-state within ~2 min. The accompanying low energy dissipation shift ($\Delta D = 0.26 \times 10^{-6}$) suggests the formation of a rigidly adsorbed film on PS, which justifies the Sauerbrey-derived quantification of the adsorbed mass.

The adsorption of LK_{14} onto SiO_2 produces a multi-step pattern (in both Δf and ΔD), suggesting a step-wise growth of the peptide layer on the hydrophilic surface. Similar multi-step adsorption behavior has previously been observed in QCM studies of charged biomolecules in multi-layer assemblies.[55] The response in Δf and ΔD reflects the average adsorption across the active surface area of the crystal, and does not necessarily imply saturated coverage of the surface. Thus, the stepwise adsorption observed can correspond to either formation of unique layers of LK_{14} and/or increasing fractional coverage of the surface. The 3-D conformation and footprint of the adsorbed LK_{14} must be known to differentiate between these two possibilities.[52] However, the AFM data, discussed below, show a time-dependant adsorption of laterally irregular islands with constant heights of 2.5 and 5 nm, suggesting the formation of some layers, which may cause the step-like changes in frequency observed by QCM. The time-dependent results suggest that the beginning step involves the rapid adsorption to form several nucleation sites on the surface (i.e. several LK_{14} molecules adsorbed overtop one another). Slower adsorption processes

subsequently follow, including island growth and spreading over the SiO_2, leading to larger laterally-coalesced domains.

The nonequivalence of the adsorption steps is also evidence for a multi-step process which involves different types of surface interactions occurring on SiO_2 (i.e. peptide/surface and peptide/peptide interactions). Figure 3.3 shows that the frequency change associated with the initial adsorption step (Δf_1 = -9 Hz) is dissimilar to subsequent adsorption processes ($\Delta f_{2,3,4} \approx$ -1 Hz) with respect to the adsorbed amount and time of each step. This suggests that several adsorption mechanisms contribute. The later stages of adsorption (t = 10-40 min) involve much weaker interactions (i.e. peptide/peptide) than the initial LK_{14}/SiO_2 surface interaction. Approximately 10% of the adsorbed mass can be removed by washing (Δf_{wash} = 1.6 Hz). This indicates the presence of weaker interactions within the uppermost peptide layers.

A significant change in dissipation also occurs following peptide adsorption onto SiO_2, ΔD = 1.5-2.0($\times 10^{-6}$), in contrast to the small dissipation response ($\Delta D = 0.26 \times 10^{-6}$) accompanying adsorption onto PS. The difference in dissipation behavior further supports that the peptide adsorbs very differently on the two surfaces. Although the total decrease in frequency on SiO_2 (Δf_1 = -15.4 Hz) is approximately twice greater than that on PS (Δf_1 = -7.4 Hz), the large net change in dissipation on the hydrophilic SiO_2 implies significant viscoelastic behavior of non rigid LK_{14} adlayers. Thus, the Sauerbrey relation is not valid on the hydrophilic surface, and quantitative analysis of the steps (i.e. conversion of the shift in to a hydrated peptide mass) is difficult.[39] At the onset of each adsorption step, a gradual decrease in ΔD is followed, implying that adsorbed LK_{14} molecules on SiO_2 are more dynamic than on PS. Initially, adsorbed LK_{14} on SiO_2 is highly mobile (exhibiting high viscous losses) and undergoing observable rearrangements on the surface. As adsorption continues, a reduced ΔD indicates a decrease in the mobility of peptide molecules over time.

The effect of the surface hydrophobicity is also expressed in the different adsorption time-scales observed. For instance, LK_{14} exhibits rapid initial adsorption on both surfaces (on the order of seconds) as indicated by the initial large decrease in the frequency in both cases (Δf_1 = -9 Hz for SiO_2 and Δf = -7.4 Hz for PS). The adsorption reaches equilibrium in ∼2 min on hydrophobic PS surface, while on hydrophilic SiO_2 the multi-step mechanism requires ∼35 min.

3.5.2 AFM Studies of LK_{14} Adsorption on Hydrophobic and Hydrophilic Surfaces

Topographical analysis of LK_{14} (0.1 mg/mL) adsorbed onto the hydrophobic surface shows feature heights of 1.5 nm. Under similar solution conditions, circular dichroism studies indicate that the LK_{14} is α-helical.[5] The secondary structure of the adsorbed peptide can not be definitively identified here, this height is similar to the calculated (defect-free) van der Waals diameter of the LK_{14} α-helix in solution ∼1.4 nm = width of helical barrel plus the K and L side-chains as shown in Figure 3.1). The tetrameric aggregation state is a consequence of the hydrophobic leucine residues segregating to create a hydrophobic core, with the free energy of dehydration being the driving force. Despite using a peptide and buffer salt concentration which stabilizes tetramer formation of LK_{14} in solution, the measured feature heights of 1.5 nm suggest that some peptides undergo an adsorption-induced reduction in aggregation state. When the amphiphilic peptide is adsorbed on a hydrophobic surface, the unfolding of the tetrameric aggregates is likely stabilized by the strong hydrophobic interactions with PS. A hydrophobic driven adsorption would reduce the interfacial energy by exposing the hydrophobic residues of the interior tetramer to the hydrophobic surface. Similar observations have been reported in fluorescence and circular dichroism studies by Kiyota et. al which examined aggregated small-chain LK pep-

tides interacting with a lipid bilayer, an analogous liquid/solid interface.[56] Here, the small-chain amphiphilic peptide undergoes gradual transition from a self-aggregated state in buffer solution to a single α-helix upon interaction with lipid bilayers.[56] This reduction in aggregation is primarily attributed to the hydrophobic-mediated interactions of hydrophobic residues with the interior of the lipid bilayer, with the absence of electrostatic interactions. No dynamic effects were detected on the time-scale of the AFM measurements (5 min to 2 h) for LK_{14} adsorbed on PS, in agreement with the rapid adsorption ($t \sim 2$ min) observed by QCM on PS.

AFM measurements of adsorption onto a hydrophilic surface show dynamics in both the adsorbed amount and the lateral growth of the peptide. Over the 30 min adsorption process, a significant increase in the density of adsorbed peptide occurred via the transition of small spherical agglomerates (150-300 nm in width) to large laterally disperse islands (up to 1.5 μm in width). A time-dependent increase in the rms surface roughness from 0.2 ± 0.1 nm (bare silica) to 0.7 ± 0.1 nm (LK_{14} on SiO_2 at $t < 5$ min) and finally to 1.3 ± 0.1 nm (LK_{14} on SiO_2 at $t > 30$ min) confirms that gradual adsorption, over $t > 30$ min, occurs on hydrophilic surface, which is much different than the $t < 2$ min time-scale on the hydrophobic PS (rms roughness $= 0.8 \pm 0.2$ nm). The multi-step behavior observed by QCM, the increase in adsorbed amount measured by AFM is likely due to gradual mass deposition via aggregation processes at the surface. While the lateral size distribution changes significantly throughout the LK_{14} deposition, the topographical heights remain constant (2.5 nm and 5.0 nm) over time. The initial step likely involves the formation of discrete stacked LK_{14} molecules (i.e. nucleation sites), which may be similar in orientation and height. At higher concentrations, many layers of stacked LK_{14} molecules are formed on top of the SiO_2 as suggested by AFM measured heights of >10 nm. In this case, the lateral dimensions and geometry of the features observed in the uppermost layers of peptide appear to be homogeneous (around 150-200 nm) and similar to that of the exposed lower layers,

as seen in Figure 3.5d. This suggests that at higher concentrations of LK_{14}, the adsorption is influenced by peptide self-association in solution prior to interaction with the SiO_2 surface. This mechanism is consistent with previous research which has shown that higher concentrations of LK_{14} peptide promotes self-aggregation.[5]

The difference in the friction behavior obtained on the two LK_{14}-coated surfaces is due to the different surface interactions occurring upon adsorption onto PS vs. that on SiO_2. As suggested by the AFM topographic data, different driving forces are likely responsible for adsorption of LK_{14} on hydrophobic vs. hydrophilic surfaces. A rough surface containing features of 5 nm (i.e. produced by LK_{14} on SiO_2) should exhibit a larger lateral force on a dragging tip due to contact with a large number of surface molecules, compared to a smooth film containing a lower density of adsorbed LK_{14} and features heights of 1.5 nm on PS. Normal forces up to 17 nN could be exerted onto to the thick multilayers of the LK_{14}/SiO_2 system before inducing permanent deformation to the surface (shown in Figure 3.5d), while the damage threshold on LK_{14}/PS layer was significantly less at 2 nN.

3.5.3 SFG Spectroscopic Studies of LK_{14} Adsorption on Hydrophobic and Hydrophilic Surfaces

The presence of ordered methyl groups of the adsorbed leucine side-chains on the PS-d_8 vs. ordered NH on SiO_2 indicate very different adsorption behavior on the two surfaces. The SFG data suggests that the preferential average orientation of the LK_{14} peptide on the surface is dictated by the nature of the interactions occurring at the solid/liquid interface. While these SFG studies in the CH region can not confirm the precise structure on the surface (requiring SFG experiments in the spectral region between 1200-1800 cm^{-1}),[27; 57] AFM and QCM data suggest the formation of a rigid 1.5 nm thick monolayer on PS-d_8. The hydrophobic interaction of the

leucine side-chains with the PS-d_8 surface is likely driven by the dissociation of the solution-phase tetramers. This surface-mediated dehydration of the side-chains would minimize the surface energy. Surface interaction of the peptide through the leucine residues on the hydrophobic surface allows interaction of the charged lysine residues with the aqueous bulk.

On silica, the observation of NH stretching modes (and the absence of CH stretching modes) indicates that the LK_{14} peptide bonds with different ordering at this hydrophilic solid/water interface. The hydrophilic SiO_2 is negatively charged in pH = 7.4 solution ($pK_a = 2$), which suggests an electrostatic adsorption mechanism on this surface possibly occuring through the positively-charged lysine side chains (pK_a = 10). AFM data show that multiple peptide layers are formed on SiO_2, which may be driven from the intermolecular self-association of the leucine side-chains to minimize the interfacial energy from contact with the bulk water. It is feasible that the detected NH mode is from the side chains of the lysine residues, in agreement with a recent SFG study of proteins adsorbed on silica.[58] However, the NH assignment to an Amide A mode can not be ruled out, since Amide A is normally observed between 3270 cm^{-1} and 3310 cm^{-1}.[59] Regardless of the exact origin of the observed signal, the difference in SFG spectra between the hydrophobic and hydrophilic surface indicates the peptide has completely different average orientations at these interfaces.

We also observe different peaks in the water region on the hydrophilic vs. hydrophobic surface. A broad OH peak centered at 3092 cm^{-1} is always observed for LK_{14}/PS-d_8 (Figure 3.7) in comparison to a much weaker peak at 3190 cm^{-1} for LK_{14}/SiO_2 (Figure 3.8). Although the OH peak at 3092 cm^{-1} is at low frequency for water, SFG results of hydrophobic solid/water interfaces have shown broad OH modes that span the region between 3000 cm^{-1} and 3600 cm^{-1} due to different hydrogen-bonded environments.[60] In the absence of peptide, OH peaks are typically observed

at ∼3200 cm^{-1} and ∼3400 cm^{-1} and are attributed to tetrahedrally coordinated and hydrogen bonded water, respectively.[60; 61]

On the hydrophilic surface, the water structure is significantly different. After the addition of the peptide, the OH peak at ∼3400 cm^{-1} completely disappears in the spectrum and the intensity of the ∼3200 cm^{-1} peak is reduced. This suggests a significant rearrangement of the water hydrogen bonding structure due to the peptide adsorption. The position and intensity of the OH peaks (both on the hydrophobic and hydrophilic surface) are highly dependent on the ionic strength of the buffer, the pH of the solution, and the presence of the LK_{14} peptide, and is the subject of our current investigations.

3.6 Conclusions

The combined use of the QCM-D, AFM and SFG techniques is a powerful approach that was employed for the first time to understand the in situ adsorption of a model amphiphilic peptide, LK_{14}, at a hydrophobic and hydrophilic solid/liquid interfaces. The time-dependant QCM-D and AFM studies show that LK_{14} adsorbs monotonically over 2 min, forming a rigid film on hydrophobic PS. On hydrophilic SiO_2 we observe a slower multi-step adsorption process (30-35 min) leading to a viscoelastic adsorbate with layered LK_{14} molecules, which laterally aggregate on a μm-scale. Multilayer formation on SiO_2 leads to a 2-fold increase in the friction, while submonolayer coverage of the peptide on PS results in minimal change in the exhibited friction. The SFG spectra indicate that the differences in morphology, friction, adsorbed amounts and viscoelasticity, measured by QCM and AFM on the hydrophobic and hydrophobic surface, can be attributed to the nature of the molecular interaction occurring at the interface. The SFG spectrum of LK_{14}/PS suggests that the adsorption is dominated by hydrophobic interactions at the surface through the hydrophobic

side (leucine amino acid) of the peptide. For LK_{14}/SiO_2, the hydrophilic surface promotes ordering of charged NH groups at the interface. The surface-sensitive difference in adsorption behavior is observed on a macromolecular-scaleusing AFM and QCM. This combined technique approach is highly advantageous for understanding peptide behavior at the aqueous/solid interface because it independently probes the morphological and mechanical behavior, quantitative coverage amount, and molecular-scale average orientation and interaction in response to the surface hydrophobicity.

Bibliography

[1] Horbett, T. A.; Brash, J. L. *Proteins at Interfaces II: Fundamentals and Applications*; American Chemical Society: Washington, DC, **1995**.

[2] Matsumura, M.; Fremont, D. H.; Peterson, P. A.; Wilson, I. A. *Science* **1992**, *257*, 5072.

[3] Russell, C. J.; Thorgeirsson, T. E.; Shin, Y. K. *Biochemistry* **1996**, *35*, 9526.

[4] Kruger, P.; Schalke, M.; Wang, Z.; Notter, R. H.; Dluhy, R. A; Lsche, M. *Biophys. J. 1999*, *77*, 903.

[5] DeGrado, W. F.; Lear, J. D. *J. Am. Chem. Soc.* **1985**, *107*, 7684.

[6] DeGrado, W. F.; Wasserman, Z. R.; Lear, J. D. *Science* **1989**, *243*, 622.

[7] Healy, K. E. *Curr. Opin. Solid State Mater. Sci. 1999*, *4*, 381.

[8] Tong, Y. W.; Shoichet, M. S. *J. Biomater. Sci., Polym. Ed.*, **1998**, *9*, 713.

[9] Kaiser, E. T.; Kezdy, F. J. *Proc. Natl. Acad. Sci.* **1983**, *80*, 1137.

[10] Brack, A.; Spach, G. *J. Am. Chem. Soc.* **1981**, *103*, 6319.

[11] Castano, S.; Desbat, B.; Dufourcq, J. *Biochim. Biophys. Acta*, **2000**, *1463*, 65.

[12] Castano, S.; Desbat, B.; Cornut, I.; Meleard, P.; Dufourcq, J. *Lett. Pept. Sci.* **1997**, *4*, 195.

[13] Kerth, A.; Erbe, A.; Dathe, M.; Blume, A. *Biophys. J.* **2004**, *86*, 3750.

[14] Maget-Dana, R.; Lelievre, D.; Brack, A. *Biopolymers* **1999**, *49*, 415.

[15] Castano, S.; Desbat, B.; Laguerre, M.; Dufourcq, J.; *Biochim. Biophys. Acta.* **1999**, *1416*, 176.

[16] Dieudonne, D.; Gericke, A.; Flach, C. R.; Jiang, X.; Farid, R. S.; Mendelsohn, R. *J. Am. Chem. Soc.* **1998**, *120*, 792.

[17] Blondelle, S. E.; Houghten, R. A. *Biochemistry* **1992**, *31*, 12688.

[18] Beven, L.; Castano, S.; Dufourcq, J.; Wieslander, A.; Wroblewski, H. *Eur. J. Biochem.* **2003**, *270*, 2207.

[19] Long, J. R.; Oyler, N.; Drobny, G. P.; Stayton, P. S. *J. Am. Chem. Soc.* **2002**, *124*, 6297.

[20] Stewart, S.; Fredericks, P. M. *Spectrochim. Acta, Part A.* **1999**, *55*, 1615.

[21] Herne, T. M.; Ahern, A. M.; Garrell, R. L. *Anal. Chim. Acta.* **1991**, *246*, 75.

[22] Burkett, S. L; Read, M. J. *Langmuir* **2001**, *17*, 5059.

[23] Lee, N. H.; Christensen, L. M.; Frank, C. W. *Langmuir* **2003**, *19*, 3525.

[24] Knoeson, A.; Pakalnis, S.; Wang, M.; Wise, W.; Lee, N.; Frank, C. W. *IEEE J. Sel. Top. Quant.* **2004**, *10*, 1154.

[25] Dreesen, L.; Sartenaer, Y.; Humbert, C.; Mani, A. A.; Methivier, C.; Pradier, C. M.; Thiry, P. A.; Peremans, A. *Chem. Phys. Chem.* **2004**, *5*, 1719.

[26] Kim, G.; Gurau, M. C.; Lim, S. M.; Cremer, P. S. *J. Phys. Chem. B.* **2003**, *107*, 1403.

[27] Chen, X.; Wang, J.; Sniadecki, J. J.; Even, M. A.; Chen, Z. *Langmuir* **2005**, *21*, 2662.

[28] Chen, X.; Clarke, M. L.; Wang, J.; Chen, Z. *Int. J. Mod. Phys. B.* **2005**, *19*, 691 and references therein.

[29] Kim, J.; Cremer, P. S. *Chem. Phys. Chem.* **2001**, *2*, 543.

[30] Anderson, N. A.; Yang, C. S. C.; Stephenson, J. C.; Richter, L. J.; Briggman, K. A. *Abstr. Pap. Am. Chem. Soc.* **2005**, *229*, U669-U669.

[31] Raschke, M. B.; Shen, Y. R. *Curr. Opin. Solid State Mater. Sci.* **2004**, *8,* 343.

[32] Kim, J.; Somorjai, G. *J. Am. Chem. Soc.* **2003**, *125*, 3150.

[33] King, D.; Fields, C.; Fields, G. *Int. J. Pept. Protein Res.* **1990**, *36*, 255.

[34] Sauerbrey, G. Z. *Phys.* **1959**, *155*, 206.

[35] Czanderna, A. W.; Lu, C. in *Applications of Piezoelectric Quartz Crystal Microbalances* edited by Lu, C. and Czanderna, A. W. (Elsevier, Amsterdam, **1984**), Vol. 7, p. 1.

[36] Krim, J.; Chiarello, R. J. *Vac. Sci. Technol. B.* **1991**, *9*, 1343.

[37] Widom, A.; Krim, J. *Phys. Rev. B.* **1986**, *34*, 1403.

[38] Marx, K. A. *Biomacromolecules* **2003**, *4*, 1099.

[39] Hook, F.; Rodahl, M.; Brzezinski, P.; Kasemo, B. *Langmuir* **1998**, *14*, 729.

[40] Hook, F.; Kasemo, B.; Nylander, T.; Fant, C.; Sott, K.; Elwing, H. *Anal. Chem.* **2001**, *73*, 5796.

[41] Lambert, A. G.; Davies, P. B.; Neivandt, D. J. *App. Spectrosc. Rev.* **2005**, *40*, 103.

[42] Shen, Y. R. *Nature* **1989**, *337*, 519.

[43] Wang, H. F.; Gan, W.; Lu, R.; Rao, Y. ; Wu, B. H. *Int. Rev. Phys. Chem.* **2005**, *24*, 191.

[44] Wei, X.; Hong, S. C.; Zhuang, X.; Goto, T.; Shen, Y. R. *Phys. Rev. E.* **2000**, *62*, 5160.

[45] Hirose, C.; Akamatsu, N.; Domen, K. *Appl. Spectrosc.* **1992**, *46*, 1051.

[46] Zhuang, X.; Miranda, P. B.; Kim, D.; Shen, Y. R. *Phys. Rev. B.* **1999**, *59*, 12632.

[47] Superfine, R.; Huang, J. Y.; Shen, Y. R. *Chem. Phys. Lett.* **1990**, *172*, 303.

[48] Doyle, A. W.; Fick, J.; Himmelhaus, M.; Eck, W.; Graziani, I.; Prudovsky, I.; Grunze, M.; Maciag, T.; Neivandt, D. J. *Langmuir* **2004**, *20*, 8961.

[49] Wang, J.; Buck, S.; Chen, Z. *J. Phys. Chem. B.* **2002**, *106*, 11666.

[50] Baldelli, S.; Mailhot, G.; Ross, P. N.; Somorjai, G. A. *J. Am. Chem. Soc.* **2001**, *123*, 7697.

[51] Baldelli, S.; Mailhot, G.; Ross, P.; Shen, Y. R.; Somorjai, G. A. *J. Phys. Chem. B.* **2001**, *105*, 654.

[52] Keller, C. A.; Kasemo, B. *Biophys. J.* **1998**, *75*, 1397.

[53] Ji, N.; Shen, Y. R. *J. Chem. Phys.* **2004**, *120*, 7107.

[54] Watry, M. R.; Richmond, G. L. *J. Phys. Chem. B.* **2002**, *106*, 12517.

[55] Calvo, E. J.; Danilowicz, C.; Lagier, C. M.; Manrique, J.; Otero, M. *Biosens. Bioelectron.* **2004**, *19*, 1219.

[56] Kiyota, T.; Lee, S.; Sugihara, G. *Biochemistry* **1996**, *35*, 13196.

[57] Samuel, N. T.; McCrea, K. R.; Gamble, L. J.; Ward, R. S.; Stayton, P. S.; Somorjai, G. A.; Castner, D. G. **2006**, in preparation.

[58] Jung, S. Y.; Lim, S. M.; Albertorio, F.; Kim, G.; Gurau, M. C.; Yang, R. D.; Holden, M. A.; Cremer, P. A. *J. Am. Chem. Soc.* **2003**, *125*, 12782.

[59] Krimm, S; Bandekar, J. *Adv. Protein Chem.* **1986**, *38*, 183.

[60] Du, Q.; Freysz, E.; Shen Y. R. *Science* **1994**, *264*, 826.

[61] Scatena, L. F.; Richmond, G. L. *Chem. Phys. Lett.* **2004**, *383*, 491.

Chapter 4

Adsorption Properties of Designed Peptides on Model Surfaces: Effects of Sequence and Chain Length

4.1 Abstract

The adsorption properties of model amphiphilic peptides have been studied in situ with surface-specific Sum Frequency Generation (SFG) Vibrational Spectroscopy, Quartz Crystal Microbalance (QCM), and Atomic Force Microscopy (AFM) at the hydrophobic (polystyrene) and hydrophilic (silica) solid-liquid interface. The peptides contain hydrophobic (X) and charged (Y) amino acids with sequence: Ac-XYYXXYXXYYXXYX-NH_2 or Ac-XYXYXYX-NH_2 where the X and Y combinations are Leucine (L) and Lysine (K); Alanine (A) and Lysine (K); Alanine (A) and Arginine (R); and Phenylalanine (F) and Arginine (R). Homopeptides of lysine,

leucine, and alanine have also been studied for comparison. We use SFG spectroscopy to investigate variables such as peptide chain length and sequence, and buffer concentration on adsorption on the model surfaces. SFG spectra of adsorbed peptides on polystyrene show strong CH resonances characteristic of the hydrophobic side-chains at the interface. On silica, NH modes are observed for LK_{14} peptide, whereas adsorption of the other peptides show no distinct peptide modes but drastically different surface water structure upon adsorption. QCM data indicates that the 14-amino acid peptides adsorbed strongly onto both the hydrophobic PS and the hydrophilic SiO_2 surfaces, whereas the 7-amino acid peptides adsorb weakly on both surfaces. In situ AFM topography and lateral force measurements show different surface morphologies and friction coefficients when the various peptides are adsorbed onto silica versus polystyrene surfaces.

4.2 Introduction

In Chapter 3 we reported adsorption studies of a model amphiphilic peptide on hydrophobic and hydrophilic surfaces using AFM, QCM and SFG spectroscopy. A 14-amino acid peptide, with sequence LKKLLKLLKKLLKL (LK_{14}) (structure shown in Figure 3.1), yielded very different SFG spectra when adsorbed on polystyrene and silica. This was attributed to different driving forces for surface interaction: hydrophobic interactions on polystyrene, and electrostatic interactions on SiO_2. In order to gain a more complete understanding of the mechanisms of peptide bonding on these model surfaces, a series of peptides have been synthesized using different amino acids, but with the same hydrophobic sequence as the LK_{14} peptide reported in Chapter 3. Peptides with hydrophobic and charged amino acid pairs Leucine (L) and Lysine (K), Alanine (A) and Lysine (K), Alanine (A) and Arginine (R); and Phenylalanine (F) and Arginine (R) were synthesized (amino acid structures

shown in Figure 4.1). We would like to understand whether a peptide's solution secondary structure or affinity for an induced secondary structure at the interface affects the adsorption. In order to address this question, the peptides examined here were designed to form both β-strand and α-helical secondary structures at the interface. This scheme should allow us to investigate whether solely electrostatic and hydrophobic interactions control adsorption depending on the character of the side chain; or whether the peptide's affinity for secondary structure formation at the surface drives the adsorption. SFG spectroscopy is used to isolate the effects of surface hydrophobicity, peptide sequence and chain length, peptide concentration, and buffer concentration on the adsorption of these LK, AK, AR, and FR peptides on polystyrene and silica. QCM and AFM are used to measure the mass adsorbed, and surface mechanical and topographical properties of the adsorbed peptide films, respectively.

4.3 Experimental

We have used the experimental conditions and procedures described in detail in Chapter 2 and 3 for all CD, AFM, QCM and SFG experiments.[1]

4.3.1 Peptide Synthesis

Peptides were synthesized using an Applied Biosystems ABI 431A synthesizer using rink amide 4-methylbenzhydrylamine (MBHA) resin (Nova Biochem) and standard 9-fluorenylmethyloxycarbonyl (FMOC) chemistry.[2] Approximately 200 mg of rink amide resin was used in the synthesis, with a 9-equivalents excess of reagents. The N-terminus of the peptide was acetylated by adding acetic anhydride to the resin-bound peptide prior to cleaving in a solution of 95% trifluoroacetic acid in water. The

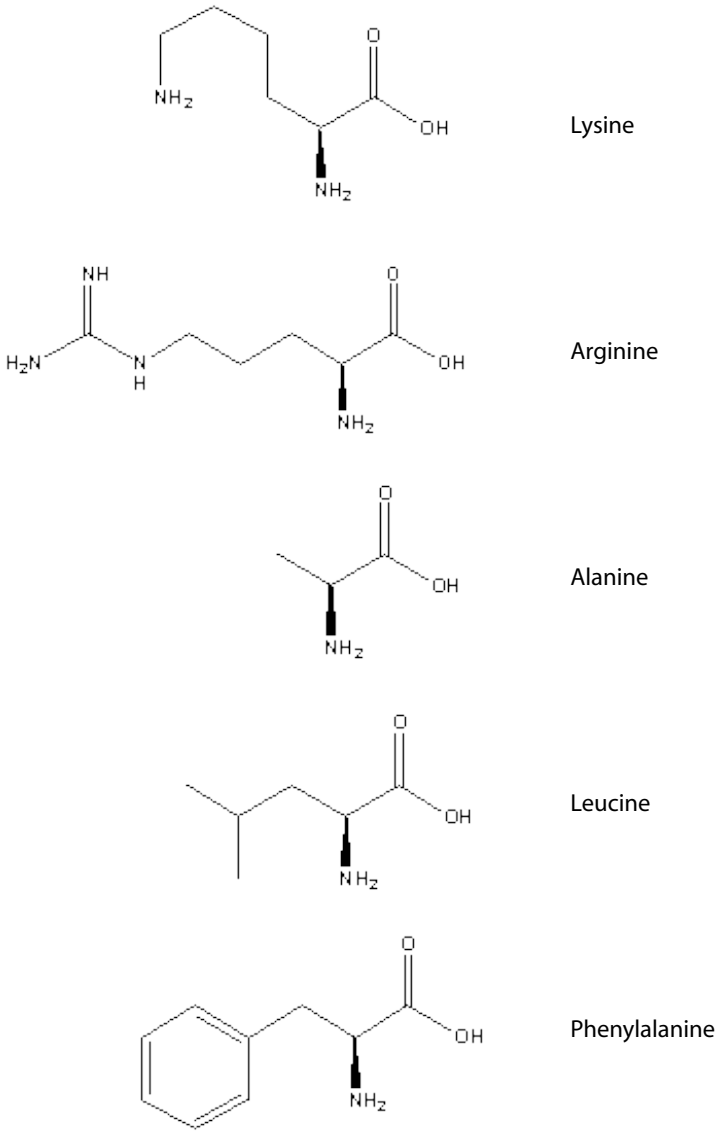

Figure 4.1. Amino acids used in model synthetic peptides

crude peptides were purified by reversed-phase high pressure liquid chromatography (rp-HPLC) with a C-18 column (Vydac), where possible. Hydrophobic peptides were not HPLC purified due to low solubility and retention on the HPLC column (see note on synthesis in Appendix A.) The purity and composition of the peptides was characterized using LC-ESI-MS (electrospray ionization) mass spectrometry. Peptides were precipitated in cold methyl-tert-butylether and lyophilized to dryness.

The peptides contain hydrophobic (X) and charged (Y) amino acids with sequence: Ac-XYYXXYXXYYXXYX-NH_2 or Ac-XYXYXYX-NH_2 where the X and Y combinations are Leucine (L) and Lysine (K); Alanine (A) and Lysine (K); Alanine (A) and Arginine (R); and Phenylalanine (F) and Arginine (R). The 14 amino acid peptides are sequenced to induce α-helical formation at an apolar interface, while the 7 amino acid peptides should form β-strands.[3; 4] One additional 7 amino acid peptide was synthesized, with sequence LKKLKKL. This peptide is designed to form a helix, however is below the nominal number of residues required to stabilize helix formation. Table 4.1 gives the mass and theoretical isoelectric point, pI, for each peptide (based on the pK_a of the side-chains) before acetylation of the N-terminus.

Table 4.1. List of Peptides Synthesized

Peptide	Molecular Weight	Theoretical pI
LK_{14}	1691.25	10.70
AK_{14}	1354.88	10.70
AR_{14}	1522.91	12.70
FR_{14}	2131.16	12.70
K_{14}	1811.34	11.11
A_{14}	1012.53	5.57
L_{14}	1601.19	5.52
LK_7	854.63	10.30
AK_7	686.44	10.30
AR_7	770.46	12.30
FR_7	1074.59	12.30
K_7	914.68	10.78
L_7	809.6	5.52

The LK, AK, AR, and FR peptides used in this study all had drastically different solution solubilities, so we were unable to perform all of the experiments at the same peptide concentration. In general, the 14-amino acid peptides were more soluble than the 7-amino acid peptides (even with equal ratio of hydrophobic to hydrophilic amino acids). The peptide solubility decreased in the order AK > AR > LK > FR.

4.4 Results

4.4.1 SFG Spectra of Reference Amino Acids

The SFG spectra of the amino acids used in our model peptides are shown in Figure 4.23-4.27 (Appendix I of this chapter). The peptides were deposited from a pH 7.4 PBS solution onto SiO_2, and allowed to dry to a thin film. Amino acids do not strongly adsorb on SiO_2 at this pH, as discussed in Chapter 2. The SFG spectra of these amino acids resemble previously published studies of amino acids at the air/water interface.[5; 6]. The amino acids slowly dry into bulk crystals, and generate very large SFG signal (in *ssp* polarization). The SFG spectrum of leucine has 3 peaks in the CH region at 2874, 2899 and 2942 cm^{-1}. These are assigned to a methyl symmetric stretch, CH_3 ν_s, CH, and a Fermi resonance of CH_3 ν_s, respectively. Alanine amino acid shows a similar SFG spectrum to leucine, with peaks at 2860, 2878, and 2950 cm^{-1}. Lysine and arginine produce similar SFG spectra, with peaks at 2850, 2879, and 2952 cm^{-1}, which are assigned to CH_2 ν_s, a Fermi resonance of CH_2 ν_s, and a Fermi resonance of CH_2 ν_a, respectively. The SFG spectrum of phenylalanine, obtained in *ppp* polarization, has peaks at 2934, 3036 and 3059 cm^{-1} due to methylene symmetric stretch, CH_2 ν_s, and phenyl asymmetric and symmetric stretches, ν_{7b} and ν_2, respectively.

4.4.2 SFG Studies of Designed Peptides Adsorbed on Hydrophobic and Hydrophilic Surfaces

Effects of Surface Hydrophobicity

The effects of surface hydrophobicity on peptide adsorption were examined by monitoring the adsorption of LK_{14} peptide on three different surfaces: hydrophobic polystyrene, charged SiO_2, and CaF_2 surfaces. Figure 4.2 shows the SFG spectra of LK_{14} on the three surfaces. We observe CH stretches between 2850-2950 cm^{-1} on both polystyrene and CaF_2. The signal-to-noise ratio is much higher on PS, and we can assign the CH resonances at 2874, 2899, and 2942 cm^{-1} to methyl symmetric stretch, CH_3 ν_s, CH stretch, and a Fermi resonance of CH_3 ν_s, respectively. An NH mode centered at 3300 cm^{-1} is present on both the charged SiO_2, and CaF_2 surfaces.

Time dependence of SFG signal

Time-dependent adsorption behavior was observed for LK_{14} on PS. SFG spectra show a time-dependent increase (on the order of min) of CH modes at the buffer/PS-d_8 interface, shown in Figure 4.3 as the growth of SFG peaks at 2869 cm^{-1} (CH_3 symmetric resonance) and 2935 cm^{-1} (methyl Fermi resonance) over a half hour period. The change in intensity of the CH peaks versus time is plotted in Figure 4.4. No time dependence is observed for the SFG signal of LK_{14} at the buffer/SiO_2 interface.

Homopeptide versus Amphiphilic Peptide Adsorption

The SFG spectra of LK_{14} and homopeptides L_{14}, K_{14}, and A_{14} on PS-d_8 are shown in Figure 4.5. The SFG spectrum of K_{14} shows peaks at 2865, and 2933 cm^{-1} which are assigned to CH_2 ν_s, a Fermi resonance of CH_2 ν_s, and are from ordering of the

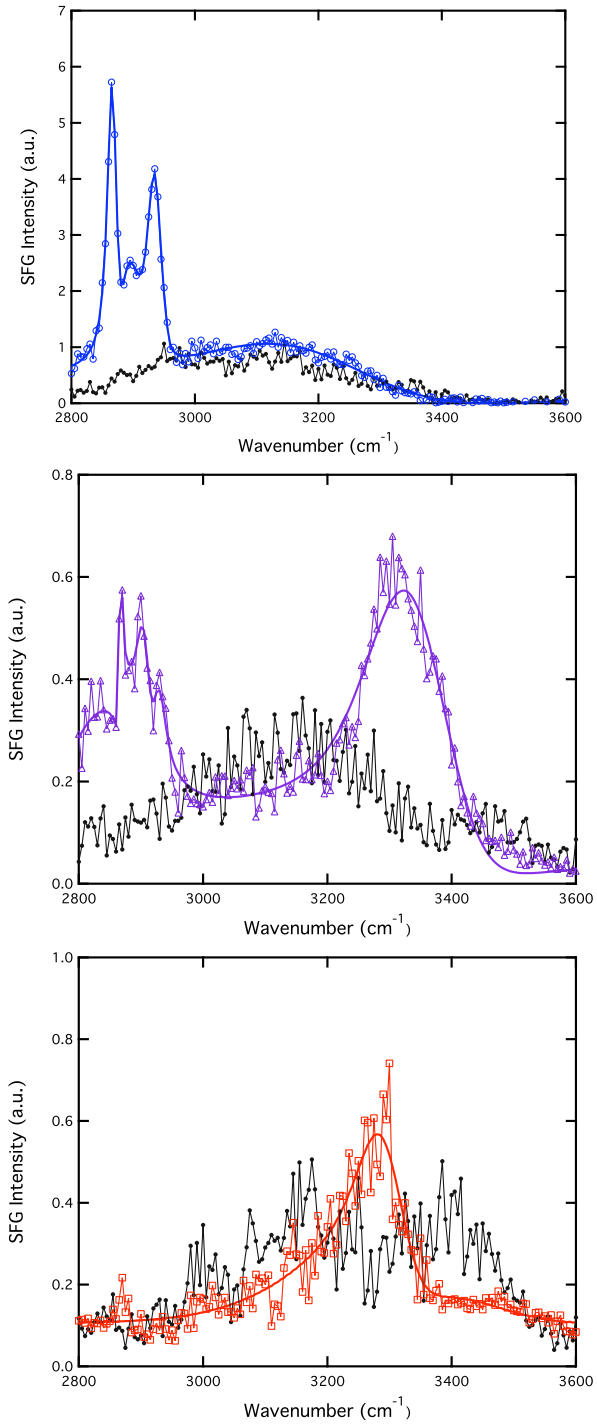

Figure 4.2. SFG spectra of LK_{14} on PS-d_8 (blue, top), CaF_2 (purple, middle) and SiO_2 (red, bottom). CH resonances are observed on PS-d_8 and CaF_2 which correspond to stretches of the hydrophobic leucine side chain. NH stretched are observed on CaF_2 and SiO_2 which correspond to stretches of the lysine side chain. PBS background spectra (black) are shown for each surface.

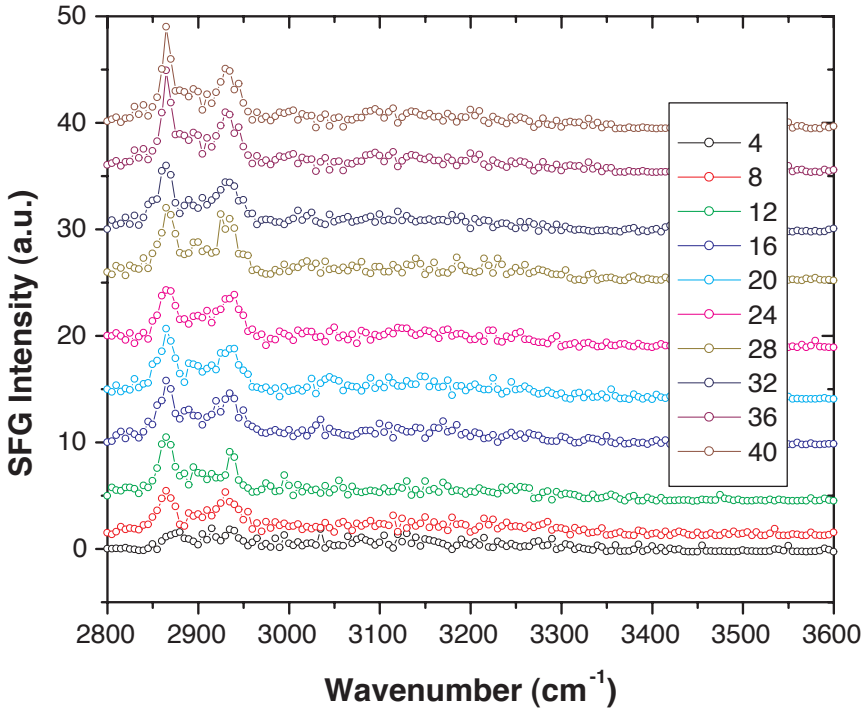

Figure 4.3. SFG spectra of LK_{14} on PS-d_8. The signal intensity in the CH region increases over ∼10 minutes. This may be due to rearrangment and ordering of molecules at the surface.

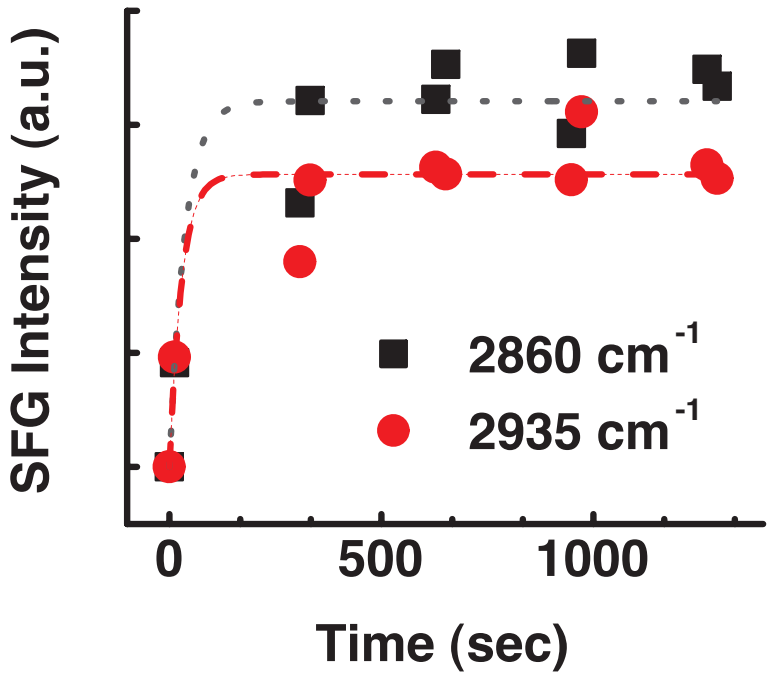

Figure 4.4. The signal intensity in the CH region increases over ∼40 minutes when LK_{14} peptide is exposed to PS. This may be due to rearrangment and ordering of molecules at the surface.

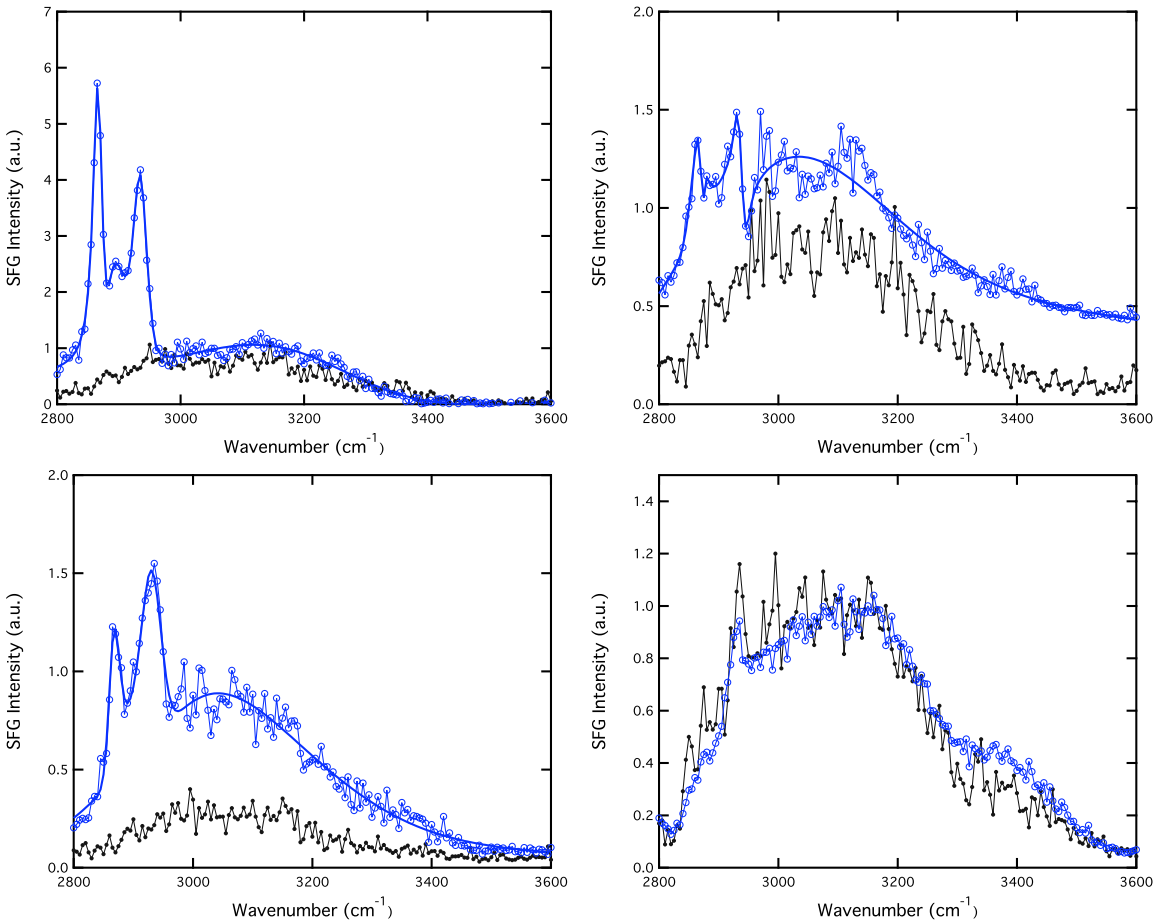

Figure 4.5. SFG spectra of LK_{14}, L_{14}, A_{14}, and K_{14} (clockwise from top left) on PS-d_8. All spectra show background PBS data in black. The CH modes in the spectra of LK_{14} and L_{14} are assigned to methyl stretches from the leucine side chain. The CH_2 modes in the spectrum of K_{14} are from the alkyl portion of the lysine side chain. The signal intensity is much larger for LK_{14} than for the homopeptides, indicating higher surface coverage and/or ordering.

alkyl chain portion of the lysine side chain. The SFG spectrum of A_{14} is similar to the PBS background, but may have a weak CH_3 ν_s mode at 2864 cm^{-1}. The hydrophobic leucine side chains modes at 2868, 2887, and 2935 cm^{-1} are observed in the spectra of LK_{14} and L_{14}, and are assigned to CH_3 ν_s, CH stretch, and a Fermi resonance of CH_3 ν_s, respectively. The signal intensity for LK_{14} is more than five times that of L_{14}. As discussed in Chapter 3, LK_{14} forms a smooth monolayer on PS, with hydrophobic leucine side-chains ordering at the PS surface, resulting in charged lysine residues interacting with the bulk water. The amphiphilic nature of LK_{14} may allow for a higher degree of surface coverage, which leads to a more intense SFG signal.

Isosequentional Amphiphilic Peptides: Effects of Sequence and Chain Length

The SFG spectra of the 14- and 7-amino acid peptides adsorbed on polystyrene and silica are shown in Figures 4.6-4.12 (polystyrene surfaces) and Figure 4.13-4.16 (silica surfaces). Background SFG spectra of PBS on the bare surfaces are plotted in the lower (black) traces of each figure.

Intense peptide modes are visible for all of the peptides adsorbed on hydrophobic polystyrene surfaces. SFG spectra of the LK peptides (Figure 4.6) show strong CH resonances at 2870, 2895, and 2935 cm^{-1} for LK_{14}, and 2880, 2910, and 2936 cm^{-1} for LK_7. These peaks are from the leucine side-chains and are assigned to a methyl symmetric stretch, CH_3 ν_s, CH stretch, and a Fermi resonance of CH_3 ν_s, respectively. Figure 4.7 shows the SFG spectra of the two 7 amino acid LK peptides, with α and β sequences. The spectra are nearly identical, except for a shift in the 2910 peak from the β LK_7 peptide to 2880 for the α LK_7 peptide. The differences in the SFG peaks indicates a slightly different average orientation of the methyl groups at the PS surface. The other noticeable different in the spectra is in the water region: there

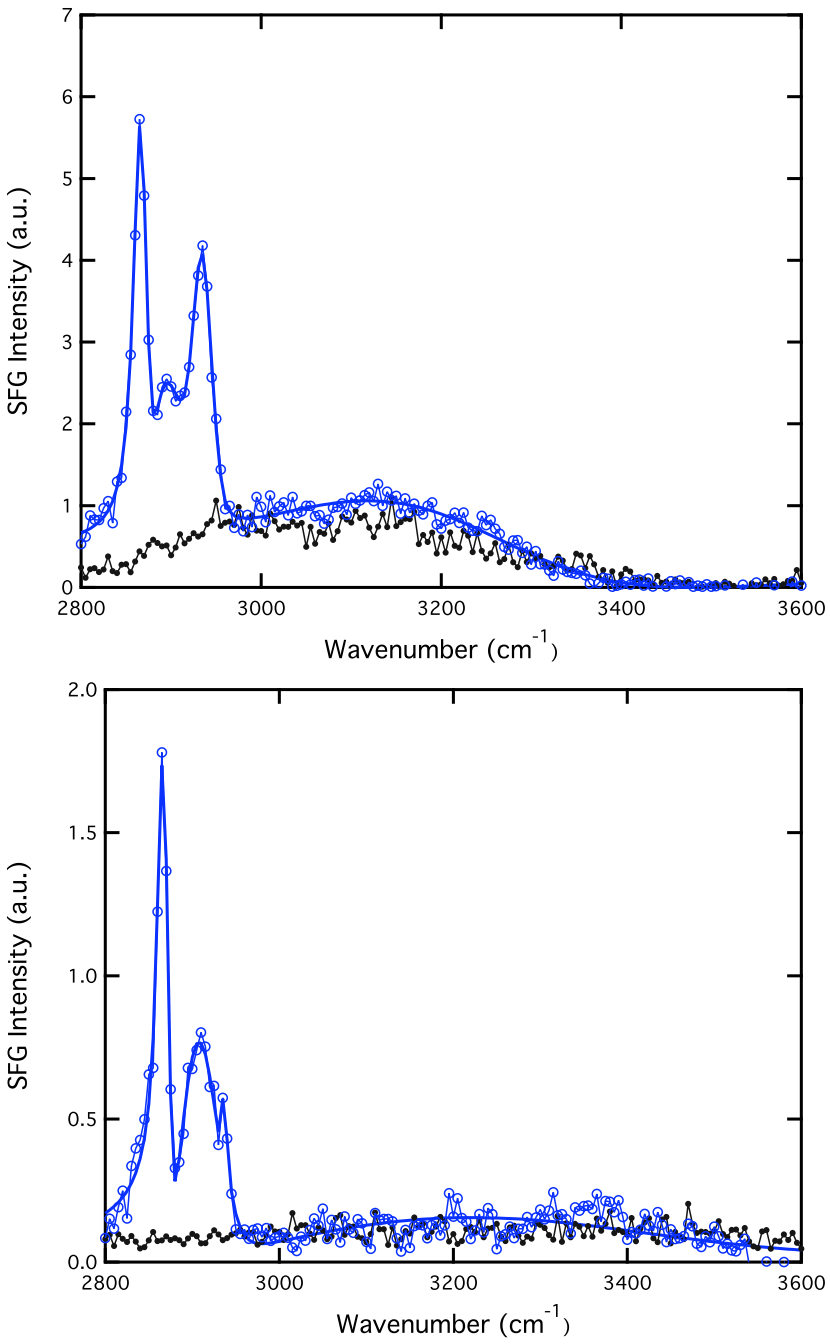

Figure 4.6. SFG spectra of PBS (black) and LK_{14} (blue), top figure. Bottom figure is PBS (black) LK_7 (blue) on PS-d_8. LK_{14} peaks at 2869, 2895 and 2935 cm^{-1}, LK_7 peaks at 2880, 2910, 2936 cm^{-1}.

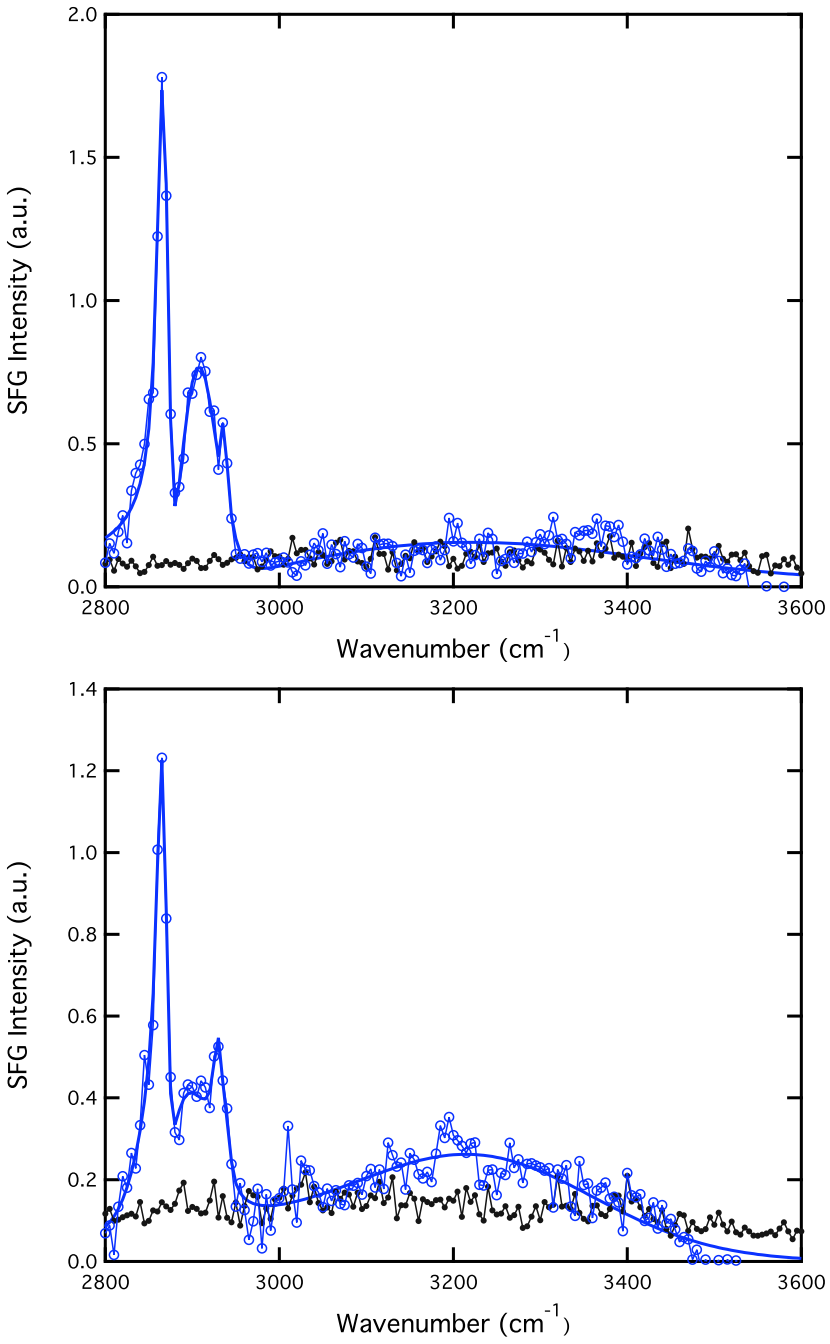

Figure 4.7. SFG spectra of PBS (black) and LK_7 α, top figure. Bottom figure is PBS (black) LK_7 β on PS-d_8. LK_7 α peaks at 2868, 2880 and 2936 cm^{-1}.

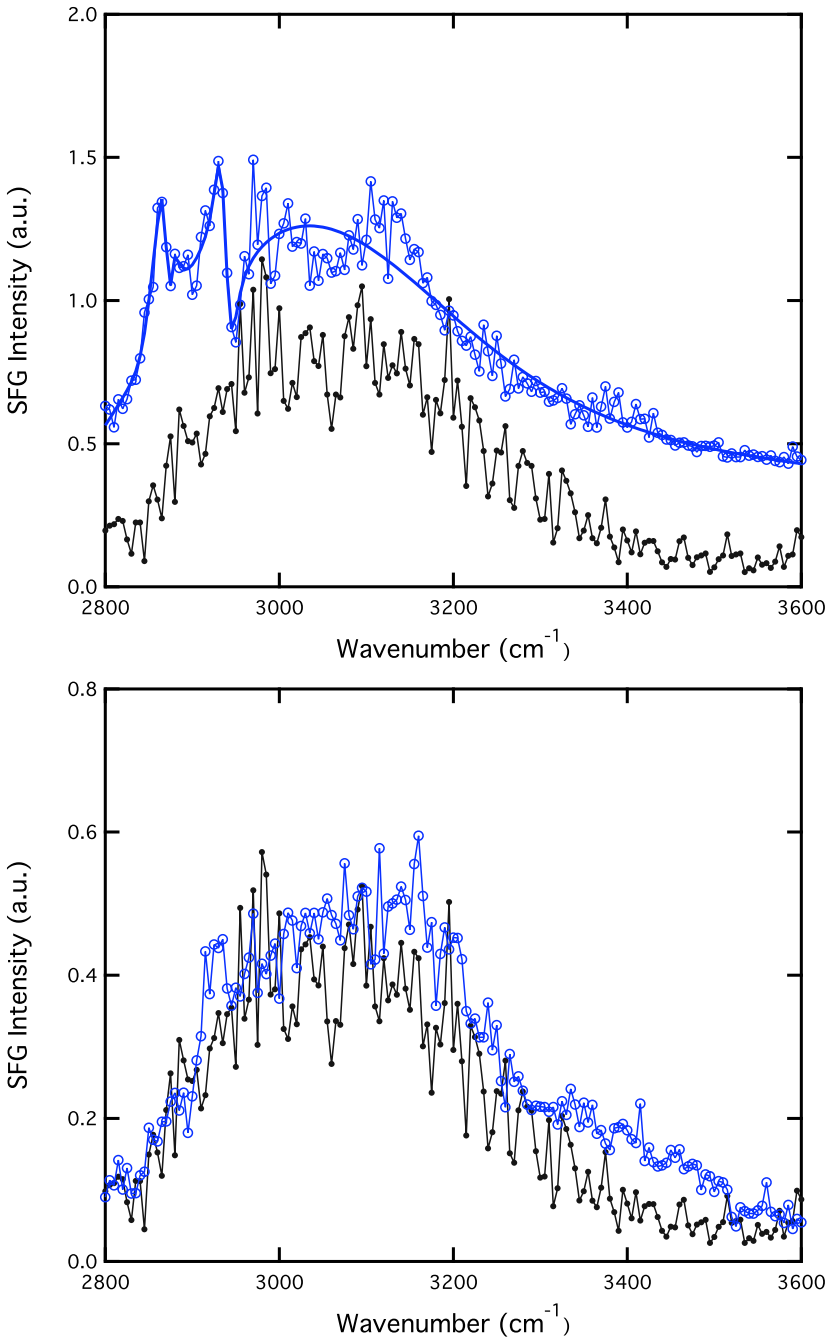

Figure 4.8. SFG spectra of PBS (black) and L_{14} (blue) on PS-d_8, top figure. SFG spectra of PBS (black) and L_7 (blue) on PS-d_8, bottom figure.

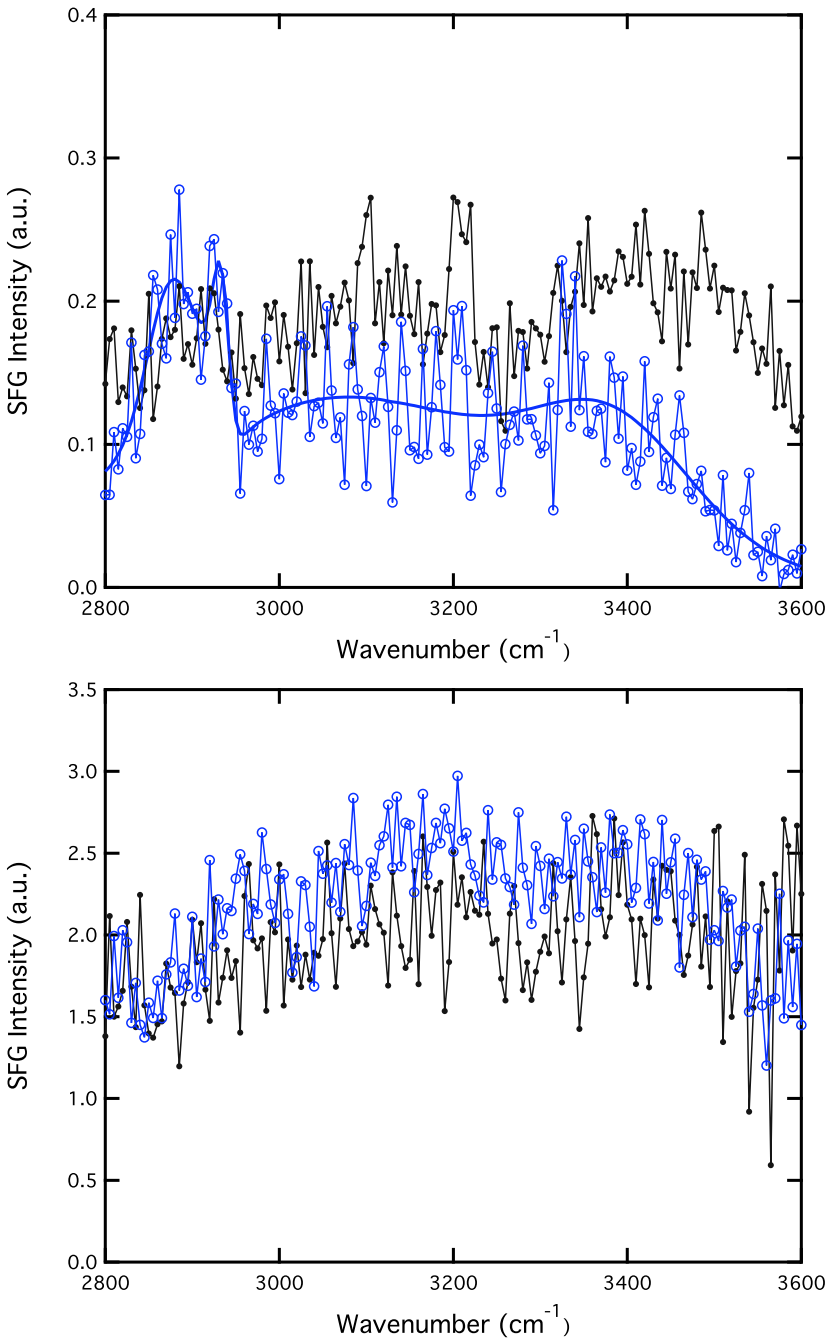

Figure 4.9. SFG spectra of PBS (black) and AK_{14} (blue) on PS-d_8, top figure. Bottom figure are SFG spectra of PBS (black) and AK_7 (blue) on PS-d_8. The peaks at 2874 and 2936 cm^{-1} are assigned the methyl symmetric stretches of the alanine side chain.

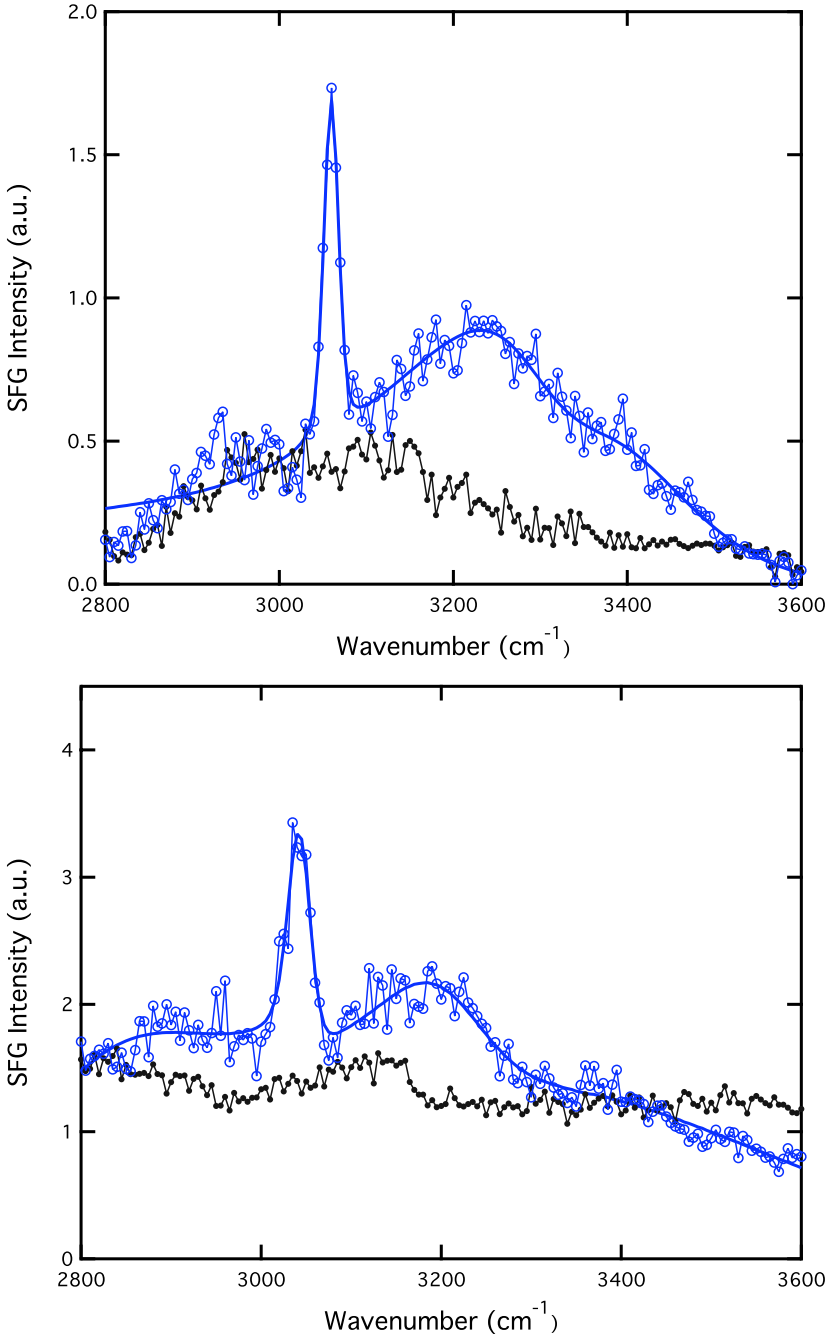

Figure 4.10. SFG spectra of PBS (black) and FR_{14} (blue) on PS-d_8, top figure. The peak at 3059 cm^{-1} is assigned to the symmetric phenyl ring stretch ν_2. SFG spectra of PBS (black) and FR_7 (blue) on PS-d_8, bottom figure. The peak at 3043 cm^{-1} is also assigned to the symmetric phenyl ring stretch, ν_2 of the phenyalanine side chain.

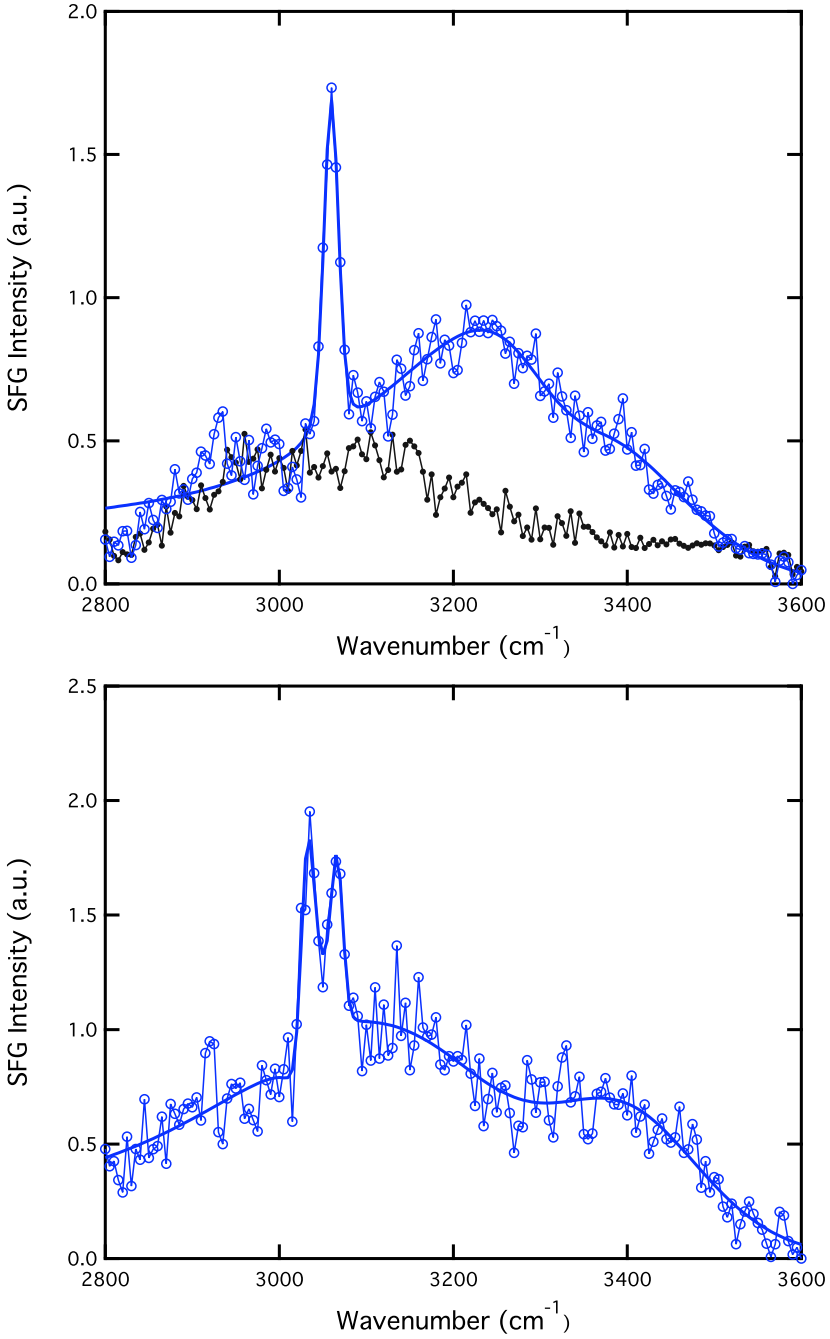

Figure 4.11. SFG spectra of PBS (black) and FR_{14} (blue) on PS-d_8, *ssp* polarization, top figure. The peak at 3059 cm^{-1} is assigned to the symmetric phenyl ring stretch ν_2. SFG spectra of PBS (black) and FR_{14} (blue) on PS-d_8, *sps* polarization, bottom figure. The peaks at 3029 and 3067 cm^{-1} are asymmetric and symmetric, ν_{7b} and ν_2, ring stretching modes, respectively.

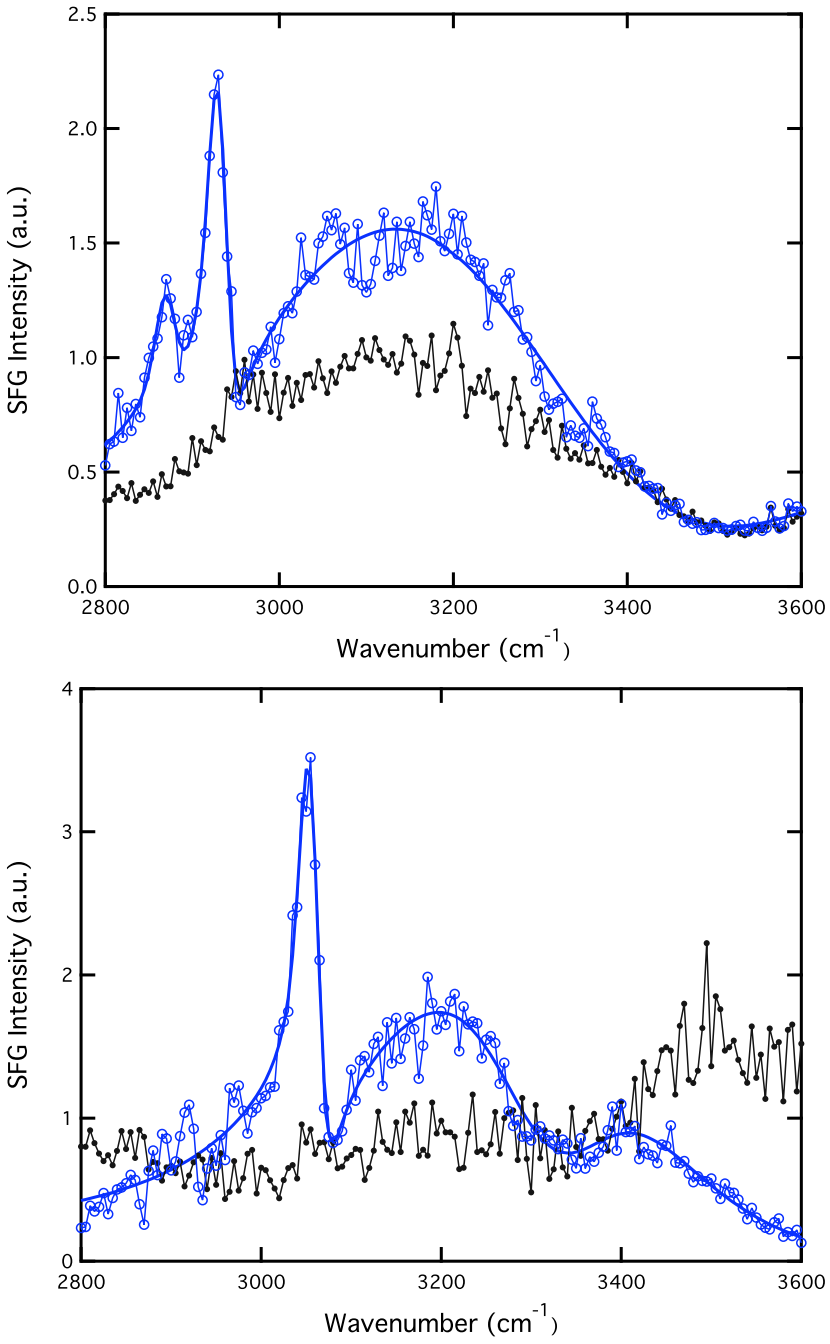

Figure 4.12. SFG spectra of PBS (black) and AR_{14} (blue) on PS-d_8, top figure. CH resonances are observed at 2861 and 2933 cm^{-1}. SFG spectra of PBS (black) and AR_7 (blue) on PS-d_8, bottom figure.

is almost no structured water in the spectrum of β LK_7, whereas the water peak centered at 3150 cm^{-1} for α LK_7 is similar to the peak in the spectrum of LK_{14} on PS. The intensity of OH peaks varies with peptide hydrophobicity. The SFG spectrum of the most hydrophobic peptide we have studied, L_{14}, shows the same leucine methyl stretches seen in the LK peptide spectra, but has a much stronger hydrogen bonded water peak centered at 3150 cm^{-1} (Figure 4.8). The adsorption of L_7 results in little change in the SFG spectrum relative to PBS, most likely indicating that the peptide surface coverage is low.

The SFG spectra of AK peptides (Figure 4.9) on PS is similar to the LK peptides. Peaks corresponding to methyl resonances of the alanine side chains are observed and 2874 and 2936 cm^{-1} for AK_{14}. These peaks are weaker in intensity than those observed in the LK spectra, and are assigned to methyl symmetric stretch (2874 cm^{-1}) and a Fermi resonance of the methl symmetric stretch (2936 cm^{-1}). There are no peptide modes visible following adsorption of AK_7. The surface water structure remains the same, showing that the peptide does not have a high affinity for surface adsorption.

SFG spectra of FR peptides (Figure 4.10) on PS show a single intense peptide mode around 3050 cm^{-1}, in addition to structured water peaks around 3200 cm^{-1}. Polarization studies of FR_{14} (Figure 4.11) allow for the assignment of the 3050 cm^{-1} mode to the phenyl ring stretch of the phenyalanine side chains. In *ssp* polarization, the phenyl groups typically show a symmetric ring stretching mode, which splits into an asymmetric and symmetric peak in *sps* polarization (Figure 4.11).

The SFG spectrum of AR_{14} (Figure 4.12) on PS shows the expected methyl symmetric stretching modes associated with the alanine side chains, as well as the structured water mode centered at 3150 cm^{-1}. The SFG spectrum of AR_7 was rather surprising, showing only one mode at 3040 cm^{-1}. This mode does not appear to be

from the arginine side chain (based on the reference SFG spectrum of arginine amino acid), and may be an unknown mode of the backbone.

The SFG spectra of the LK, AK, AR, and FR peptides adsorbed on SiO_2 (Figure 4.13-4.16) show that all of the 14 amino acid peptides adsorb to the surface, but do not generate unique peptide modes. The SFG spectrum of LK_{14} on SiO_2 is the only spectrum that yields an NH mode (at 3300 cm^{-1}). The spectra of AK_{14}, AR_{14}, and FR_{14} only result in a change in the surface water structure upon adsorption. The 7 amino acid peptides do not generate SFG signal, and adsorption results in minimal changes the surface water modes.

Effects of Peptide Concentration

We have observed concentration dependent adsorption on hydrophobic polystyrene. Figure 4.17 shows the SFG spectra of AR_{14} adsorbed on PS from low (1 mg/mL) and high (3 mg/mL) solution. At low concentration, there are no observable vibrational modes from the peptide, but a change in surface water structure occurs following adsorption. On polystyrene, we typically observe an "ice-like" (or tetrahedrally hydrogen bonded) water OH mode centered around 3150 cm^{-1}. Upon adsorption of the peptide, we see water OH modes appear at 3200 and 3400 cm^{-1}, which are peaks associated with less hydrogen-bonded water molecules. This indicates that the peptide does interact with the surface and breaks up the hydrogen bonding of the highly structured surface water molecules, but the average orientation of the side-chains may not be uniform enough (no net dipole field) to give a measurable SFG signal. At a higher concentration of peptide, we observe CH modes at the PS interface, which are associated with the alanine side-chains. The disordered water mode at 3400 cm^{-1} disappears, and the hydrogen-bonded water peak at 3200 cm^{-1} increase in intensity. This change suggests that water molecules

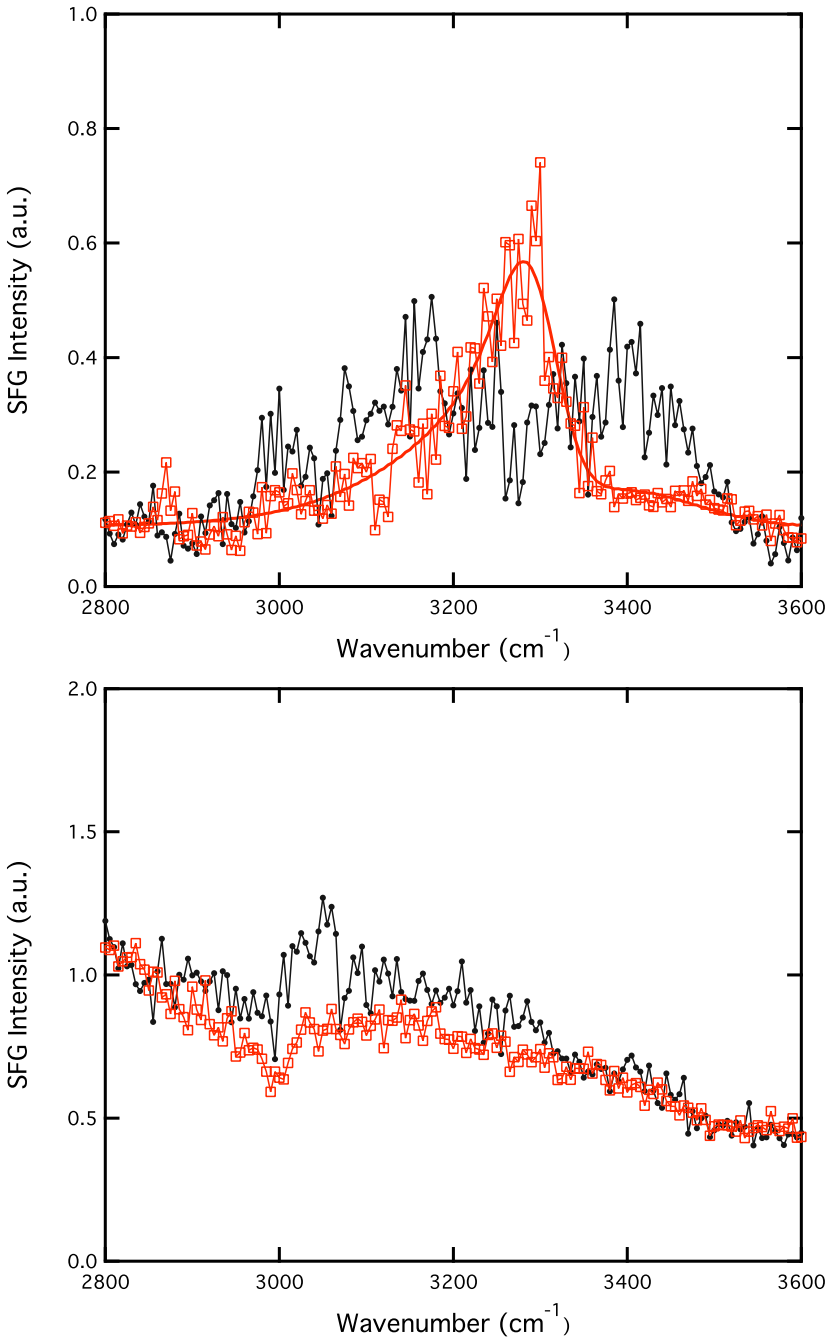

Figure 4.13. SFG spectra of PBS (black) and LK_{14} (red) on SiO_2, top. The peak centered at 3300 cm^{-1} is assigned to an Amide A band of the peptide backbone. SFG spectra of PBS (black) and LK_7 (red) on SiO_2, bottom.

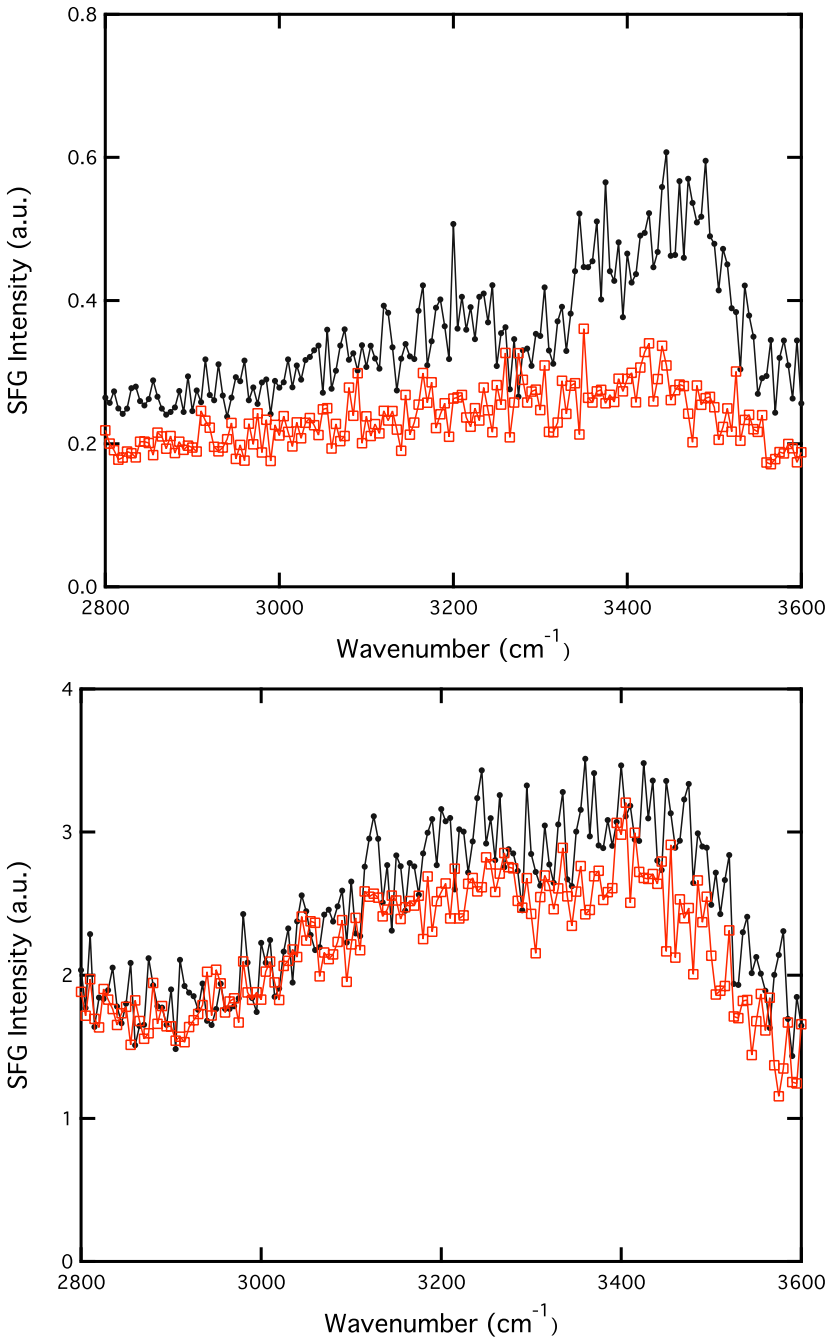

Figure 4.14. SFG spectra of PBS (black) and AK_{14} (red) on SiO_2, top. SFG spectra of PBS (black) and AK_7 (red) on SiO_2, bottom.

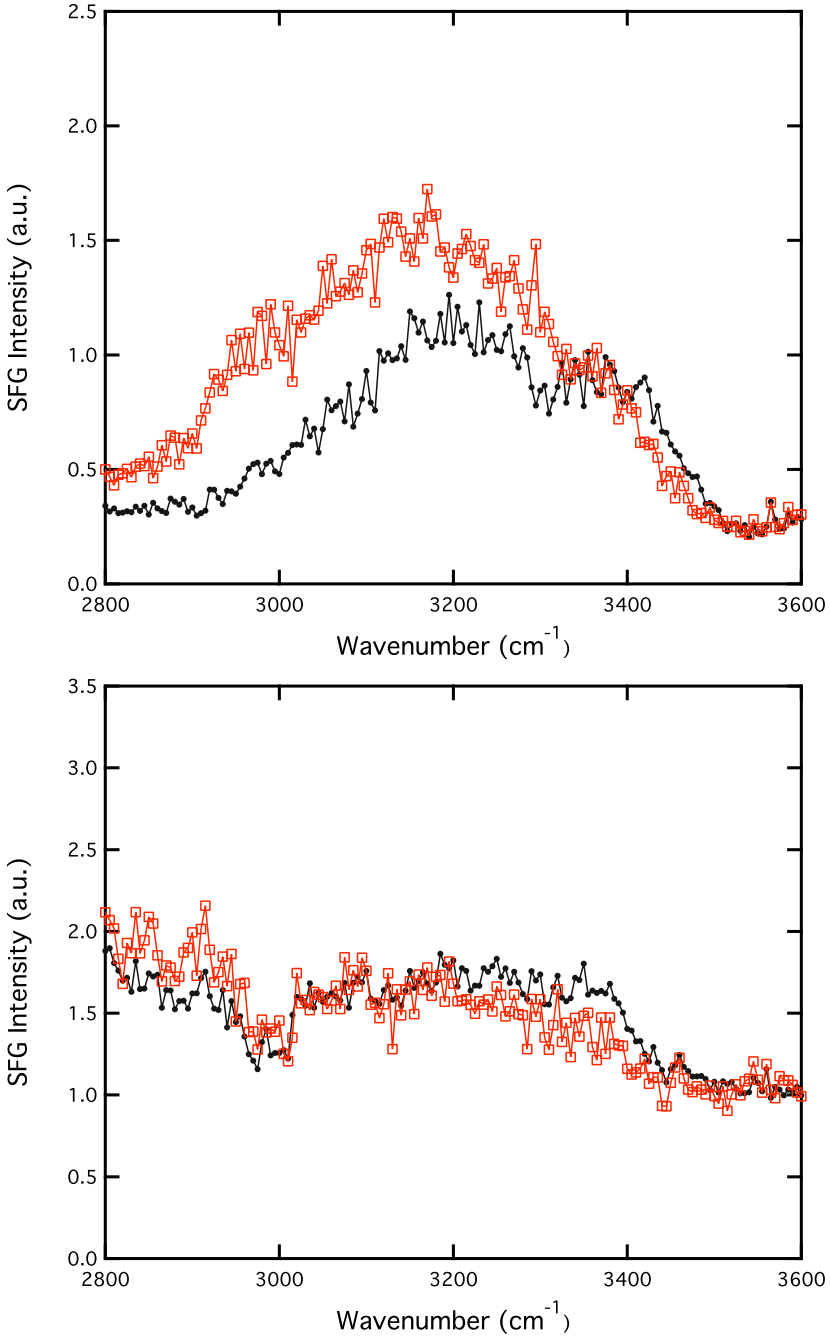

Figure 4.15. SFG spectra of PBS (black) and AR_{14} (red) on SiO_2, top. The water OH stretching mode at 3400 cm^{-1} decreases, and the hydrogen bonded "ice-like" water mode centered at 3200 cm^{-1} increases following peptide adsorption. SFG spectra of PBS (black) and AR_7 (red) on SiO_2, bottom, indicates little or no change upon peptide adsorption.

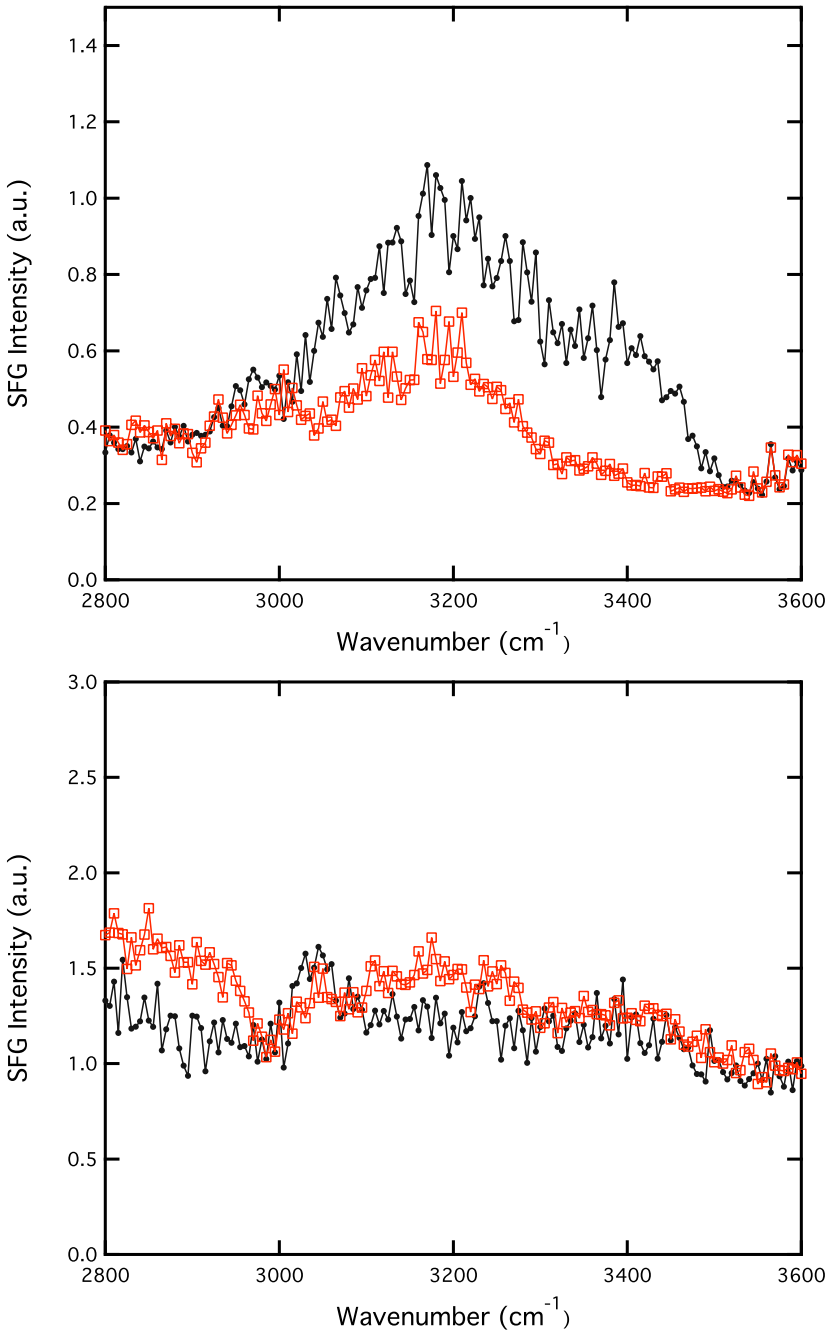

Figure 4.16. SFG spectra of PBS (black) and FR_{14} (red) on SiO_2, top. SFG spectra of PBS (black) and FR_7 (red) on SiO_2, bottom.

order around the peptide, but have fewer hydrogen bonds than water at the bare polystyrene surface.

Effects of Buffer Concentration

The SFG spectra of LK_{14} adsorbed on SiO_2 from different concentrations of PBS solution is shown in Figure 4.18. Using standard pH 7.4 PBS solution concentration (0.01 M phosphate buffered saline, 0.14 M NaCl, 0.0027 M KCl), an NH mode is present at 3300 cm^{-1}. Using a 10 times higher concentration of PBS gives a similar SFG spectrum, with the intensity of the 3300 cm^{-1} mode decreasing only slightly. Similarly, a 10 times more dilute PBS solution results in a slight increase of the NH mode. Below concentrations of 0.1 mM (100 times dilution), the peptide NH mode disappears, and an OH (structured water) mode grows in at 3200 cm^{-1} (with a slight growth of the 3400 cm^{-1} OH mode).

4.4.3 QCM Adsorption Studies

QCM adsorption data was collected for the 14- and 7-amino acid peptides adsorbed onto hydrophilic SiO_2 and hydrophobic PS surfaces. The results summarized in Table 4.2 show the absolute magnitude of the measured change in frequency, $|\Delta f|$ ($\times 10^{-6}$ Hz), at the 3rd overtone upon adsorption onto either polystyrene or silica, and the solution concentration used in the experiment. The peptides all showed monotonic adsorption behavior, where the dissipation mirrored the change in frequency. Only LK_{14} peptide adsorbed on SiO_2 showed multi-step behavior, as discussed in Chapter 3. QCM data for the peptides on PS and SiO_2 are shown in Figures 4.29-4.36 in Appendix II of this chapter.

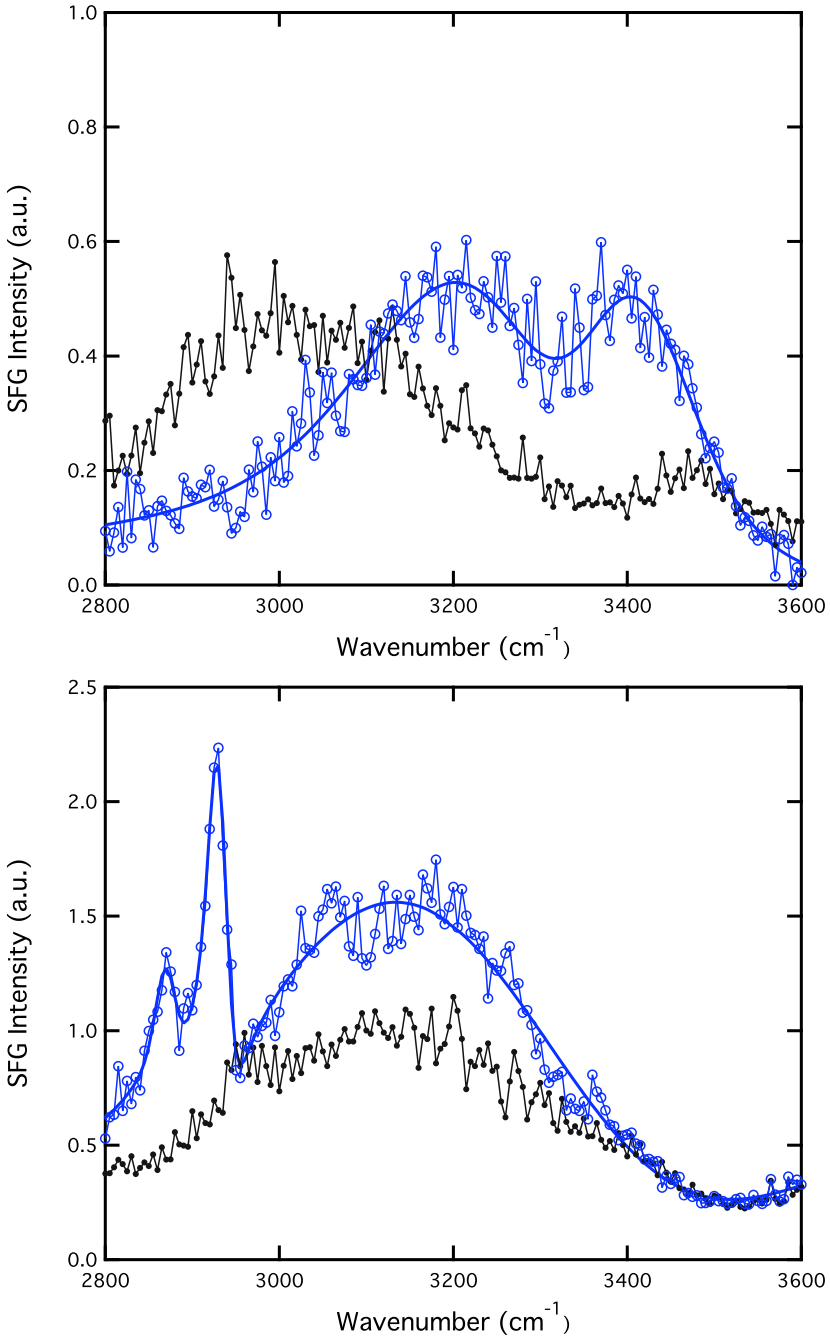

Figure 4.17. SFG spectra of PBS (black) and AR_{14} (blue) on PS-d_8 at low concentration, top figure. The broad peaks centered at 3200 and 3400 cm^{-1} are due to structured water modes. Bottom figure are the SFG spectra of PBS (black) and AR_{14} (blue) on PS-d_8 at high concentration. CH resonances are observed at 2861 and 2933 cm^{-1}.

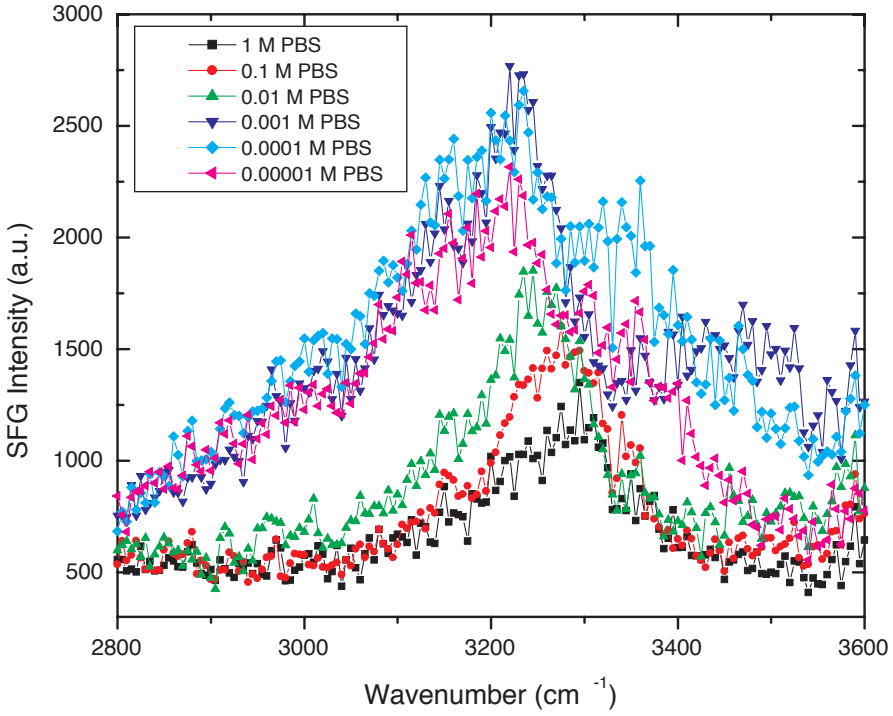

Figure 4.18. SFG spectra of LK_{14} adsorbed on PS-d_8 from PBS solutions with varying concentration. The signal intensity of the NH mode due to LK_{14} disappears in PBS solution below 0.1 mM PBS.

Table 4.2. QCM Results: Frequency Change, $|\Delta f_3|$ ($\times 10^{-6}$ Hz), Upon Adsorption

Peptide	PS	SiO_2	Solution Concentration
LK_{14}	8	16	1 mg/mL
AK_{14}	6	9	1 mg/mL
AR_{14}	5	12	1 and 3 mg/mL
FR_{14}	12	12	100 μg/mL
LK_7	1	0	100 μg/mL
AK_7	3	1	1 mg/mL
AR_7	6	12	1 mg/mL
FR_7	5	0	50 μg/mL

4.4.4 AFM Topographical Studies

The AFM topographical data presented in Chapter 3 for LK_{14} peptide adsorbed on SiO_2 and PS showed significant differences in the feature height, surface roughness, and surface friction for each surface. AFM topographic data for the LK, AK, AR, and FR peptides are collected in Figures 4.37-4.46 in Appendix III of this chapter. All of the peptides adsorbed on PS were difficult to image. Although PS is a relatively smooth surface (roughness $\sim$ 0.3 nm), peptide features were difficult to distinguish from the polymer surface. Friction measurements of the adsorbed peptides typically showed a slight decrease relative to the bare PS surface, and an increase in friction relative to the bare SiO_2 surface. The AFM results of peptides adsorbed on SiO_2 were more varied. The 14 amino acid peptides all were imaged on the atomically flat SiO_2 surface. It was difficult to obtain AFM results for the 7 amino acid peptides on SiO_2. QCM data indicates that AK_7, LK_7, and FR_7 all had a low affinity for adsorption on SiO_2, which explains the lack of features measured using AFM. In contrast, AR_7 adsorbed on SiO_2 (Figure 4.43) shows strand-like features of regular widths ($\sim$1 μm) and heights (2-3 nm).

4.4.5 Circular Dichroism Studies of Solution Phase Peptides

CD spectra for the LK, AK, AR, and FR peptides are presented in Appendix IV (Figure 4.47-4.55) of this chapter. CD spectra were collected between 190 and 240 nm in phosphate buffered saline (PBS) solution. The PBS solution cut-off occurs around 200 nm, so this is not an ideal buffer for use in CD measurements (but was used for consistency with other measurements). The CD spectrum of LK_{14} was presented in Chapter 2, and shows that LK_{14} has a predominantly α-helical structure in solution. With the exception of LK_{14}, none of the peptides examined in this study had a preferred solution secondary structure under the typical solution concentrations used here. The CD spectrum of LK_{14} was also dependent on the concentration of buffer used, and shows the loss of helical structure at PBS concentration below 0.1 mM (Figure 4.20). At very high solution concentration (4 mg/mL), AK_{14} and AR_{14} peptides show a peak at 222 nm, which is characteristic of an α-helix (Figure 4.21, 4.54).

4.5 Discussion

We have performed adsorption experiments of short model polypeptides on hydrophobic PS and hydrophilic SiO_2 substrates aimed at understanding the role of peptide sequence and secondary structure on adsorption. The SFG spectra of polypeptides adsorbed to hydrophobic and hydrophilic surfaces indicate that adsorption is strongly dependent on surface hydrophobicity. The molecular interactions and ordering of LK_{14} at the solid/water interface was compared on three different surfaces. As shown in Figure 4.1, ordered methyl groups of leucine side-chains are observed at the buffer/PS-d_8 interface: (CH_3 vs at 2869 cm^{-1}, CH or the Fermi Resonance of a CH_2 mode at 2895 cm^{-1}, and the Fermi Resonance of a CH_3 mode at 2935 cm^{-1}).[1; 5]

Only ordered NH resonances are detected at the buffer/SiO_2 interface. Both CH and NH peaks are present on CaF_2, since the surface charge is close to neutral and there is not as strong of a driving force for specific adsorption of the LK_{14} molecules. On SiO_2, with an isoelectric point of 2, adsorption through charged lysine side chains is likely the driving force, while dehydration of the hydrophobic leucine side chains causes adsorption on PS through the leucine side-chains. The difference in SFG spectra indicates that the amphiphilic LK_{14} peptide adopts completely different average orientations in response to different surfaces. A significant difference in the structure of water is observed on these surfaces: on PS-d_8 a broad OH mode centered at 3092 cm^{-1} as compared to a much weaker OH mode at 3190 cm^{-1} on SiO_2 and CaF_2 in the presence of adsorbed LK_{14} peptide. Time-dependent adsorption was observed on PS-d_8, which may be related to diffusion or kinetic effects. Current studies by Samuel et al. of LK_{14} adsorbed on a fluorocarbon surface do not show a time dependence in the CH region.[7] The different dynamic aspects observed in the molecular bonding behavior (as examined by SFG), as compared to the measured adsorbed mass and morphology (obtained by QCM and AFM), demonstrate that each technique is also capable of providing unique kinetic information and warrants more detailed study.

To investigate the effects of side chain character on adsorption, we have studied amphiphilic peptides with a range of hydrophobic side chain hydrophobicities: alanine, phenylalanine, and leucine. On PS, adsorption of the 14-mer peptides seems to be controlled by the hydrophobic character of the side chains. The SFG spectra of the reference bulk amino acids and the 14-mer peptides adsorbed on PS spectra are strikingly similar. This suggests that only the hydrophobic residues are interacting with the surface, and in an extremely dehydrated environment (equivalent to the air/solid interface). The 7-mer β-strand peptides do not show a clear trend. Both of the LK_7 (α and β sequences) adsorb via hydrophobic interactions of the leucine side chains. The SFG spectra of AR_7 and AK_7 do not show modes associated with alanine, so

it is likely that the these peptides are adsorbed onto the surface through the amide backbone, with side-chains interdigitating parallel to the surface. The phenyl groups of the F side-chain may interact with the PS surface through π-stacking. The SFG spectra shown here, obtained in *ssp* polarization, are more sensitive to molecules or functional groups with dipoles oscillating normal to the surface (i.e. have a strong dipole component in the z direction). Polarization experiments which measure dipoles oscillating more parallel to the surface are necessary (*sps* polarization) for assignment of the modes observed in the spectra of AR_7, AK_7, and FR_7.

We have observed similar spectroscopic results for adsorption on PS which are irrespective of the exact secondary structure of the polypeptide or protein backbone. This is evident in Figure 4.7 which shows similar spectra for α and β LK_7 peptides; and in Figure 4.22 comparing the CH region of LK_{14}, leucine amino acid, and bovine serum albumin protein. This may be due to the conformational flexibility in the large, branched side-chains (leucine, lysine, arginine, etc.) of the peptides we have examined. The forces driving surface orientation (hydrophobic or electrostatic interactions associated with the side chains) appear to be local interactions, and are determined by the properties of the interface. This may explain why we do not observe the Amide A mode for LK_{14} on SiO_2, or CH modes for LK_{14} on PS. On a surface where the driving forces for ordering via hydrophobic or electrostatic interactions is similar, it is possible to observe both types of surface interactions (e.g. LK_{14} on CaF_2, Figure 4.2). The similarities between the SFG spectra of LK_{14}, leucine amino acid, and BSA on PS are striking, given the range of structural levels. Similar SFG spectra have been reported for various proteins, including fibrinogen and lysozyme, adsorbed on polystyrene surfaces.[12; 14; 13] This strongly suggests that local interactions dominate the SFG response.

SFG spectra of LK, AK, AR and FR peptides adsorbed on SiO_2 do not show vibrational modes associated with the peptides, except for an NH mode observed fol-

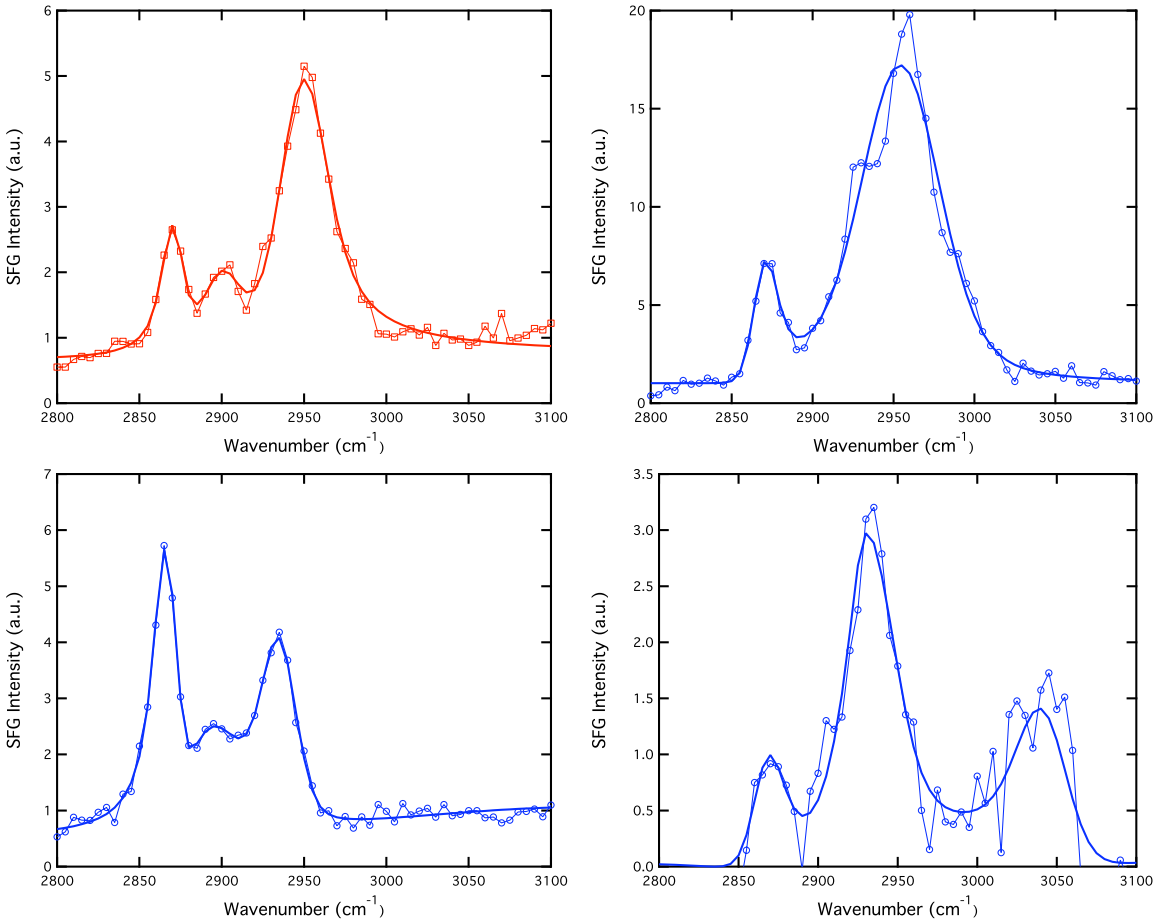

Figure 4.19. SFG spectrum of dried Leucine amino acid on SiO_2, dried Leucine on PS-d_8, LK_{14} on PS-d_8, and BSA on PS-d_3.

lowing LK_{14} adsorption. QCM data shows that the 14 amino acid peptides all adsorb strongly onto both PS and SiO_2, while the 7 amino acid peptides interact weakly with both surfaces. LK_7 and FR_7 have very low solubility, which may contribute to weak adsorption. Both peptides show negligible SFG signal, and no measurable adsorption on SiO_2 using QCM or AFM. AR_7 and AK_7 are highly soluble, and show a high affinity for the SiO_2 surface. However, no SFG signal is detected on SiO_2, indicating a lack of a specific orientation at the surface.

The NH stretch on SiO_2 observed following LK_{14} adsorption is assigned to the Amide A mode of the peptide backbone.[9; 13; 14] The presence of this backbone mode suggests that LK_{14} maintains its solution phase helical structure upon adsorption. Others have reported that the helical structure is stable on polystyrene.[8] Evidence for this is given by our SFG studies performed at different buffer concentrations. When LK_{14} is adsorbed from 1 M and 0.1 M PBS solution, the Amide A band is present. Below 0.1 mM buffer concentration, the NH mode disappears(Figure 4.18). CD studies of the solution structure at these same concentrations reveal the loss of secondary structure of LK_{14} in PBS solutions of below 0.01 M (Figure 4.19). Salt is known to stabilize secondary structure in peptides and proteins, and is likely too dilute in PBS solutions below 0.01 M.[3; 4; 15; 18] AFM and QCM data presented in Chapter 3 shows multilayer adsorption for LK_{14} on SiO_2, and surface features that likely correspond to helical aggregates.

The nominal chain length necessary for secondary structure formation is 4 residues for β-strand formation and 14 residues for α-helix formation. Short peptides (< 20 amino acids) have many more degrees of conformational freedom than proteins, and it is unusual for a peptide to adopt a single predominant solution structure.[10] Degrado and Lear have shown that the LK_{14} peptide aggregates to form tetramers in solution, which stabilizes the helical structure.[4] Leucine is the most nonpolar amino acid, so we hypothesize that the driving forces for secondary structure formation is larger

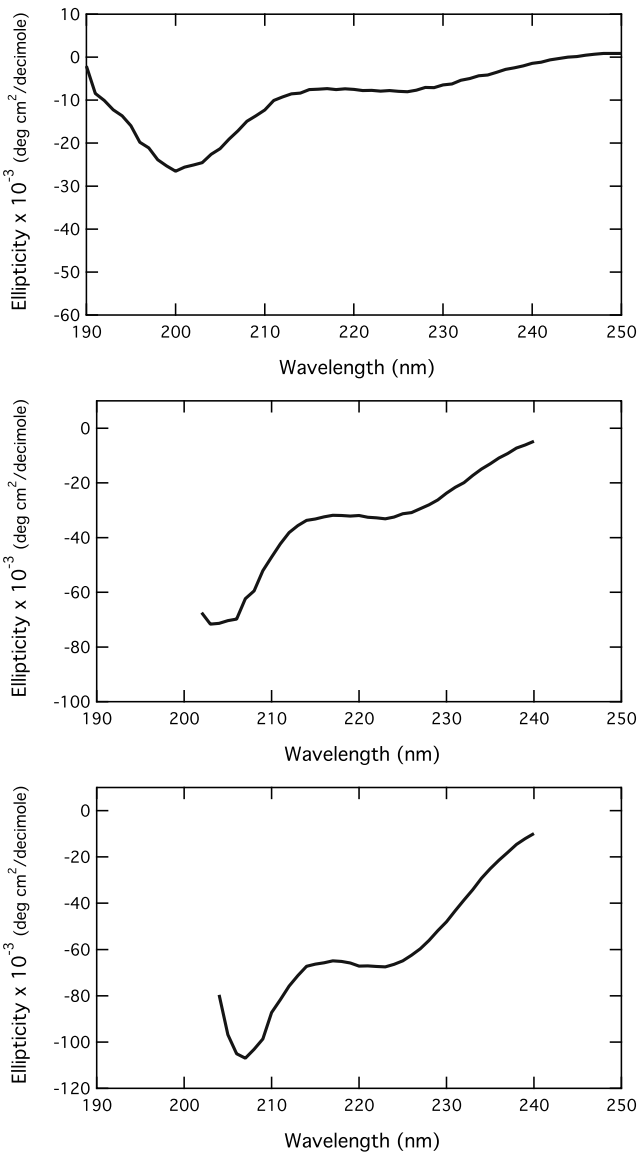

Figure 4.20. CD spectra of LK_{14} at different buffer concentration: in 0.005 M the peptide is a random coil (top); helical secondary structure appears in 0.01 M PBS and a textbook α-helical signature (strong residual ellipticity at 208 and 222 nm) is obtained in the 0.1 M PBS solution (bottom).

for the L containing peptides than A or F peptides. It has been shown that for LK_{14} concentrations below 0.01 mM, the peptide is primarily a random coil.[16] It is possible that the critical concentration for secondary structure formation for the AK, AR, and FR peptides is higher than the concentrations used in this study. The SFG spectra of AR_{14} (Figure 4.17) adsorbed from a 1 mg/mL and 3 mg/mL show concentration dependent adsorption behavior. At 1 mg/mL, the peptide interacts with the surface as indicated by the change in surface water structure. However, no peaks associated with the peptide are present, which may be due to a lack of specific adsorption (no net dipole field at the surface). At 3 mg/mL, strong CH resonances from the alanine side chain appear. CD spectra of AR_{14} peptide measured at two concentrations (Figure 4.20) shows a measurable change in the CD spectrum. The CD spectrum obtained using a 1 mg/mL solution appears to be random coil. At higher concentration, a strong residual absorbance appears at 224 nm, which is indicative of α-helical structure. However, at the higher concentration in PBS solution it was difficult to measure meaningful CD data over the necessary range (190-240 nm) due to solvent cut-off, so the full spectrum could not be obtained. A thorough concentration study using CD is needed. QCM data for adsorption at these concentrations shows a similar change in frequency upon adsorption, which is proportional to a similar adsorbed mass, despite any difference in solution or secondary structure (Figure 4.22). This is further evidence that the solution secondary structure is important, and results in a different adsorption orientation than for identical peptides with random coil solution structure (i.e. lower concentration solutions).

It is unclear how the solution phase secondary structure affects the adsorbed peptide orientation, but CD and SFG data strongly suggest that solution secondary structure leads to a specific adsorbed orientation in the cases of LK_{14} on SiO_2 and AR_{14} on PS. A thorough concentration study using CD and SFG (including polarization experiments) is required in order to fully understand this puzzling data. The

following quote appeared in an article published during the writing of this thesis: "Some of our observations do not lend themselves to straightforward interpretation. However, from discussions with other researchers in the field we have come to appreciate that we are not the only group to obtain results that defy a simple explanation. We have chosen to include these puzzling data in this paper, partly to illustrate the enigmas that exist in sum-frequency experiments on confined monolayers, partly as encouragement to other researchers confronted by similar phenomena, but principally in the belief that rational physical explanation do underly our results, even if that explanation is not always apparent from the available evidence."[21]

4.6 Conclusions

Peptides designed to form both α-helical and β-strand structures were studied to determine whether the intrinsic affinity of a peptide for a given secondary structure mediates adsorption. The model LK, AK, AR and FR peptides we have studied readily adsorb and order on hydrophobic PS-d_8 surface, as expected based on their designed sequence. We can not confirm the exact secondary structure at the surface without SFG data in the Amide I region of infrared (1500-1800 cm^{-1}). The similarity between the peptides adsorbed on PS-d_8, and the bulk amino acids indicate the separation of hydrophobic and charged amino acid residues is occurring. The complete separation of the hydrophilic and hydrophobic side chains in these peptides is only possible through secondary structure formation. Simple aggregation of the peptides, with the lack of secondary structure, would not likely lead to the strong SFG signal observed (which is proportional to the degree of molecular orientation).

The 14- and 7-amino acid peptides do not appear to specifically adsorb when exposed to SiO_2, but do interact with the surface resulting in a change in the structure of surface water molecules. The exception is LK_{14} which has a high degree of sec-

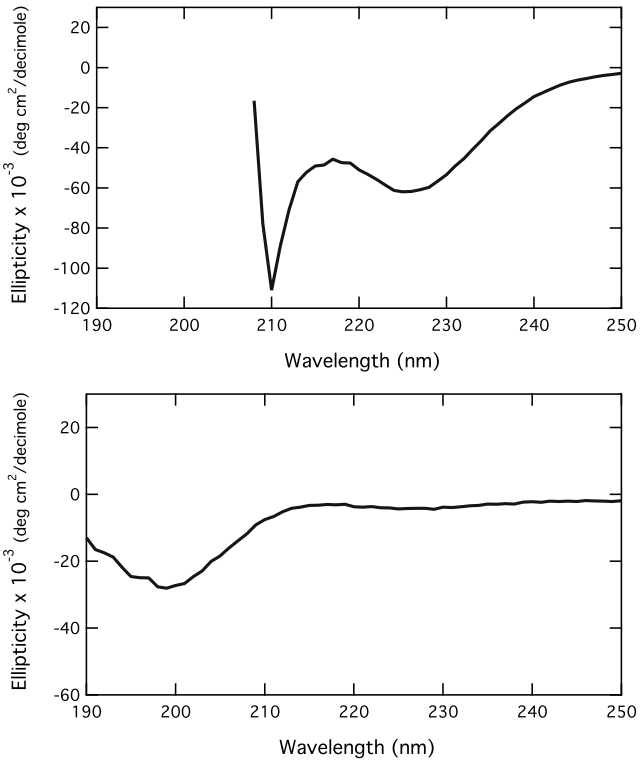

Figure 4.21. CD data of AR_{14}. The strong residual ellipticity at 223 nm (top figure) from a 3 mg/mL solution of AR_{14} is characteristic of α-helical secondary structure. At 1 mg/mL, no residual ellipticity is detected (bottom figure), indicating that the peptide is primarily random coil at this concentration.

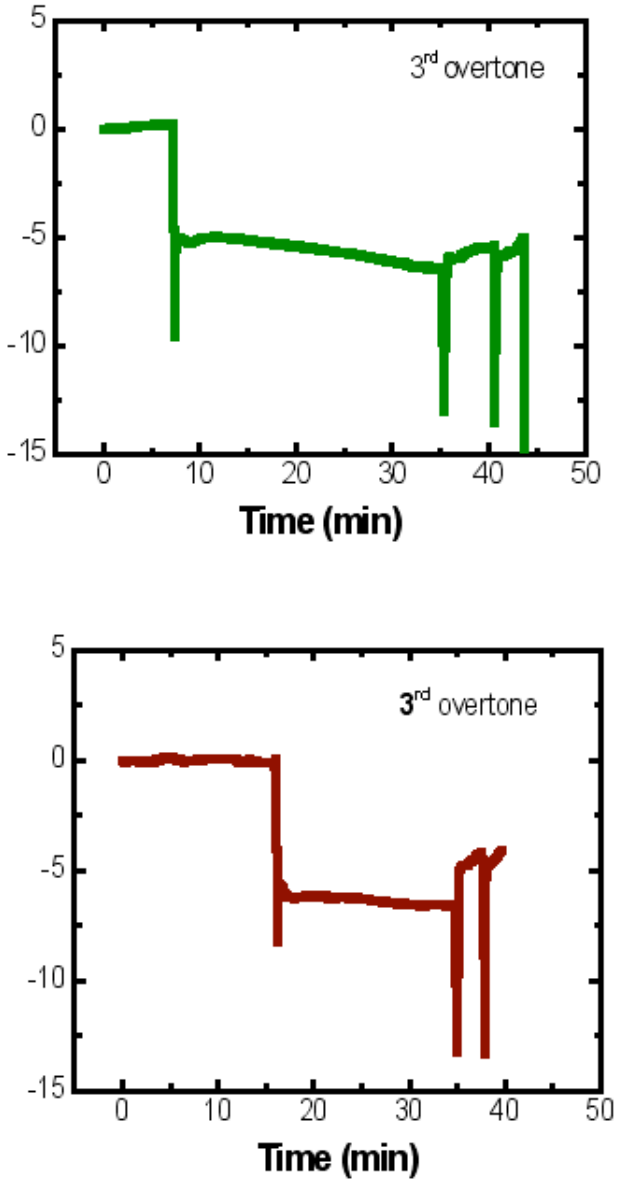

Figure 4.22. QCM data of AR_{14} adsorbed on PS-d_8 from a 1 mg/mL (top) and 3 mg/mL (bottom) solution. The change in frequency upon adsorption is nearly equal, indicating similar adsorbed amounts from the high and low concentration solutions.

ondary structure in solution (α-helical tetramers). This solution structure appears to be maintained on the surface, where a backbone Amide A (NH) stretch is observed. QCM and AFM data, presented in Chapter 3, suggest multilayer adsorption on SiO_2 and adsorbate features which match the dimensions of helical aggregates. CD data shows that none of the AK, AR and FR peptides have a predominant secondary structure in solution. QCM confirms adsorption on SiO_2, so a difference in molecular orientation is responsible for the lack of SFG spectral features. This data also suggests that electrostatic interactions represent a weaker driving force for secondary structure formation (i.e. ordering) on SiO_2 than hydrophobic interactions on PS.

In addition to SFG measurements in the Amide region, future experiments should include polarization measurements to allow for definitive mode assignments and determination of the degree of orientation which leads to the observed differences in the SFG spectra. Additional amphiphilic peptides should be synthesized by replacing positively charged lysine and arginine with negatively charged amino acids, which may allow for definitive assignment of the Amide A mode.

Bibliography

[1] Mermut, O.; Phillips, D. C.; York, R. L.; McCrea, K. R.; Ward, R. S.; Somorjai, G. A. *J. Am. Chem. Soc.*, **2006**, *128*, 3598.

[2] King, D.; Fields, C.; Fields, G. *Int. J. Pept. Protein Res.* **1990**, *36*, 255.

[3] DeGrado, W. F.; Lear, J. D. *J. Am. Chem. Soc.* **1985**, *107*, 7684.

[4] DeGrado, W. F.; Wasserman, Z. R.; Lear, J. D. *Science* **1989**, *243*, 622.

[5] Ji, N.; Shen, Y. R. *J. Chem. Phys.* **2004**, *120*, 7107.

[6] Watry, M. R.; Richmond, G. L. *J. Phys. Chem. B.* **2002**, *106*, 12517.

[7] Samuel, N. T.; McCrea, K. R.; Gamble, L. J.; Ward, R. S.; Stayton, P. S.; Somorjai, G. A.; Castner, D. G. **2006**, in preparation.

[8] Long, J. R.; Oyler, N.; Drobny, G. P.; Stayton, P. S. *J. Am. Chem. Soc.* **2002**, *124*, 6297.

[9] Knoeson, A.; Pakalnis, S.; Wang, M.; Wise, W.; Lee, N.; Frank, C. W. *IEEE J. Sel. Top. Quant.* **2004**, *10*, 1154.

[10] Marqusee, S.; Baldwin, R. L. *Proc. Natl. Acad. Sci. USA*, **1987**, *84*, 8898.

[11] Lee, N. H.; Christensen, L. M.; Frank, C. W. *Langmuir* **2003**, *19*, 3525.

[12] Cremer, P. *Langmuir*, **2002**, *18*, 2807.

[13] Wang, J.; Chen, X.; Clarke, M. L.; Chen, Z. *J. Phys. Chem. B.*, **2006**, *110*, 5017.

[14] Clarke, M. L.; Wang, J.; Chen, Z. *J. Phys. Chem. B.*, **2005**, *109*, 22027.

[15] Kerth, A.; Erbe, A.; Dathe, M.; Blume, A. *Biophys. J.* **2004**, *86*, 3750.

[16] Dieudonne, D.; Gericke, A.; Flach, C. R.; Jiang, X.; Farid, R. S.; Mendelsohn, R. *J. Am. Chem. Soc.* **1998**, *120*, 792.

[17] Castano, S.; Desbat, B.; Laguerre, M.; Dufourcq, J.; *Biochim. Biophys. Acta.* **1999**, *1416*, 176.

[18] Maget-Dana, R.; Lelievre, D.; Brack, A. *Biopolymers* **1999**, *49*, 415.

[19] Shoichet, M. S., and McCarthy, T. J., *Macromolecules*, **24**, 1441, (1991)

[20] Yasui, S. C., and Keiderling, T. A., *J. Am. Chem. Soc.*, **108**, 5576, (1986)

[21] Beattie, D. J.; Fraenkel, R.; Winget, S. A.; Peterson, A.; Bain, C. D. *J. Phys. Chem. B*, **2006**, *110*, 2278.

4.7 Appendix I: SFG Gallery

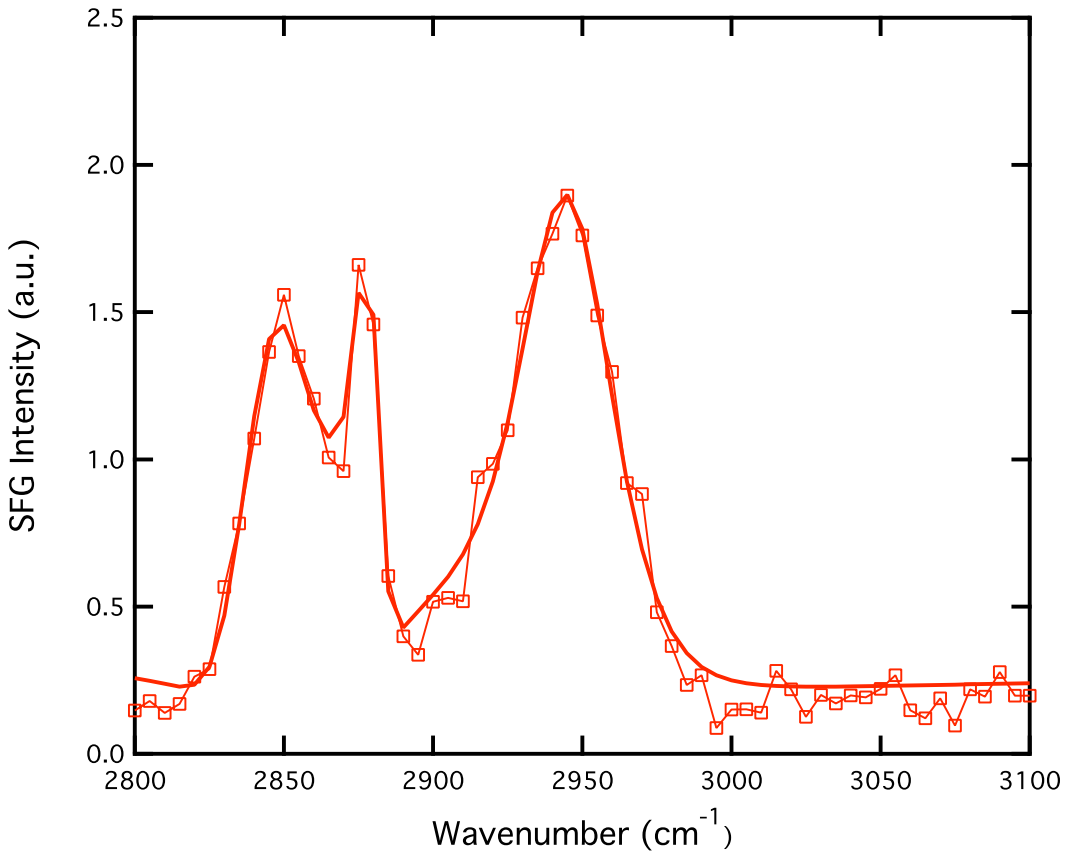

Figure 4.23. SFG spectrum of dried Lysine on SiO_2. The peaks at 2850, 2879, and 2952 cm^{-1} are assigned to CH_2 ν_s, a Fermi resonance of CH_2 ν_s, and a Fermi resonance of CH_2 ν_a, respectively.

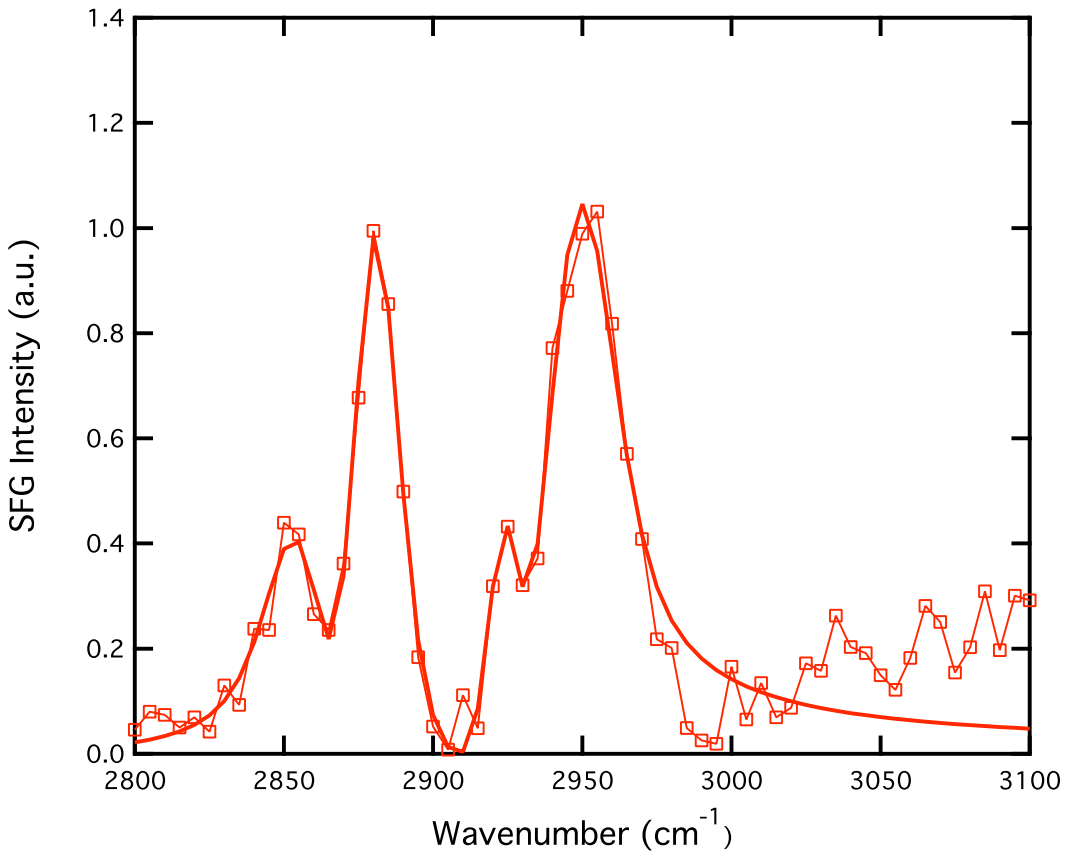

Figure 4.24. SFG spectrum of dried Arginine on SiO_2. The peaks at 2860, 2878, 2923, and 2943 cm^{-1} are assigned to CH_2 ν_s, a Fermi resonance of CH_2 ν_s, CH_2 ν_a and a Fermi resonance of CH_2 ν_a, respectively.

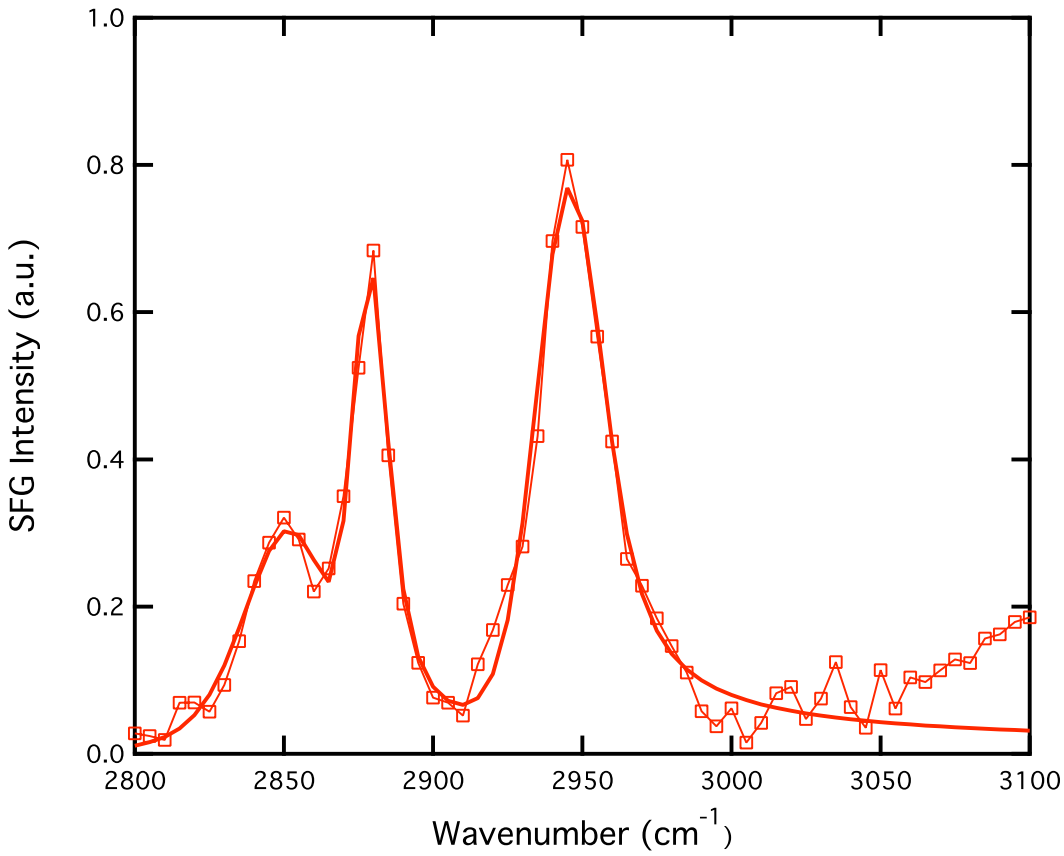

Figure 4.25. SFG spectrum of dried Alanine on SiO_2. The peaks at 2852, 2877, and 2943 cm^{-1} are assigned to CH_3 ν_a, CH_3 ν_s, and a Fermi resonance of CH_3 ν_s, respectively.

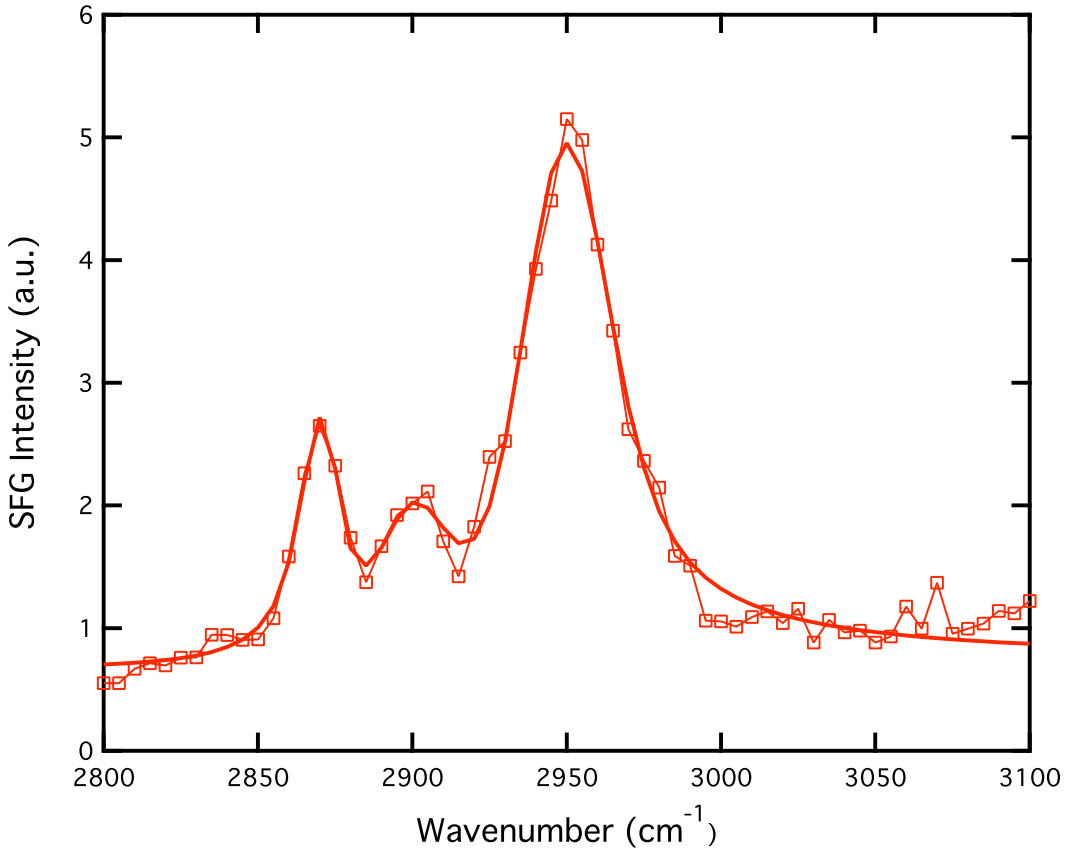

Figure 4.26. SFG spectrum of dried Leucine on SiO_2. The peaks at 2874, 2899, and 2942 cm^{-1} are assigned to methyl symmetric stretch, CH_3 ν_s, CH stretch, and a Fermi resonance of CH_3 ν_s, respectively.

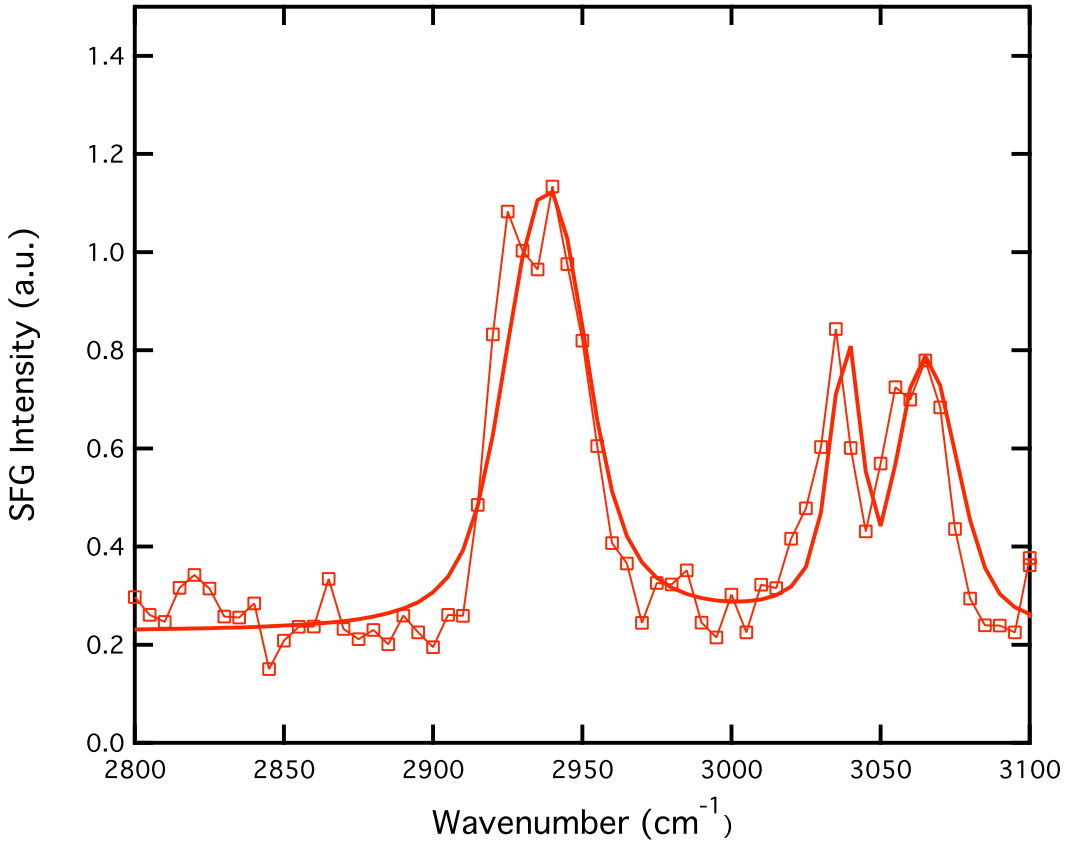

Figure 4.27. SFG spectrum of dried Phenylalanine on SiO_2, *ppp* polarization. The peaks at 2934, 3036, and 3059 cm^{-1} are assigned to methylene symmetric stretch, CH_2 ν_s, and phenyl asymmetric and symmetric stretches, ν_{7b} and ν_2, respectively.

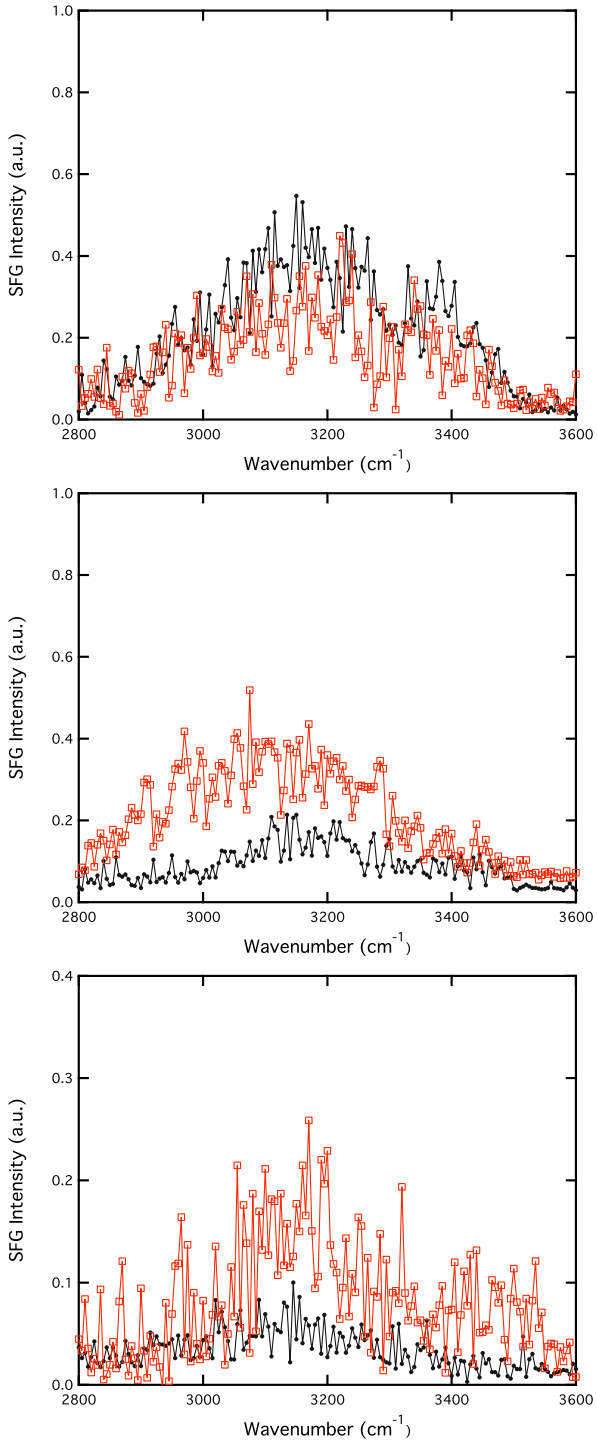

Figure 4.28. SFG spectra of A_{14} (top), K_{14} (middle) and L_{14} (bottom) on SiO_2. Background PBS spectra are shown in black. The SFG spectrum of A_{14} is nearly identical to the buffer background, indicated little interaction with the surface. Both K_{14} and L_{14} cause a change in the surface water structure, but show no unique peptide modes, indicating an interaction but lack of ordering at the surface.

4.8 Appendix II: QCM Gallery

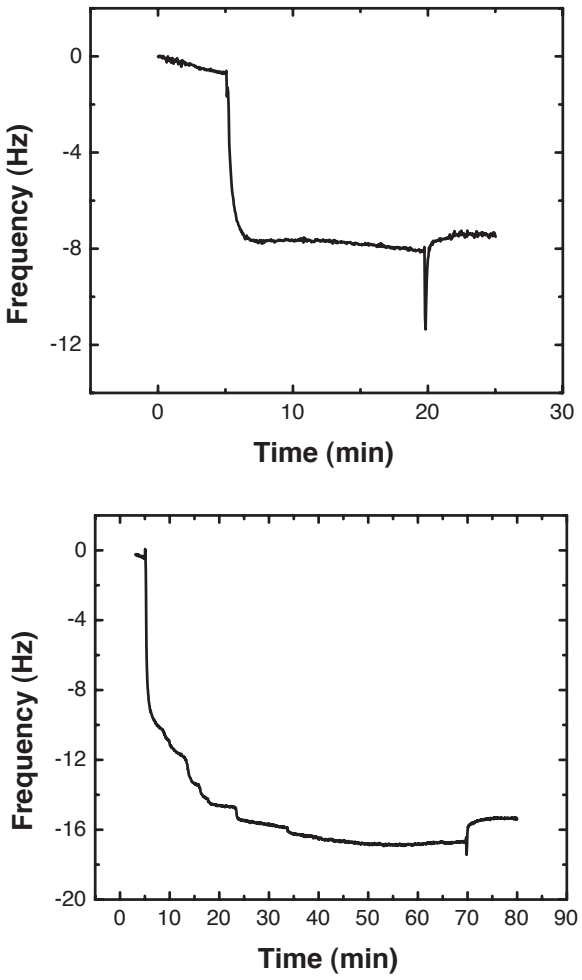

Figure 4.29. QCM data of LK_{14} on PS (top) and SiO_2 (bottom)

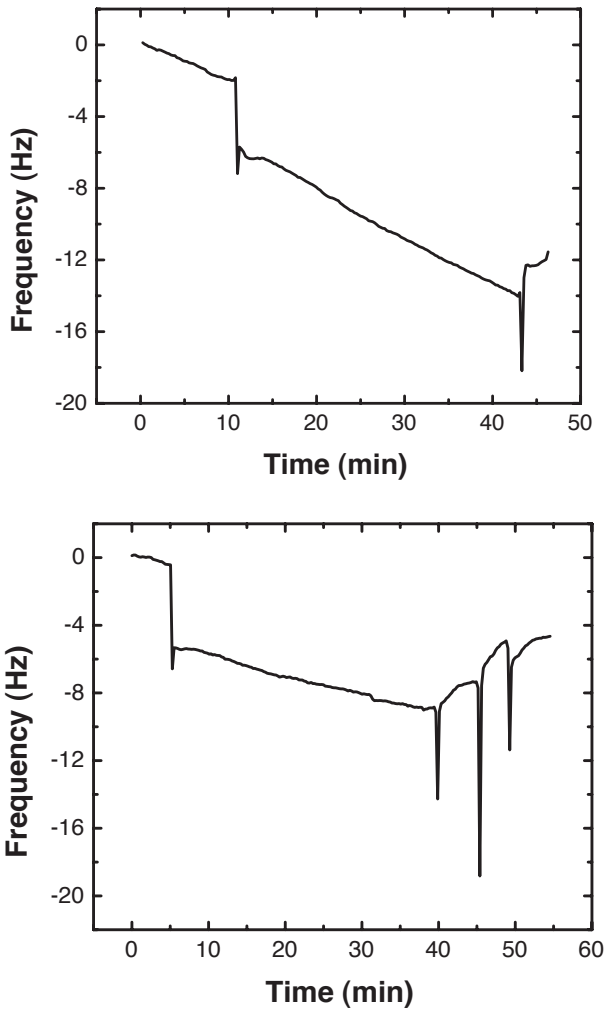

Figure 4.30. QCM data of AK_{14} on PS (left) and SiO_2 (right)

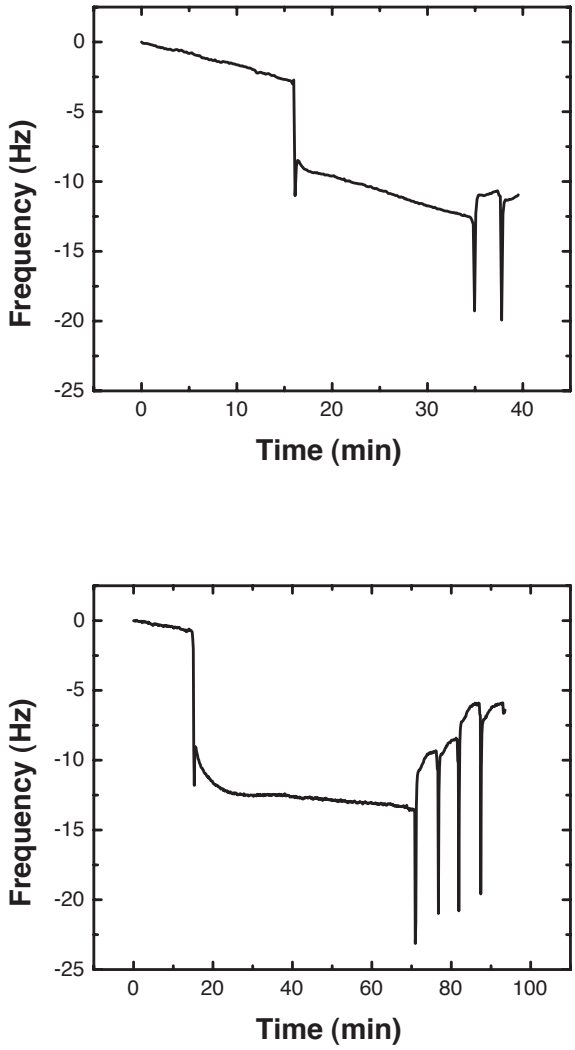

Figure 4.31. QCM data of AR_{14} on PS (top) and SiO_2 (bottom)

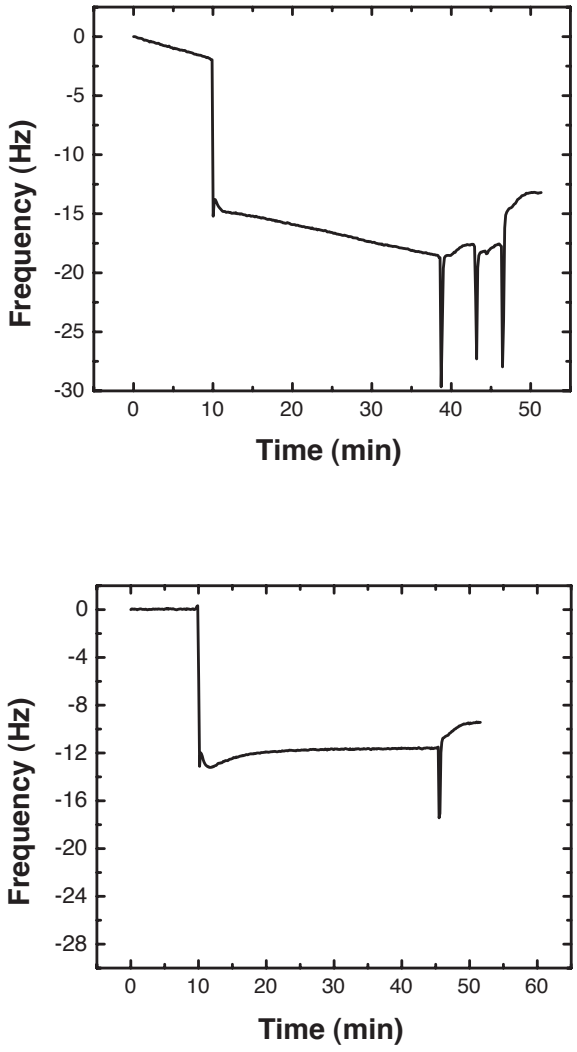

Figure 4.32. QCM data of FR_{14} on PS (top) and SiO_2 (bottom)

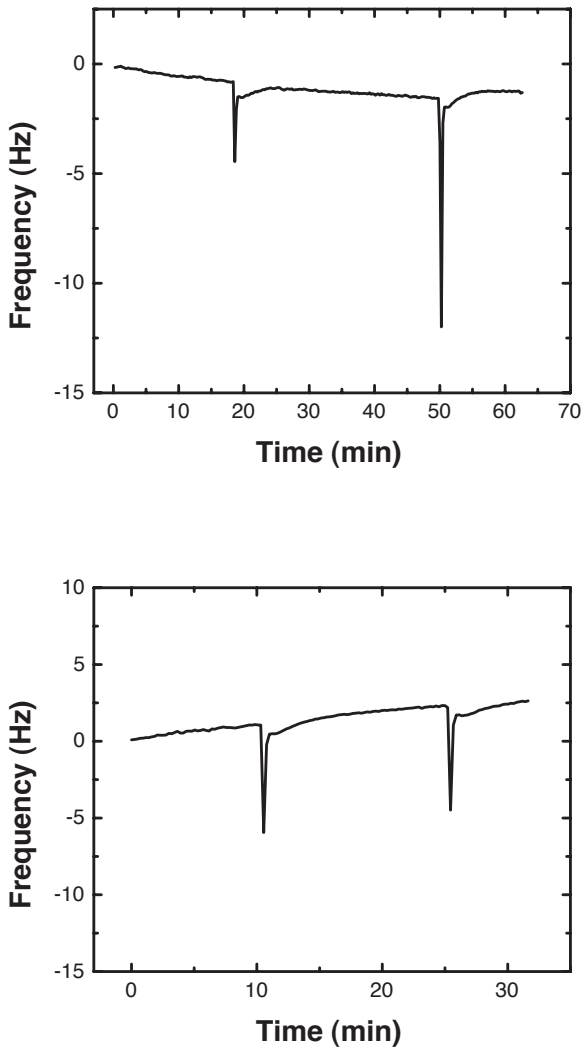

Figure 4.33. QCM data of LK_7 on PS (top) and SiO_2 (bottom)

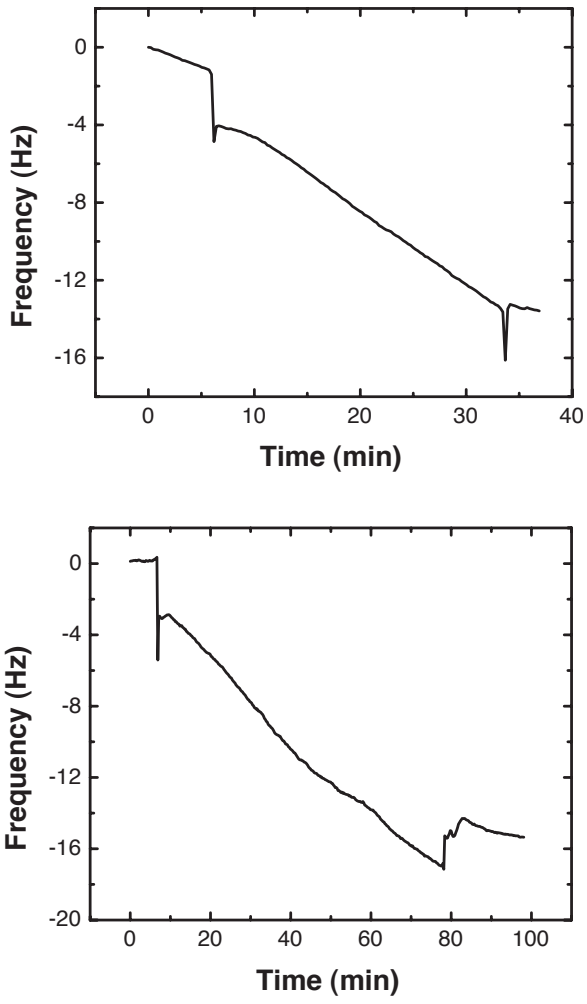

Figure 4.34. QCM data of AK_7 on PS (top) and SiO_2 (bottom)

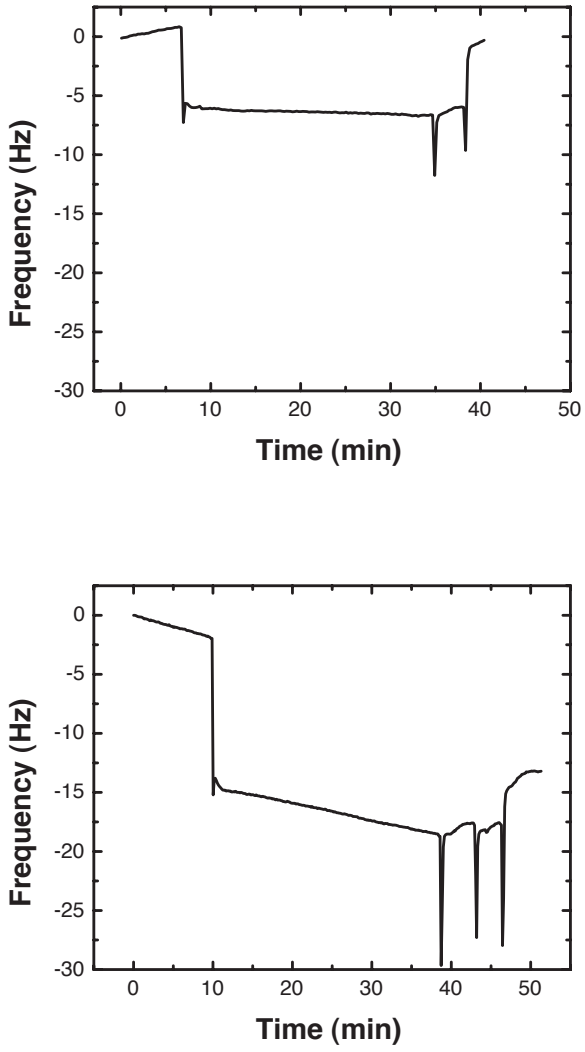

Figure 4.35. QCM data of AR_7 on PS (top) and SiO_2 (bottom)

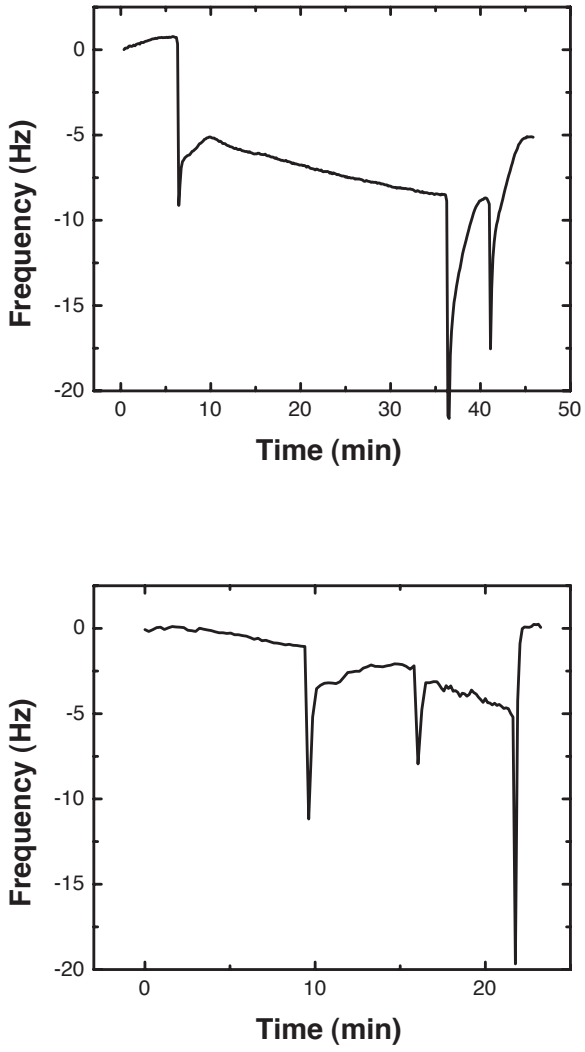

Figure 4.36. QCM data of FR_7 on PS (top) and SiO_2 (bottom)

4.9 Appendix III: AFM Gallery

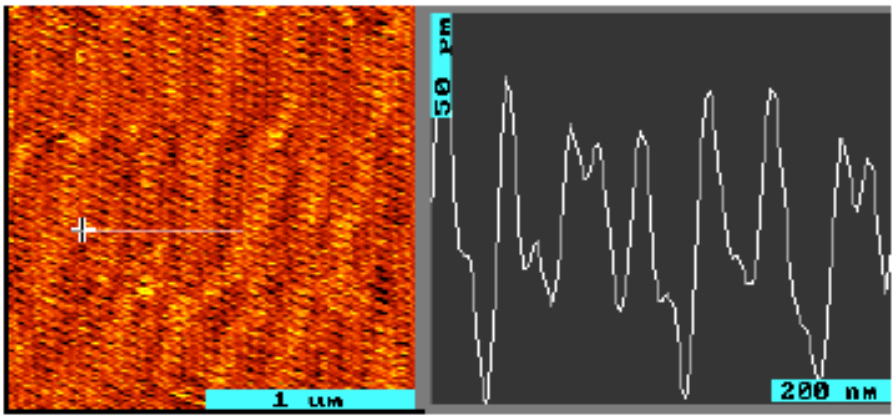

Figure 4.37. AFM topography data for bare SiO_2.

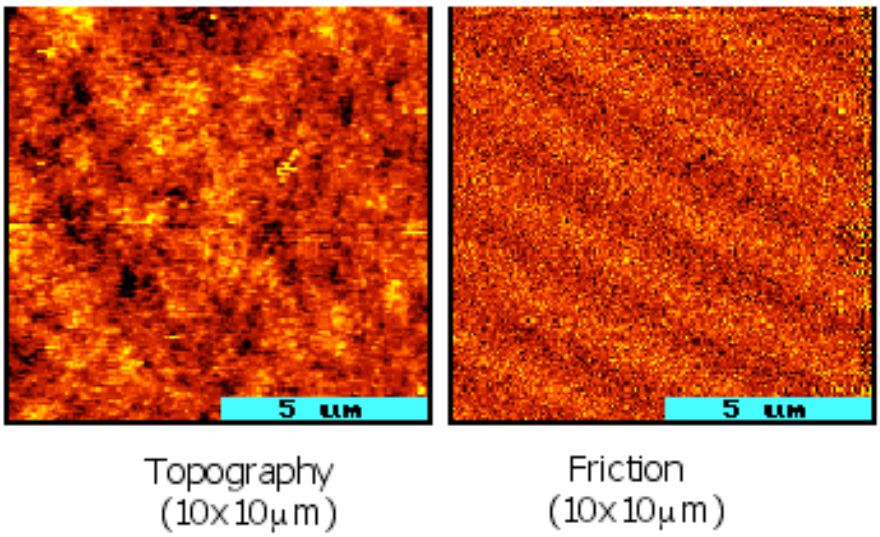

Figure 4.38. AFM topography and friction data for bare PS.

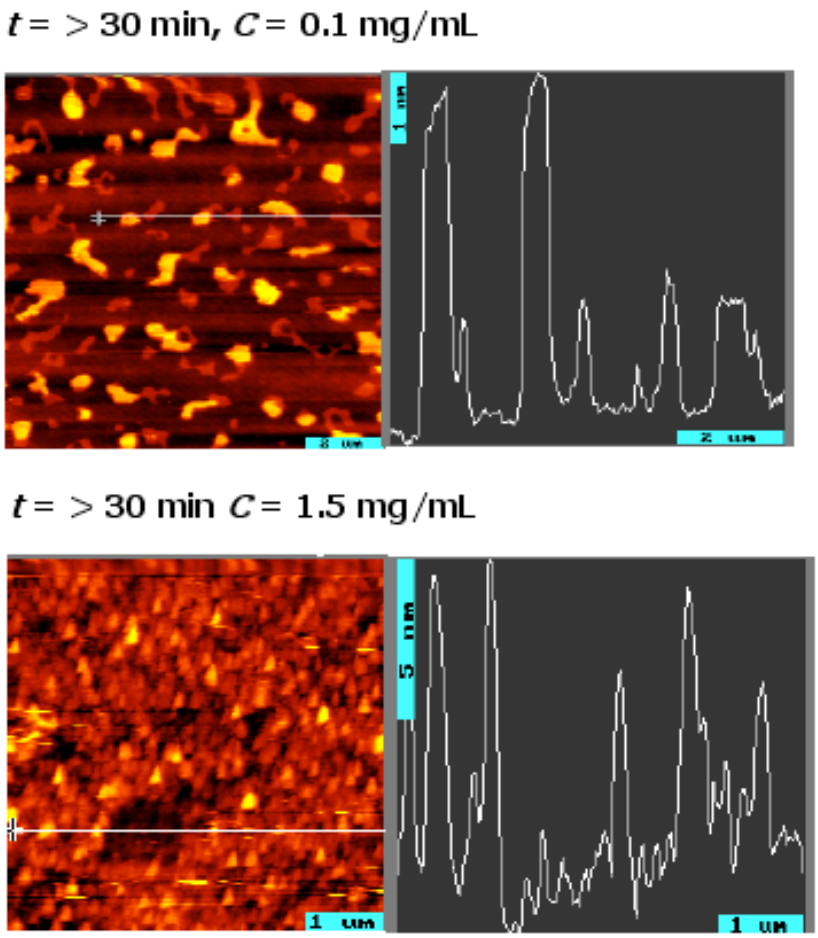

Figure 4.39. AFM topographs of LK_{14} peptide adsorbed on SiO_2 from 0.1 mg/mL and 1.5 mg/mL solutions. A thick layer is observed following adsorption from the 1.5 mg/mL solution.

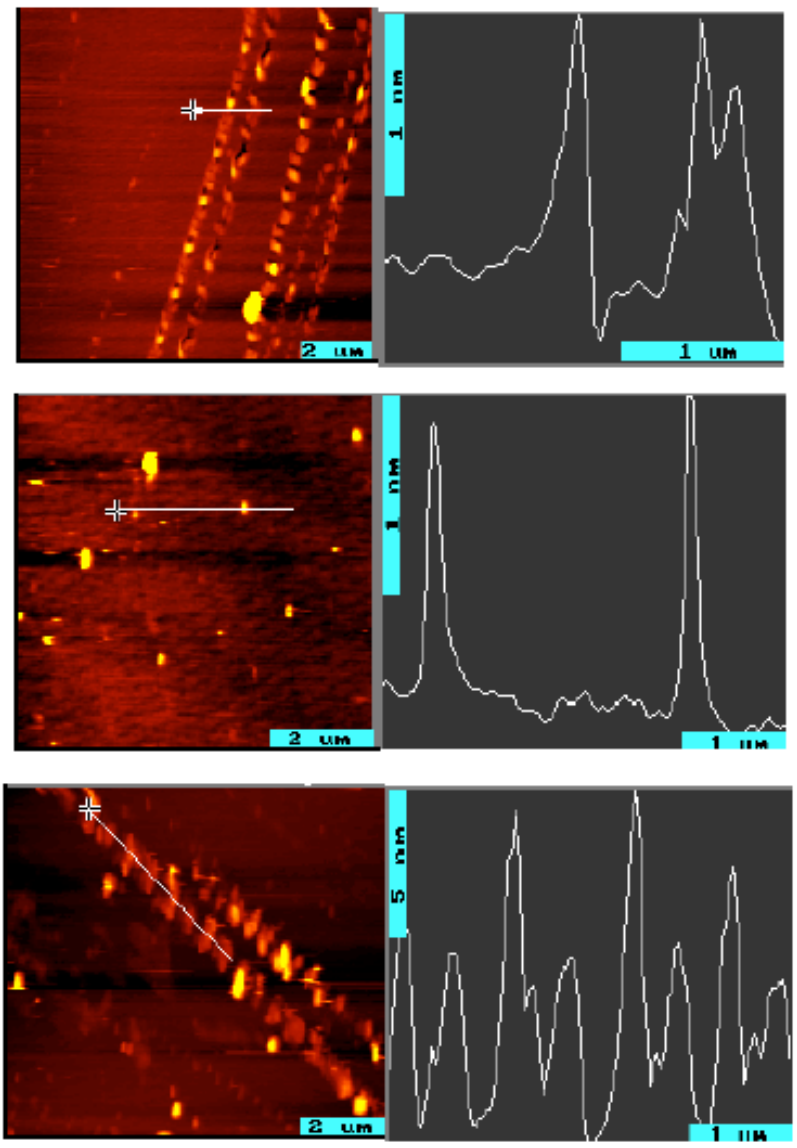

Figure 4.40. AFM data for AK_{14} peptide adsorbed on SiO_2.

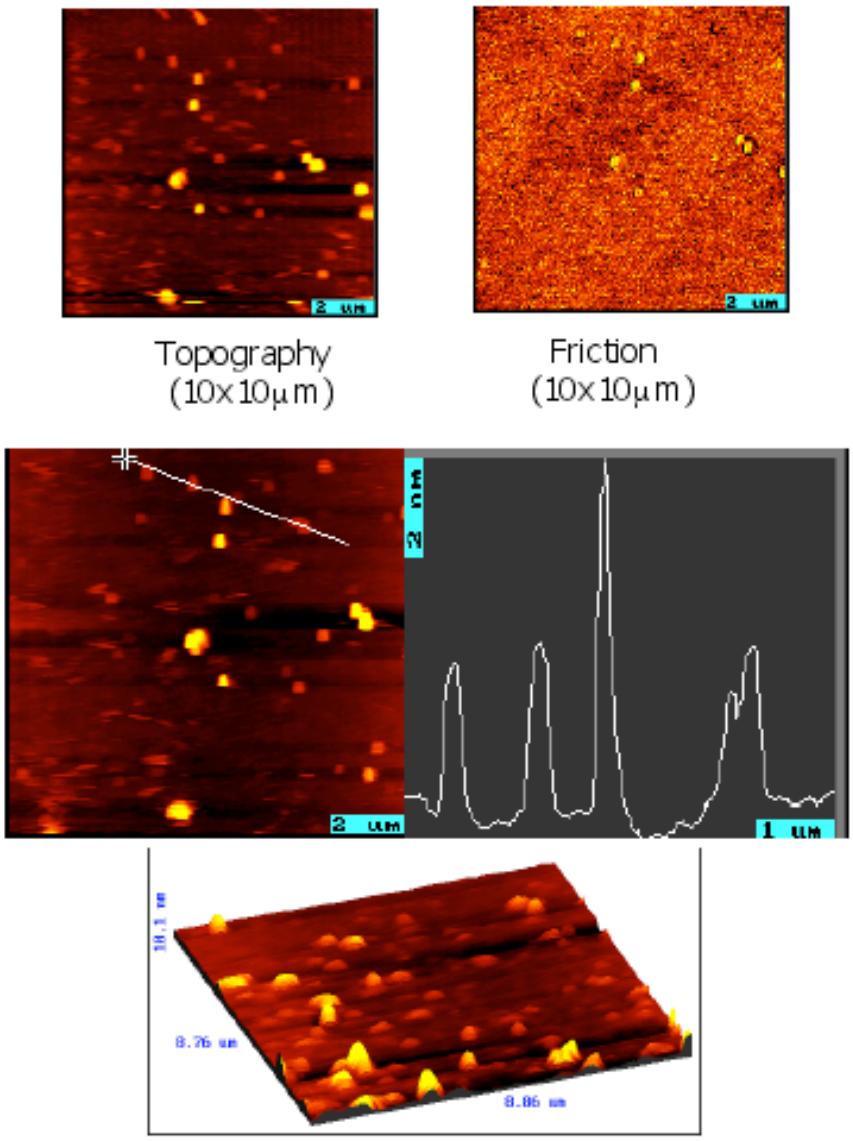

Figure 4.41. AFM data for AR_{14} peptide adsorbed on SiO_2.

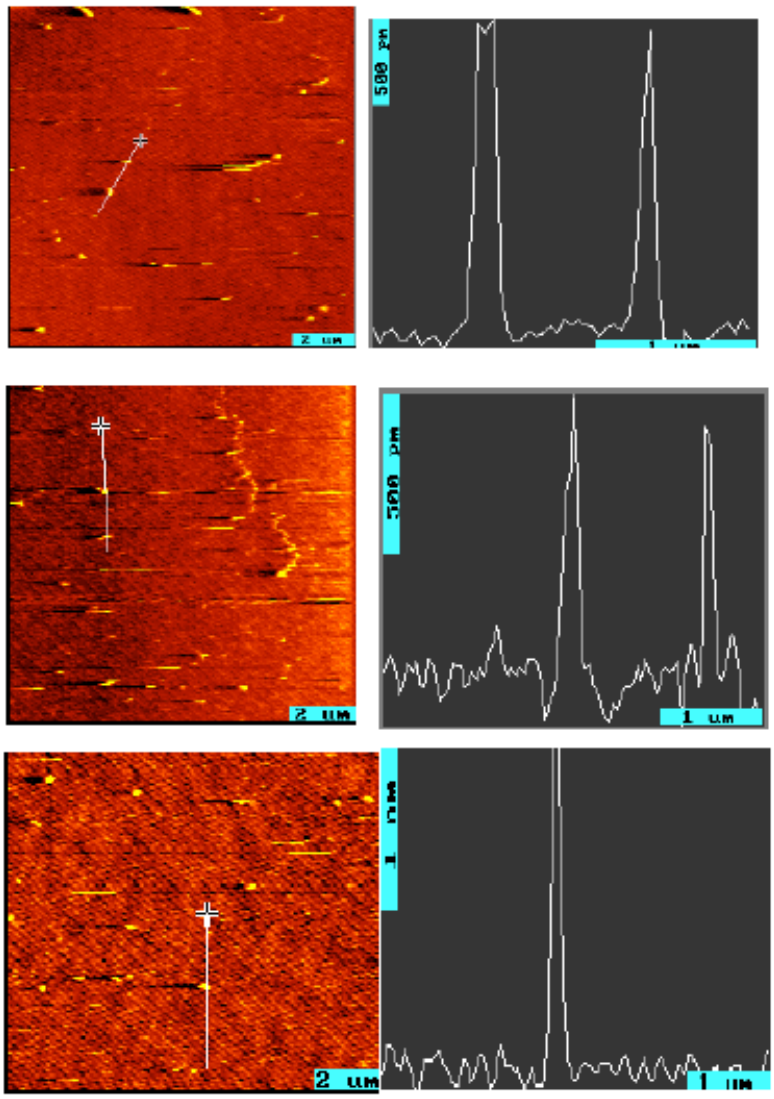

Figure 4.42. AFM data for FR_{14} peptide adsorbed on SiO_2.

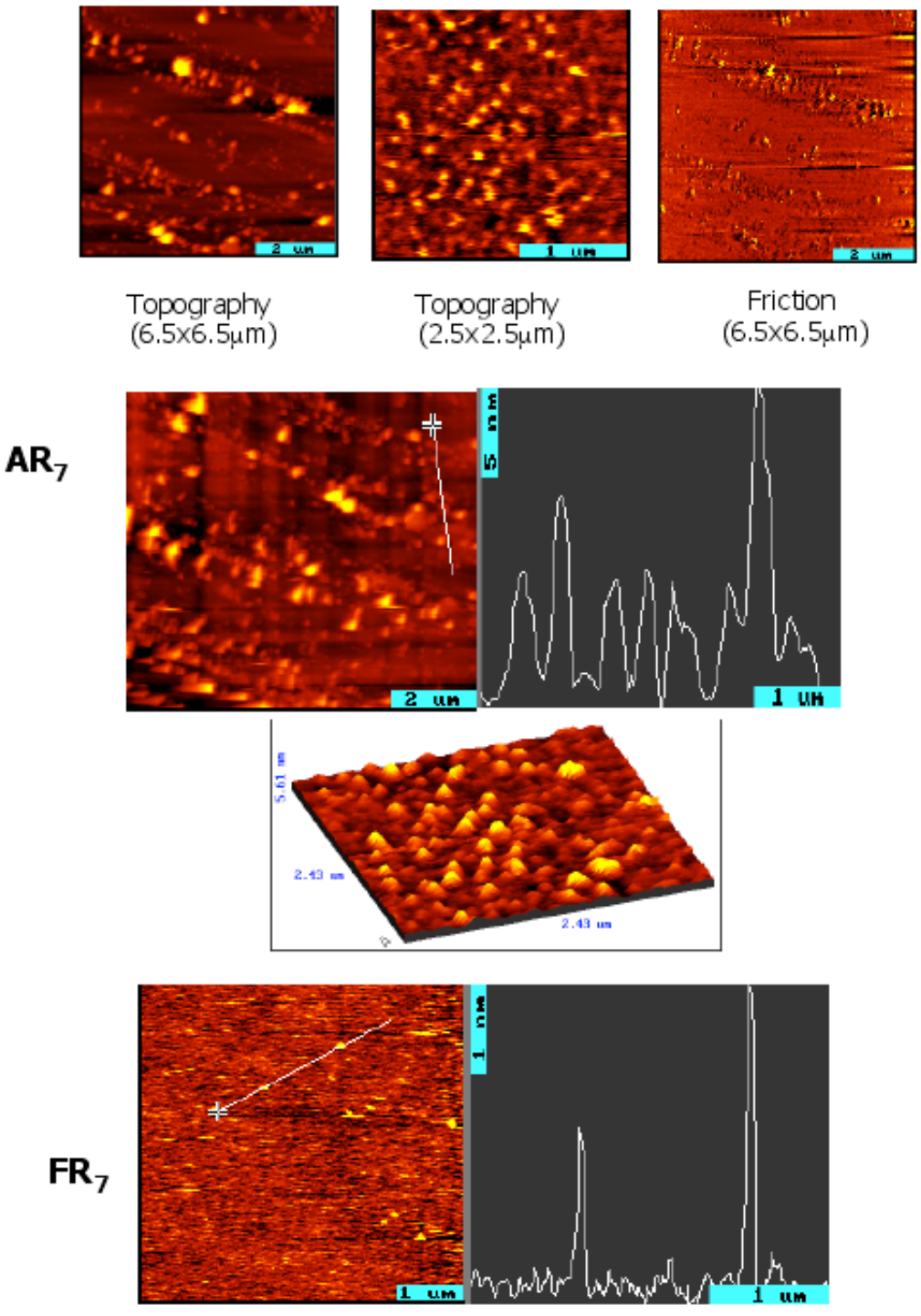

Figure 4.43. AFM data for AR_7 and FR_7 peptides adsorbed on SiO_2.

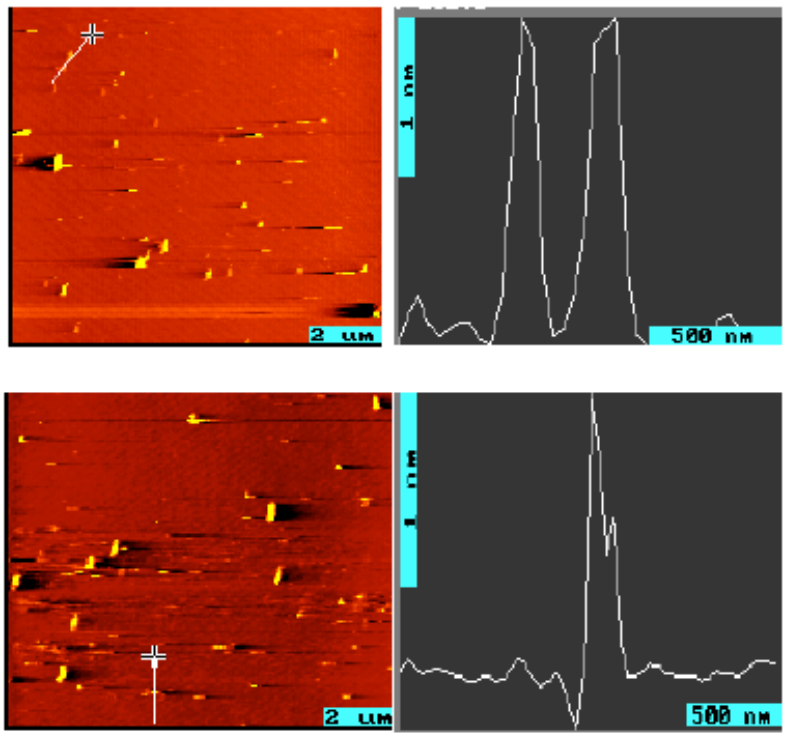

Figure 4.44. AFM data for AK_7 peptide adsorbed on SiO_2.

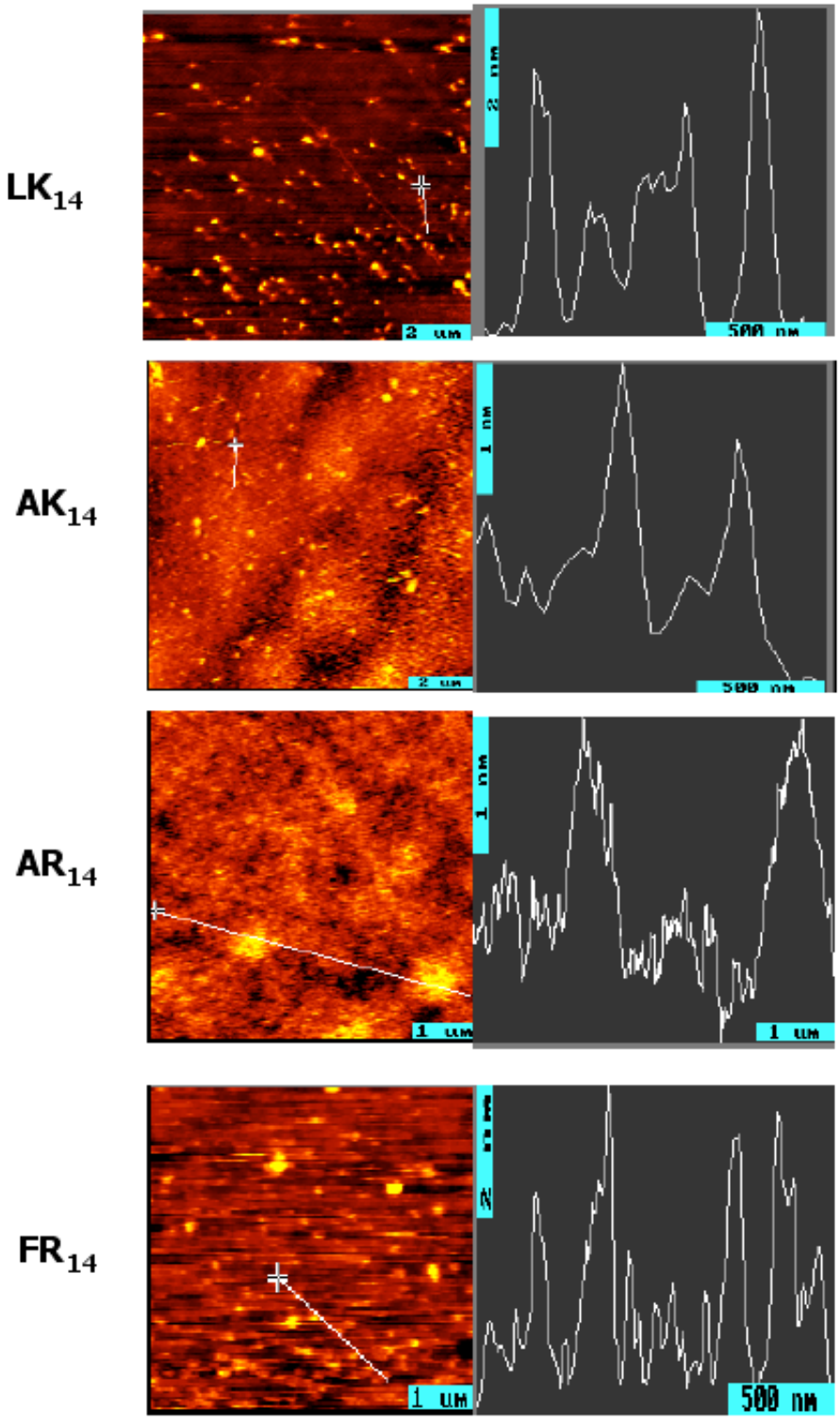

Figure 4.45. AFM data for 14 amino acid peptides PS.

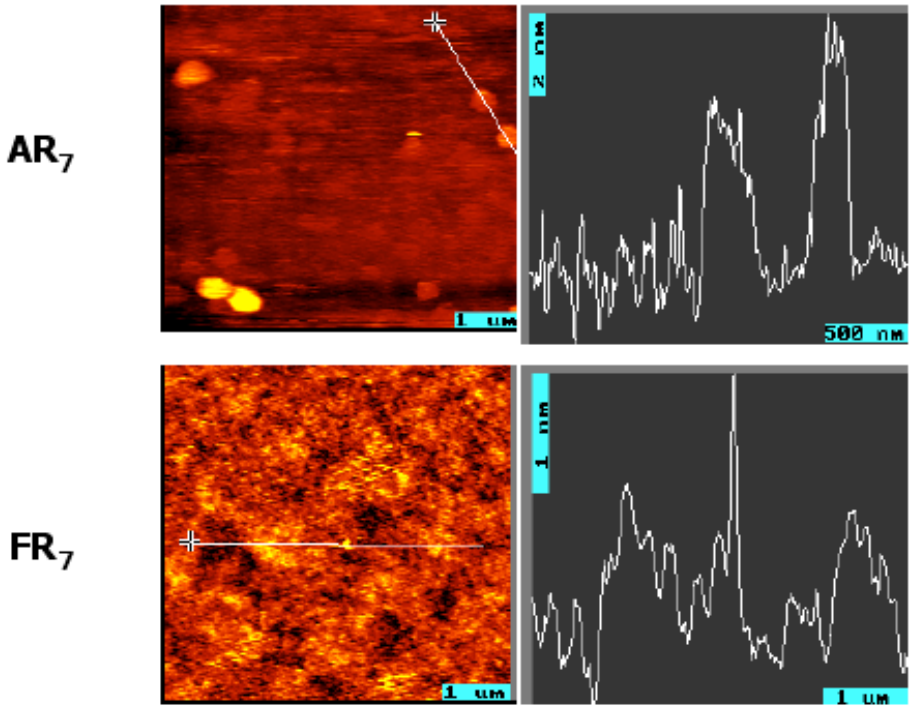

Figure 4.46. AFM data for 7 amino acid peptides PS.

4.10 Appendix IV: CD Gallery

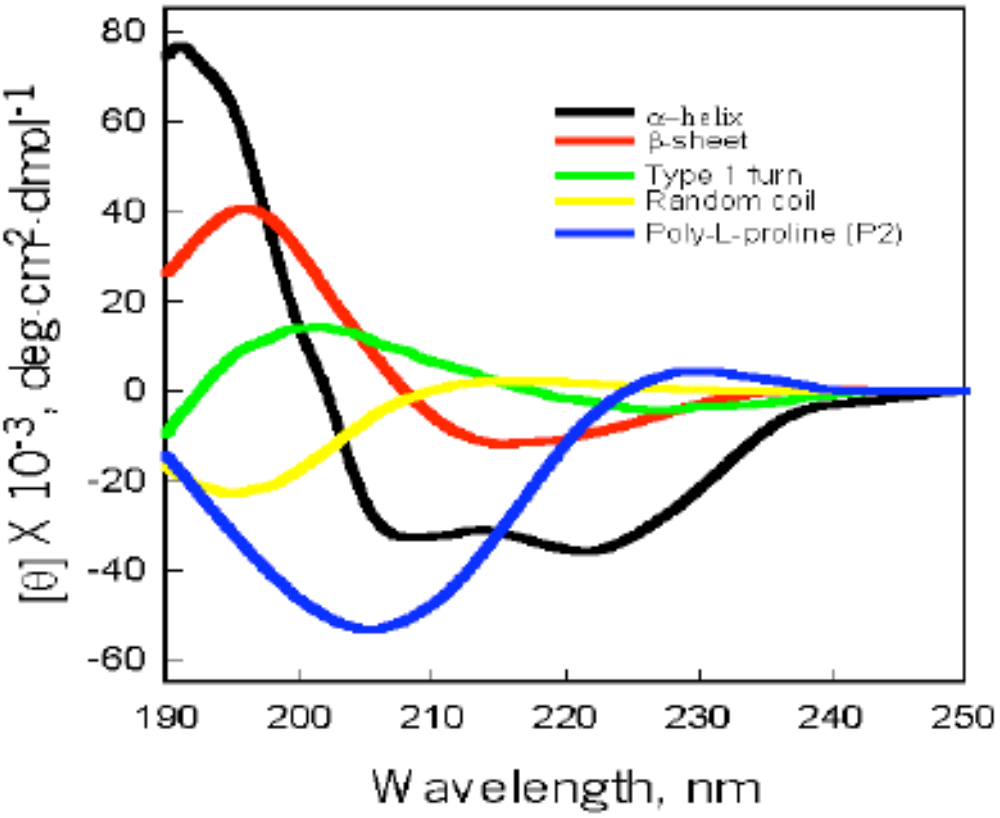

Figure 4.47. CD reference data.

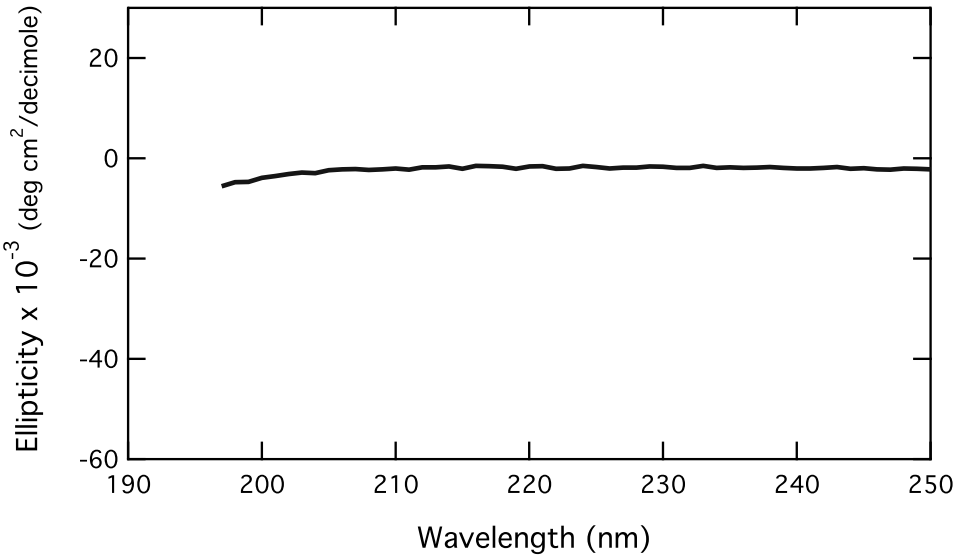

Figure 4.48. CD data of background PBS solution.

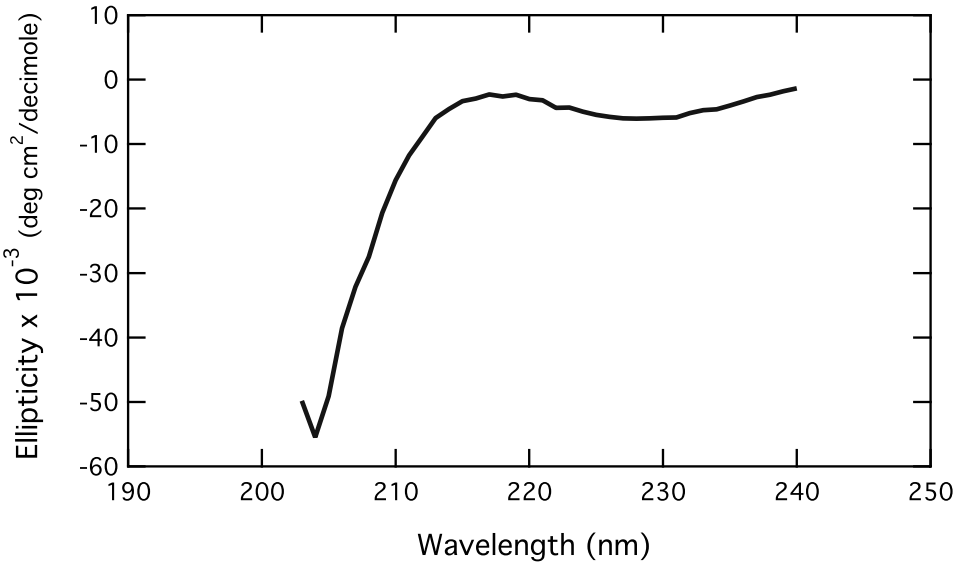

Figure 4.49. CD data of AR_7.

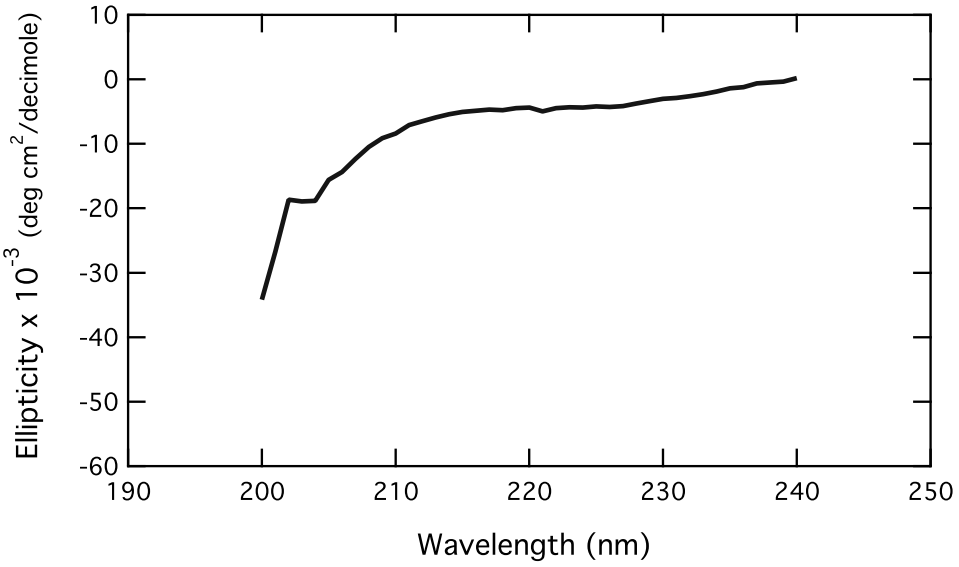

Figure 4.50. CD data of LK_7 β.

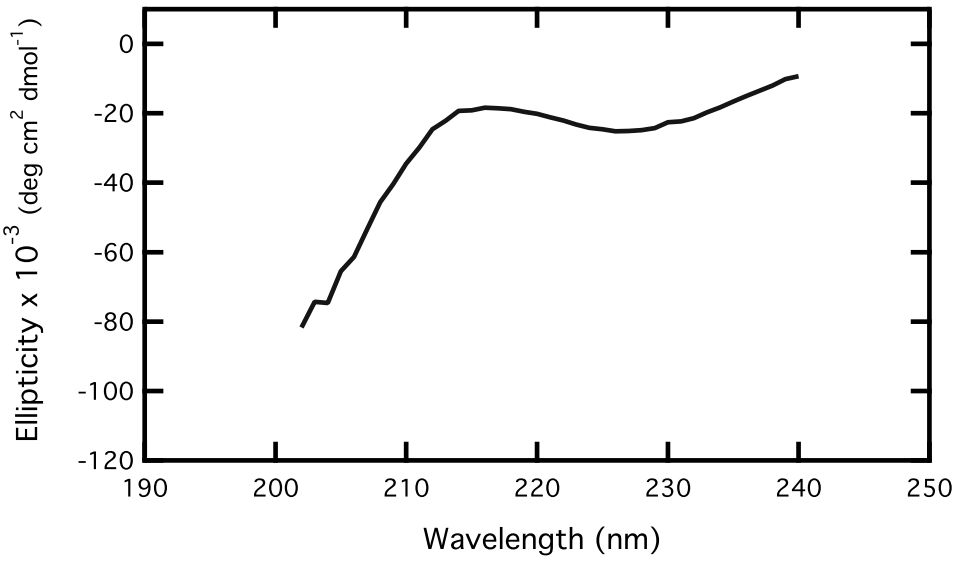

Figure 4.51. CD data of LK_7 α.

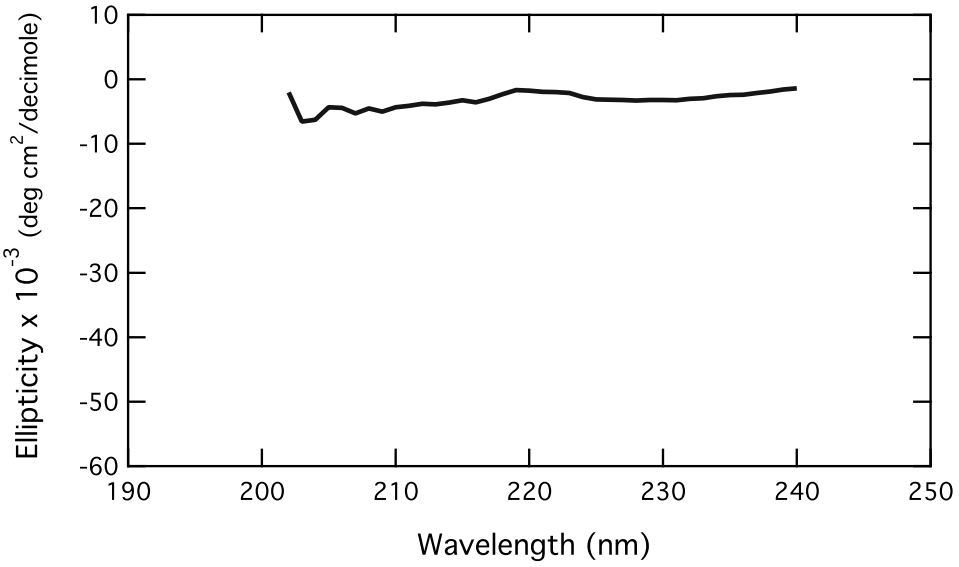

Figure 4.52. CD data of FR_7.

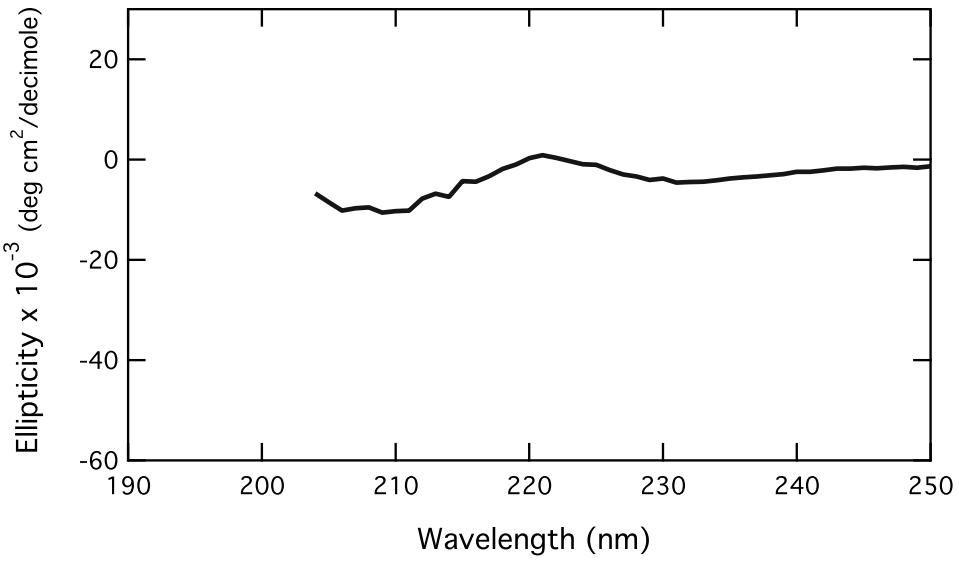

Figure 4.53. CD data of FR_{14}.

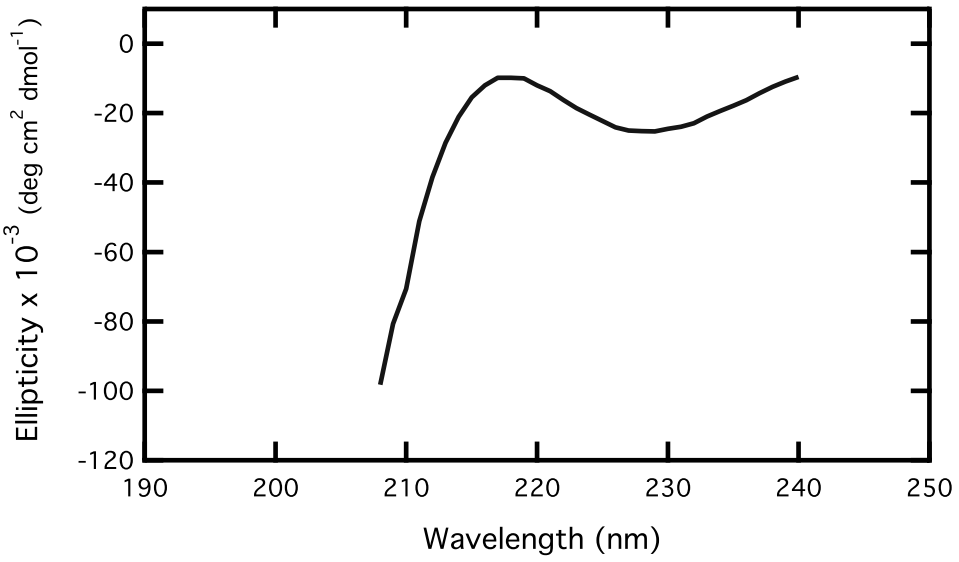

Figure 4.54. CD data of AK_{14}, 2.5 mg/mL.

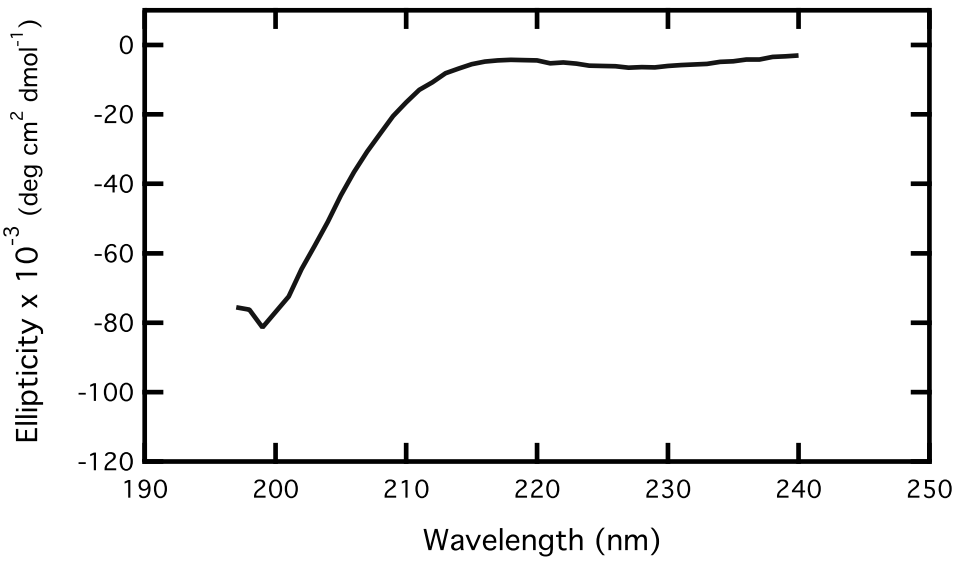

Figure 4.55. CD data of AK_{14}, 0.5 mg/mL.

Chapter 5

Characterization of Bacteria Surfaces for Actinide Bioremediation

5.1 Abstract

Microbes in soils and sediments can significantly affect transport of radionuclides in the environment. A mechanistic and molecular level understanding of the nature of actinide adsorption onto these biological surfaces is necessary for designing bioremediation methods for hazardous nuclear waste. SFG spectroscopy was used to characterize the surface of the common soil bacteria *Deinococcus radiodurans*, *Bacillus sphaericus*, and *Shewanella putrefaciens*. FTIR and SFG spectra were obtained between 2800-3050 cm^{-1}, and show differences in the CH stretching region between the bulk (FTIR) and surface (SFG) spectra. This work demonstrates that SFG spectroscopy is an effective method for studying complicated biological surfaces in situ.

5.2 Introduction

The use of nuclear energy during the last century for industrial and military purposes has resulted in the release of large quantities of radionuclides into the environment.[1] Figure 6.1 shows the common radionuclides and heavy metals in vicinally contaminated ground water and soils at Department of Energy facilities. In order to determine the potential for further migration of these species from the storage facilities, as well as design strategies for selective containment or possibly removal, it is necessary to understand many different types of interactions. The migration of radionuclides in the environment occurs mainly through transport in aqueous media. The rate of migration is determined by aqueous solubility, and interactions with solid surfaces (minerals, soil organic matter and soil microbes). There has been much research devoted to the determination of actinide solubility and sorption onto mineral surfaces.[2; 3] Recent interest in the development of biological treatment strategies for remediation of nuclear waste has prompted research aimed at understanding the interaction of radionuclides with soil microbes and soil organic matter.[4; 5] The interactions thought to be occurring at these biological interfaces include sorption, redox reactions, and complexation.[6]

Microorganisms are known to interact with heavy metals and radionuclides by the following mechanisms: 1) actinide sorption on the bacterial surface, 2) bacterial surface sorption, followed by actinide precipitation, 3) actinide interaction with species released by bacteria, involving complexation followed by precipitation, and, 4) uptake into the cell or bioaccumulation [7; 8]. Some microorganisms are also known to enzymatically reduce metals, and by changing their oxidation state can alter their aqueous solubility and mobility. Microbiologists estimate that there are over a million species of bacteria present in soils, and we only have the ability to culture 1% of bacteria.[1] Therefore the full effect of microbes on the actinide source term is not fully known.

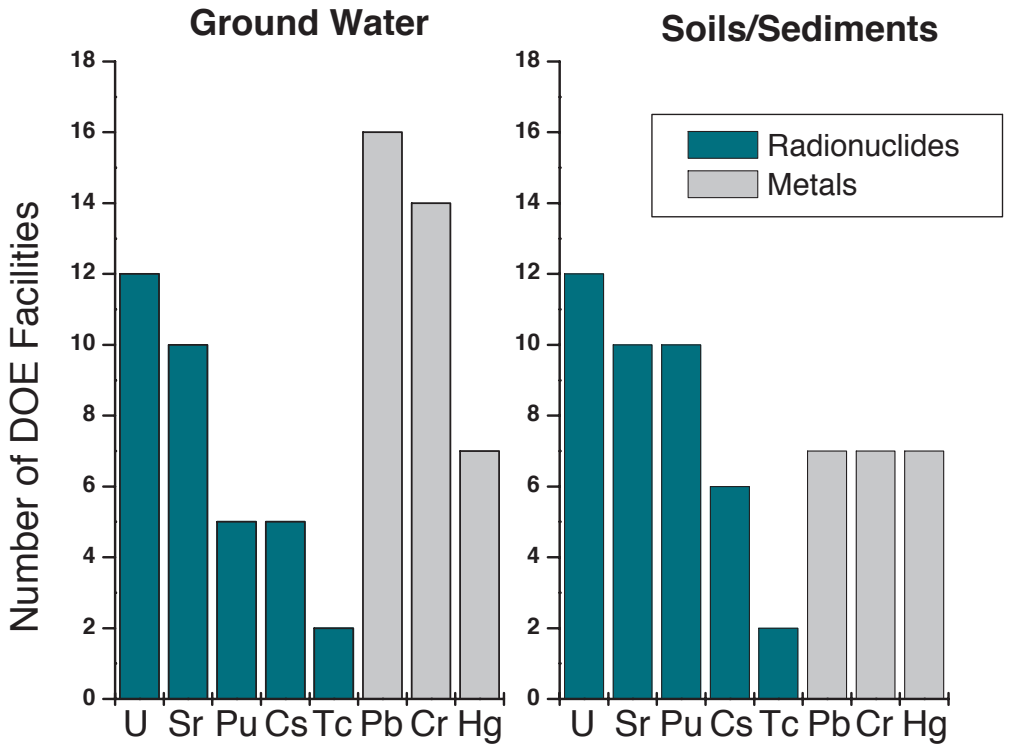

Figure 5.1. Types of heavy metal and radionuclide contamination found at Department of Energy sites in soils or groundwater.

A critical component of active bioremediation is the survival of the bacteria in contaminated environments, which are often at extreme pH and highly radioactive. Many species of bacteria have adapted to these conditions including the following Gram negative soil bacteria, which are known to interact with actinides: *Deinococcus radiodurans*, *Bacillus sphaericus*, and *Shewanella putrefaciens*.[1] *D. radiodurans* is extremely desiccation and radiation resistant, and has the ability to survive in mixed radiation fields, making it particularly suitable for remediation of high level nuclear waste. *D. radiodurans* has been shown to survive exposure to γ-radiation levels up to 1.5 million rads under certain conditions, whereas a 500 rad dose is lethal to humans.[1; 9; 10] *D. radiodurans* is aerobic, but was found to reduce metals such as Fe(III), Cr(VI), U(VI), and Tc(VII) in an anaerobic environment. The ability to survive high radiation doses makes *D. radiodurans* an excellent candidate for bioremediation of mixed radioactive waste.[11] *S. putrefaciens* is not particularly radiation resistant, but is a facultatively anaerobic species and can survive with or without oxygen in its environment.[12] This may be necessary for immobilizing contamination in deep anoxic soils, such as those found at geologic waste repositories such as Yucca Mountain. *S. putrefaciens* has been shown to enzymatically reduce soluble metals such as Cr(VI), U(IV), and Tc(VII) to yield an insoluble metal precipitate.[12] Previous studies of biosorption on the aerobic upper soil bacteria *B. sphaericus* have shown a high accumulation of Pu(VI) bound by surface complexation.[13] Determination of plutonium concentration by potentiometric titration as well as Extended X-ray Absorption Fine Structure (EXAFS) have identified carboxylate and phosphate functional groups on the cell walls of *B. sphaericus* [14]. An understanding of the mechanism of actinide stabilization is necessary to fully evaluate these bacteria species for potential bioremediation applications.

Traditional techniques used to study surfaces and interfaces, such as Low Energy Electron Diffraction (LEEDS) or photoemission spectroscopy, employ high-energy

electron or x-ray beams requiring ultra-high vacuum conditions.[16] These types of surface spectroscopy are not useful for examining biological samples, which requires non-destructive methods and ambient temperatures and pressures. The non-linear optical techniques of second harmonic and sum frequency generation (SHG and SFG) are ideal for in situ study of biological surfaces and interfaces at environmentally relevant conditions. Several excellent reviews on the application of SFG to biological surfaces and interfaces are available.[17; 18; 19; 20] In sum frequency generation spectroscopy, two input beams (typically a fixed visible and tunable infrared beam) at ω_1 and ω_2 overlap at a surface or interface and generate a surface specific sum frequency output ($\omega_{SF} = \omega_1 + \omega_2$). Second harmonic generation is one special case of sum frequency generation where $\omega_1 = \omega_2$. Second harmonic generation can probe the electronic (UV-vis region) structure of the adsorbed species at a surface or interface. If the frequency of the probe light is tuned to be in resonance with an electronic transition of an adsorbate, the SHG signal intensity can be enhanced by electronic resonances of the interfacial species with either the probe or the second harmonic light fields. Resonantly enhanced SHG measurements allow for the investigation of heterogeneous processes with surface and molecular specificity. Infrared-visible sum frequency generation vibrational (infrared region) spectroscopy probes the vibrational modes (that are both infrared and Raman active) of molecules adsorbed at the interface, and gives detailed information on surface structure and composition. The surfaces and interfaces accessible to SHG/SFG include gas/solid, gas/liquid, liquid/liquid and liquid/solid interfaces as well as heterogeneous processes occurring at these interfaces. The relevant surfaces under study for bioremediation applications include mineral oxides, biosurfactants and biopolymers (bacterial proteins), organic adlayers adsorbed on solid (mineral) surfaces and soil organic matter (including humic and fulvic acids). In the present work, SFG spectroscopy is used to characterize the cell surfaces of the soil bacteria species *D. radiodurans*, *B. sphaericus*, and *S. putrefaciens*. Both *D.*

radiodurans and *B. sphaericus* possess an S-layer (images shown in Figure 6.2 and 6.3). Crystalline bacterial cell surface layers (S-layers) represent the outermost cell envelope component of many bacteria and archaea. S-layers are composed of identical proteinaceous subunits, which assemble into oblique, square, or hexagonal lattice types.[21] The highly ordered S-layers make these bacteria particularly amendable to study using SFG spectroscopy.

5.3 Experimental

5.3.1 Sample Preparation

D. radiodurans strain R1 (ATCC #13939) was grown in aerobic conditions in TGY growth media (5 g Tryptone, 1 g Glucose, and 3 g Yeast extract per liter of deionized water). A fresh plate of bacteria (4-11 days old; room temperature for *Deinococcus radiodurans*) was used to prepare an inoculum. The benchtop was sterilized with 70-95 % alcohol, and a bunsen burner flame was used to sterilize the tops of the culture tubes. Before adding growth media to the tubes, the bottle lip and bottom of the cap were sterilized in the flame. A sterile pipet was used to transfer media to the culture tubes, and the lip of the media bottle was sterilized before and after the transfer (the bottle was capped loosely to prevent dust or other airborne contamination). A sterilized metal loop was used to add the colonies, after flaming the loop and wire and cooling the loop by touching a sterile part of the agar plate. Cultures were incubated overnight at 30 °C on a rotary shaker. Cells were harvested in stationary phase (OD_{600} 2-4) by centrifugation, washed twice with pH 7 NaCl solution (0.1 M), and resuspended in a few drops of NaCl solution, to give a concentrated suspension of bacteria.

The bacterial strain *S. putrefaciens*, and *B. sphaericus* were grown to stationary

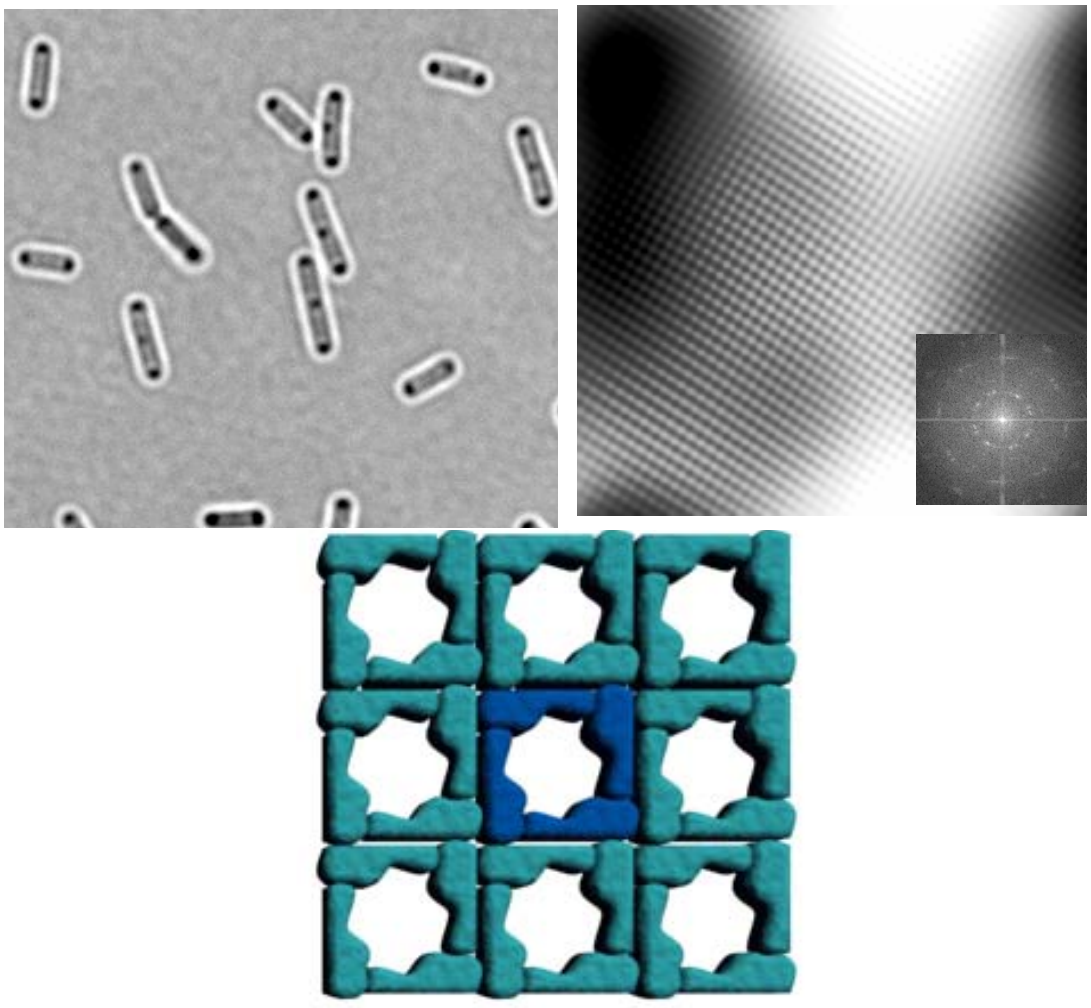

Figure 5.2. Bright field image of *B. sphaericus*, right. Computer Enhanced TEM image of S-layer of *B. sphaericus*. Inset is a Fourier Transform, left. Bottom image is Structural Model of S-layer proteins of *B. sphaericus*. Pore size 3.6 nm, lattice parameter 12.5 nm. Images courtesy of Agave Biosciences.

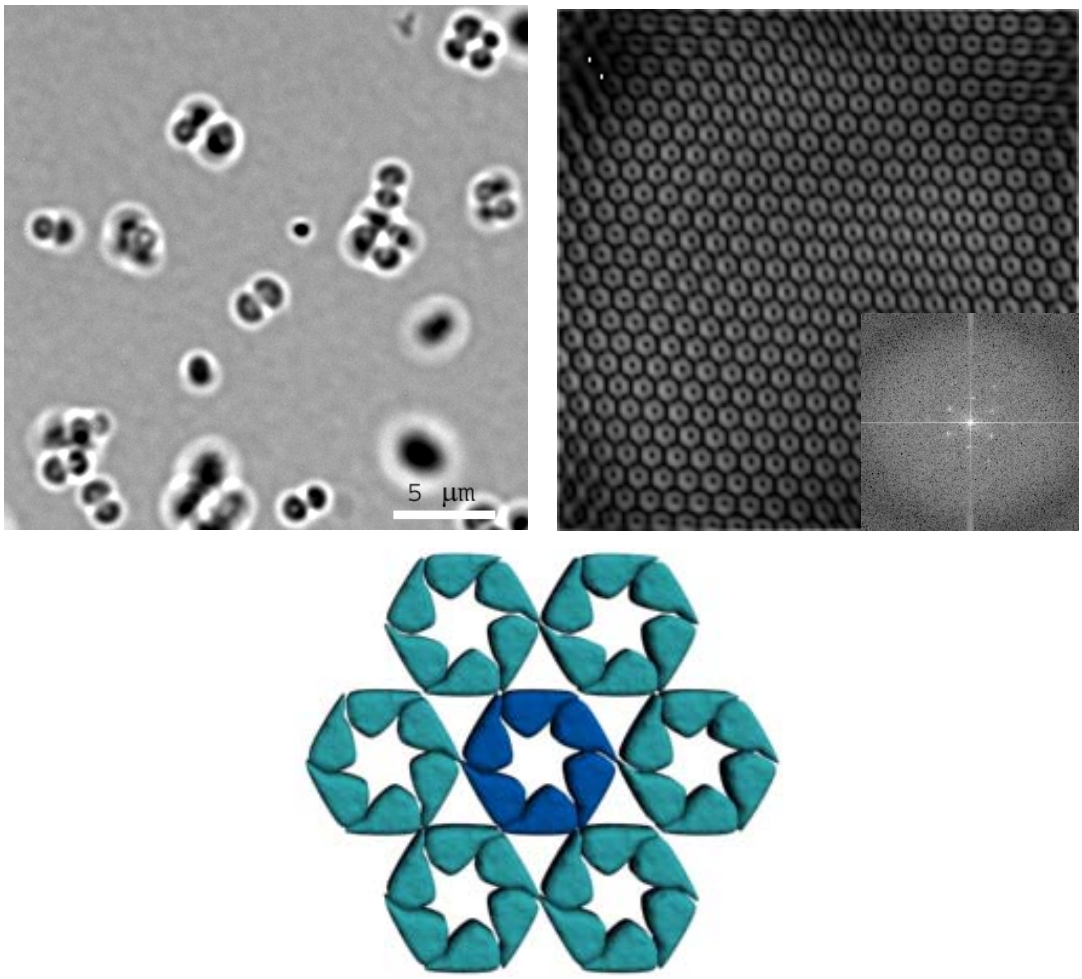

Figure 5.3. Bright field image of *D. radiodurans*, left. Computer Enhanced TEM image of S-layer of *D. radiodurans*. Inset is a Fourier Transform, right. Lower image is a Structural Model of S-layer proteins of *D. radiodurans*. Pore size 5.5 nm, lattice parameter 19 nm. Images courtesy of Agave Biosciences.

phase in LNB medium (0.44 g K_2HPO_4 (5mM), 0.89 g KH_2PO_4 (13mM), 0.1 g NaCl, 2.6 g HEPES buffer, 0.2 g Peptone, 0.2 g Vitamin-free amino acids, 10 mL Wolfe's modified minerals, 2.24 g Lactate, per liter of purified deionized water, with pH adjusted to 7.4 and the medium passed through a 0.2 μm filter). The biomass was harvested by centrifugation, rinsed twice and resuspended in phosphate buffered saline (0.01 M K_2PO_4, 0.085 % NaCl, pH 7.4).

Samples were prepared for SFG spectroscopy by spreading a thin layer of bacteria suspension over a glass slide. SFG spectra were obtained in reflection geometry, with the IR and vis beam angles of 58 and 62 degrees with respect to the surface normal. The intensity of the IR and visible beams were attenuated by defocusing, to obtain an average pulse energy at the sample of approximately 10 μJ per pulse. SFG spectra of TGY growth media and buffer were obtained to determine the background. sFourier-Transform IR spectra of the bacteria samples were obtained (Thermos Nicolet FTIR) for comparison. A thin layer of bacteria was spread on a CaF_2 window for data acquisition.

Bacteria survivability was tested using fluorescent Hoescht staining following SFG laser irradiation. The SFG signal intensity was also monitored over several scans to determine the bacteria cell wall damage threshold. Signal intensity from the first scan was compared to signal intensity from a scan 30 minutes to 2 hours later in order to detect signal attenuation which may be due to lysed cell surfaces.

5.4 Previous Research

5.4.1 Uranyl Sorption on *D. radiodurans*

Previous research in the Nitsche laboratory has studied uranyl adsorption onto *D. radiodurans* as a function of pH.[22] A 10^{-4} M uranyl solution (U-233) was added to a suspension of bacteria which had been equilibrated at various pH. The suspensions were shaken continuously, and the solution sampled at various time intervals. We used liquid scintillation counting to measure the amount of U activity in solution, which was used to calculate the distribution coefficient (U solution/U solid). Uranyl concentration of 10^{-4} M is 2 orders of magnitude below the solubility limit in this pH range. There is a significant increase in the uranyl sorption edge around pH 4.5, which is near the typical pK_a of carboxylate (Figure 6.4). Uranyl loading on the cell does not depend on whether the cells are alive or heat-killed, log or stationary growth phase, and is constant over an order of magnitude change in relative biomass, indicating sorption.

5.4.2 TRLFS measurements of Uranyl Sorption onto *D. radiodurans*, *B. sphaericus*, and *P. aeruginosa*

Another technique used in our laboratory to study bacteria-actinide systems is time resolved laser fluorescence spectroscopy (TRLFS).[13; 14] TRLFS gives species specific fluorescence lifetime and thermodynamic stability constants. Figures 6.5-6.7 show the fluorescence spectra of three different bacteria-uranyl systems. The first is of *B. sphaericus* and uranyl, and a uranyl-(nucleotide) adenosine mono-phosphate reference; *D. radiodurans*/uranyl, and malonic acid (dicarboxylic acid) reference; and *Pseudamonas aeruginosa*/uranyl and uranyl hydrolysis products. The TRLFS data are very different for each bacteria species. The fluorescence lifetimes and emis-

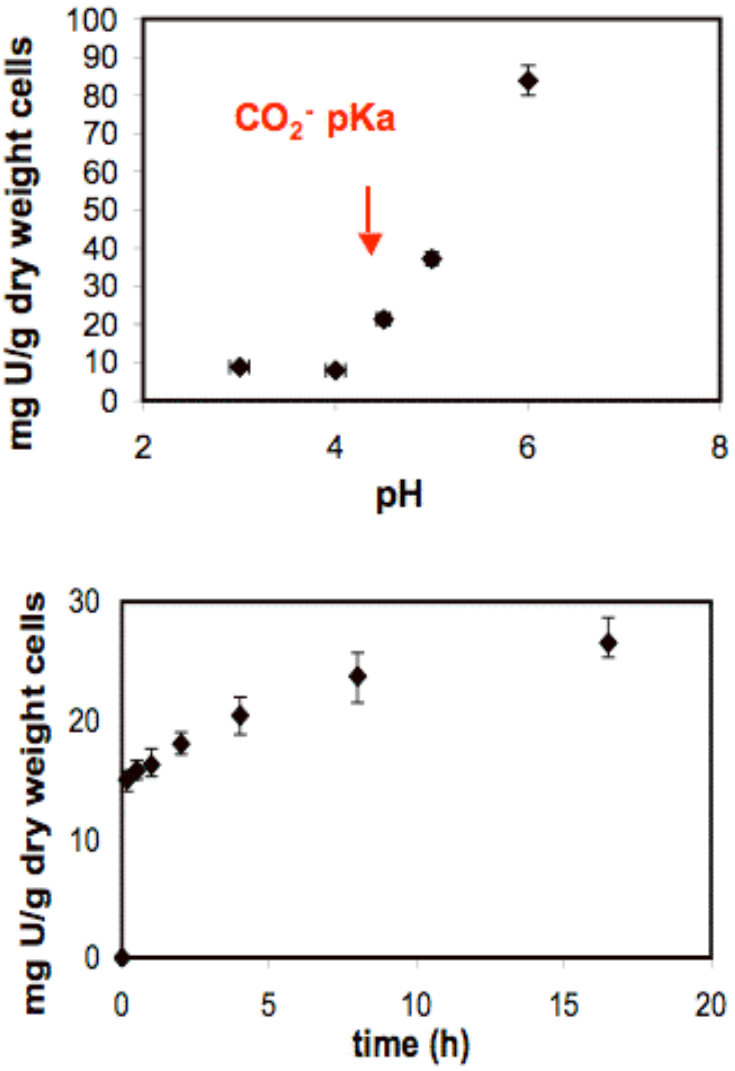

Figure 5.4. Uranyl sorption studies on *D. radiodurans*.

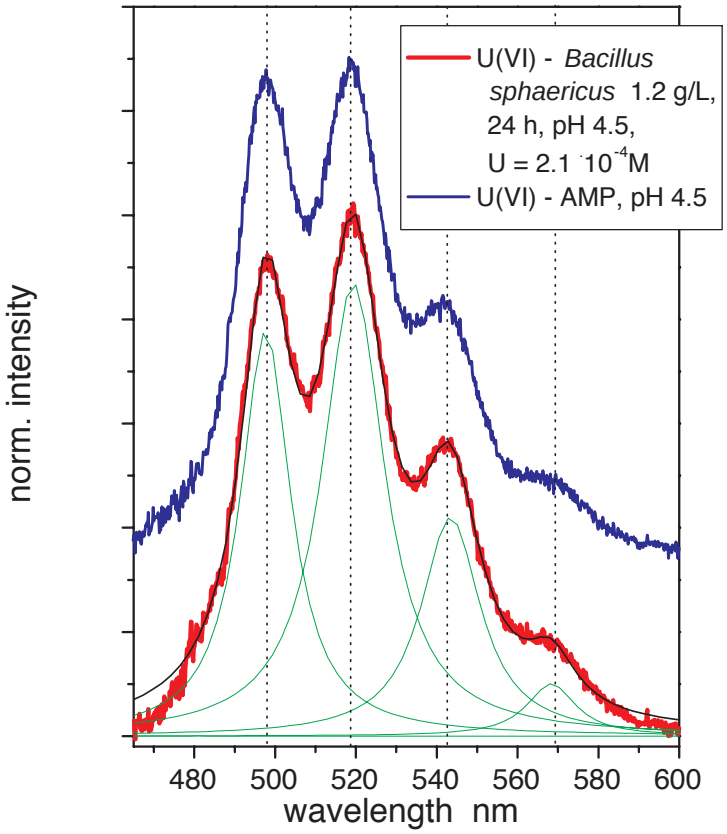

Figure 5.5. TRLFS spectrum of U(VI) sorbed onto *B. sphaericus* and reference U(VI)-AMP.

sion spectra closely match our reference compounds, suggesting that uranyl sorbs to phosphate groups on *B. sphaericus*, carboxylate groups on *D. radiodurans*, and does not sorb on *P. aeruginosa*. *Pseudamonas aeruginosa* is known to stabilize uranyl through a very different mechanismphophate secretion followed by U(VI)-phosphate precipitation.[15]

The spectroscopic data and uranyl sorption data suggests that uranyl complexes to *D. radiodurans* cell surface via carboxylate groups. *D. radiodurans* has an very complex cell wall structure, shown schematically in Figure 6.8. The S-layer of *D. radiodurans* is known to display its C-terminus, which may provide negatively charged

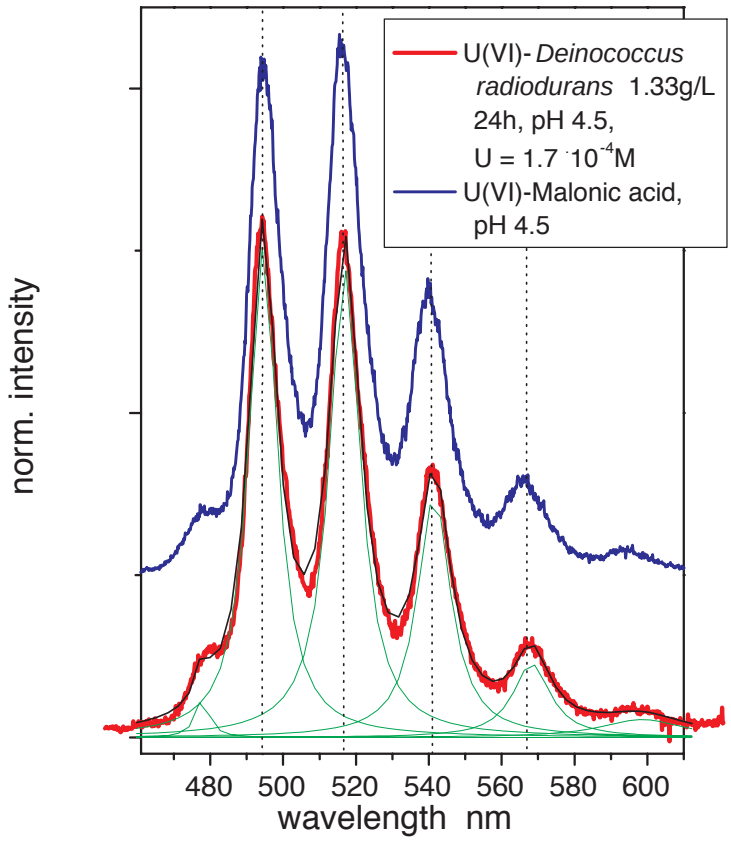

Figure 5.6. TRLFS spectrum of U(VI) sorbed onto *D. radiodurans* and reference U(VI)-malonic acid.

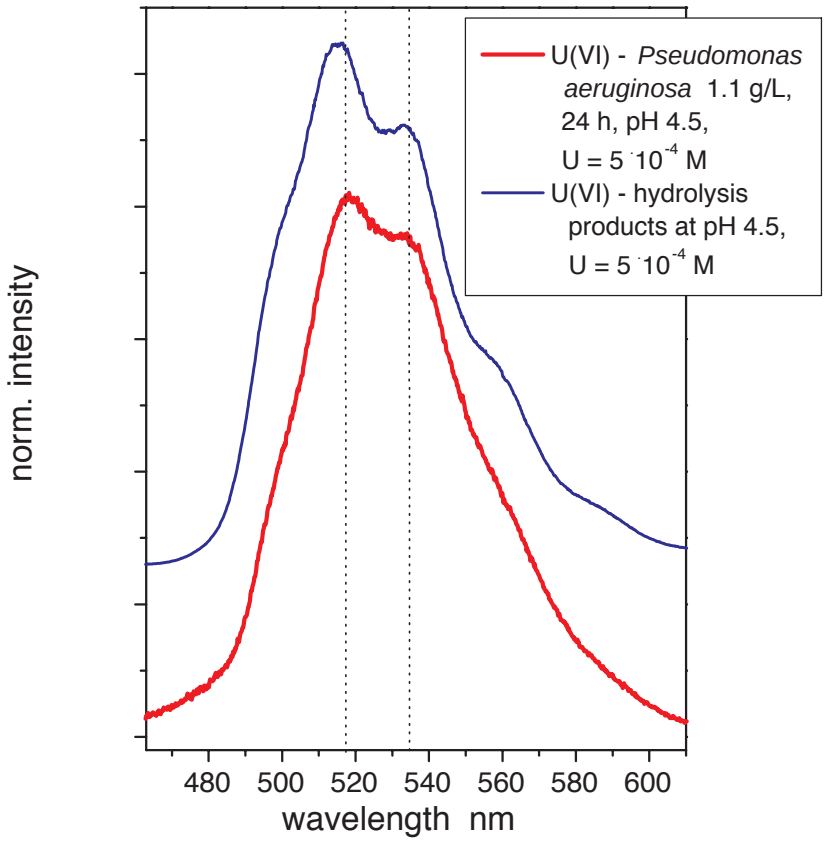

Figure 5.7. TRLFS spectrum of U(VI) and *P. aeruginosa* and reference U(VI) hydrolysis products.

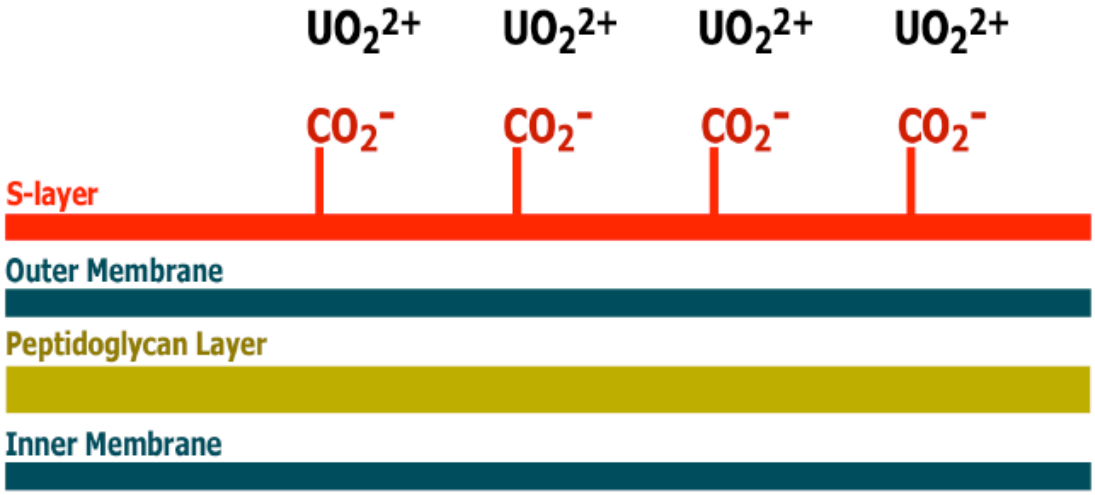

Figure 5.8. Model cell cross section of *D. radiodurans*.

groups for uranyl sorption.[23; 24] We would like to test this hypothesis by studying uranyl adsorption onto the cell surface in situ using SFG spectroscopy.

5.5 Results and Discussion

The FTIR spectra of *D. radiodurans* and *S. putrefaciens* are shown in Figure 6.9. The FTIR spectra are very similar, with broad features due to OH, CH, and Amide I and II absorbances. The OH is likely from water in the cell, the CH from lipids in the cell wall proteins, and the Amide I and II from protein backbones. In order to study the interaction of metals with the surface, it is necessary to probe the spectral regions where the more reactive functional groups absorb IR radiation (below 1800 wavenumbers). However, experiments were begun in the CH region to determine the feasibility of the technique with live, whole bacterial cells.

The FTIR and SFG spectra of *D. radiodurans* in the CH stretching region are shown in Figure 6.10 and Figure 6.11, respectively. The FTIR spectrum shows both

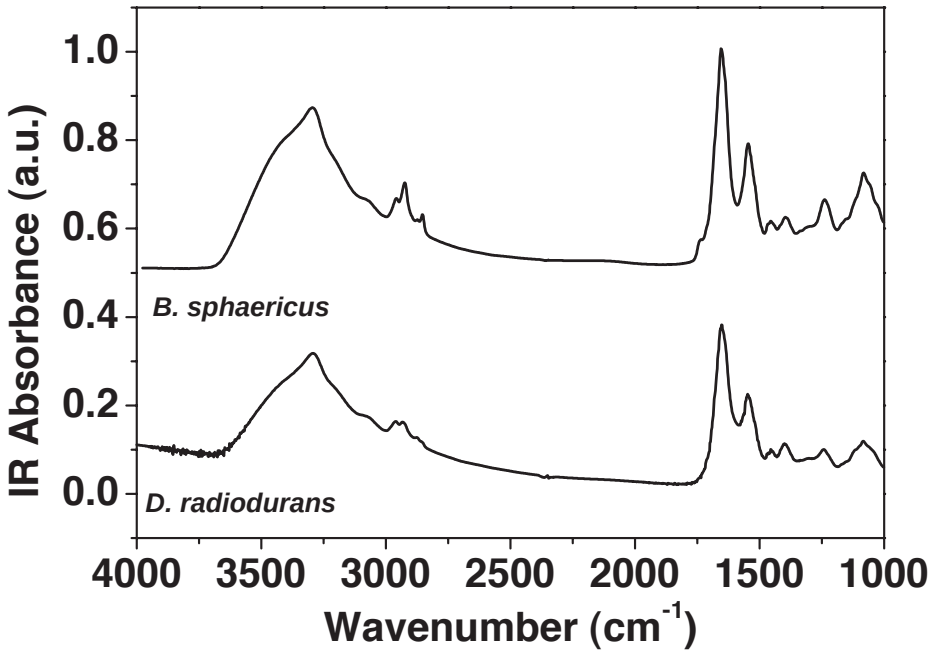

Figure 5.9. FTIR spectra of *D. radiodurans* and *B. sphaericus*.

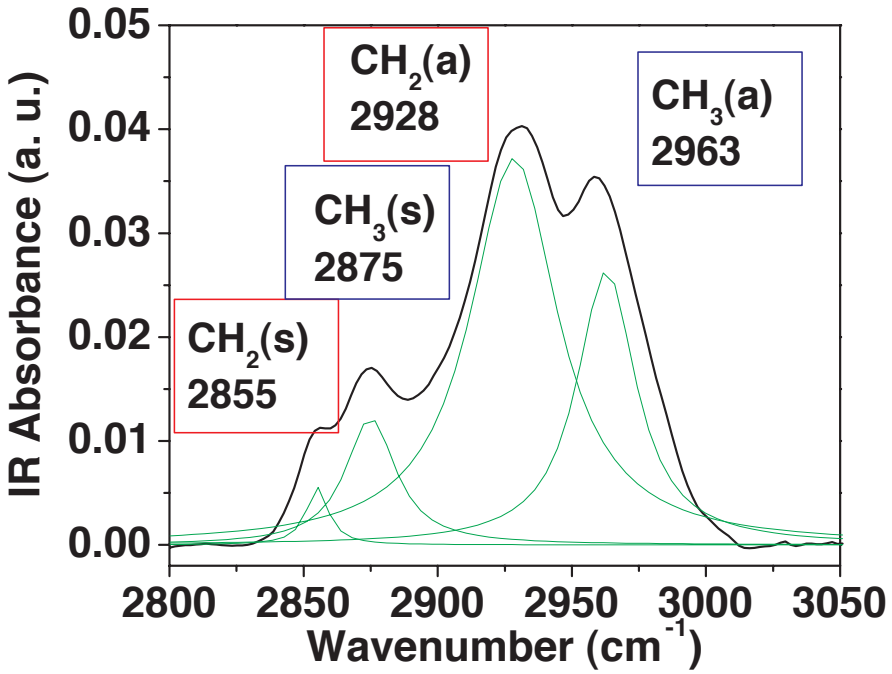

Figure 5.10. The FTIR spectrum of *D. radiodurans* in the CH stretching region (2800 - 3050 cm^{-1}).

CH_2 and CH_3 normal modes, whereas the SFG spectrum shows only CH_3 normal modes are SFG active at the surface. These modes are tentatively attributed the observed CH_2/CH_3 resonances to the S-layer surface proteins. The TGY growth media and buffer do not produce SFG signal, and the unique SFG spectra for the bacteria suggest that these are surface protein vibrational modes.

The SFG spectra of *S. putrefaciens* and *B. sphaericus* are shown in Figure 6.12 and 6.13. The SFG spectrum of *B. sphaericus*, in contrast to that of *D. radiodurans*, shows only CH_2 groups are SFG active at the surface. The SFG spectrum of *S. putrefaciens* shows only CH_3 groups observable at the surface. The signal to noise ratio of the SFG spectrum of *S. putrefaciens* is low, which may be due to a more disordered surface structure, since this species of bacteria lacks an S-layer.

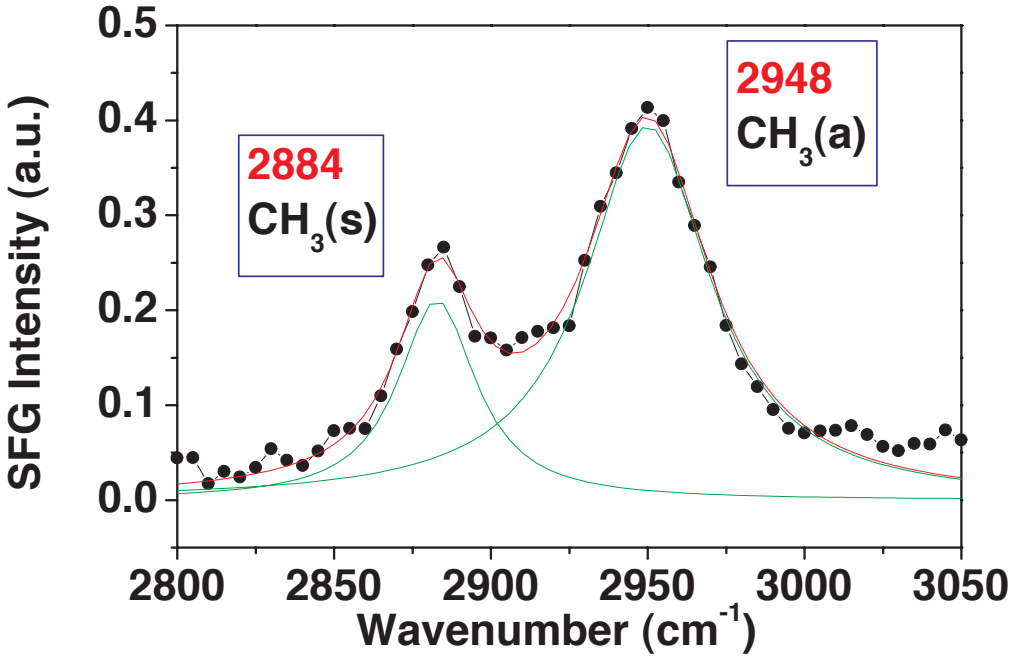

Figure 5.11. The SFG spectrum of *D. radiodurans* in the CH stretching region (2800 - 3050 cm^{-1}).

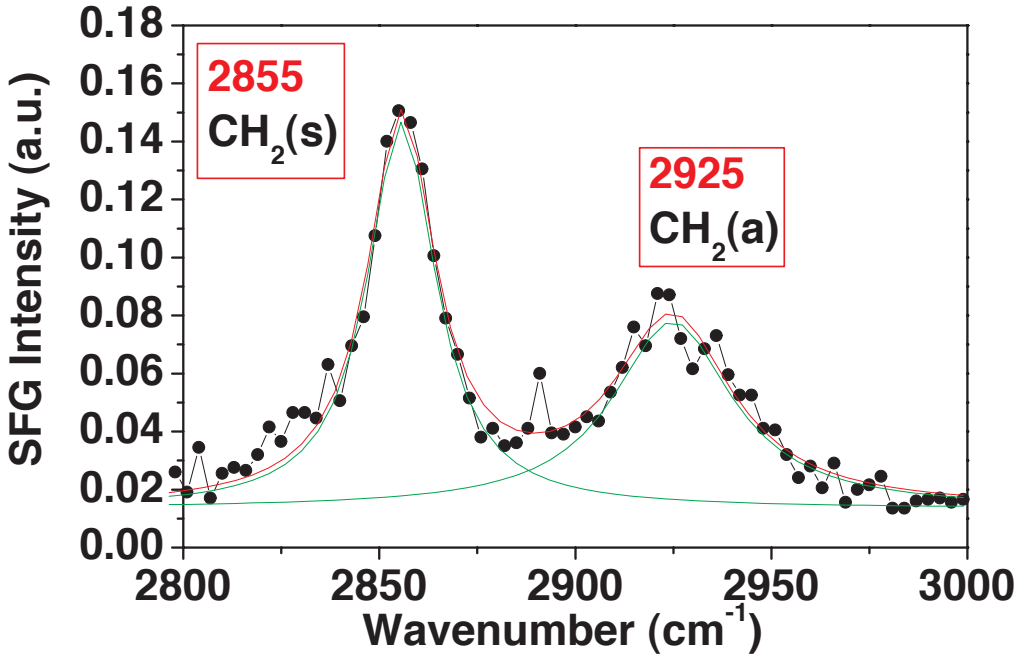

Figure 5.12. The SFG spectrum of *B. sphaericus* in the CH stretching region (2800 - 3050 cm^{-1}).

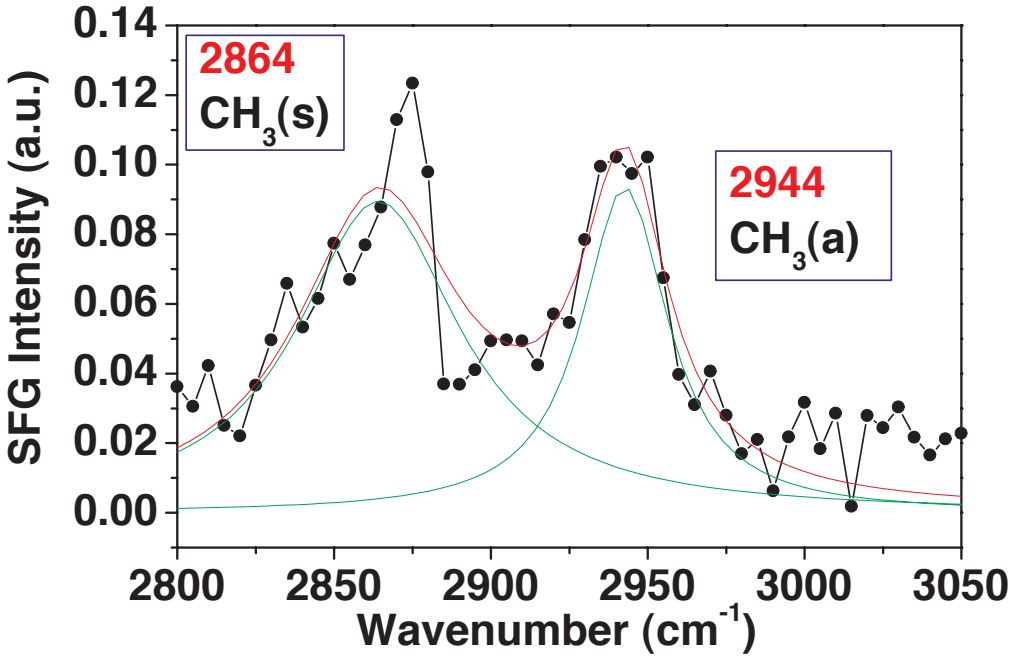

Figure 5.13. The SFG spectrum of *S. putrefaciens* in the CH stretching region (2800 - 3050 cm^{-1}).

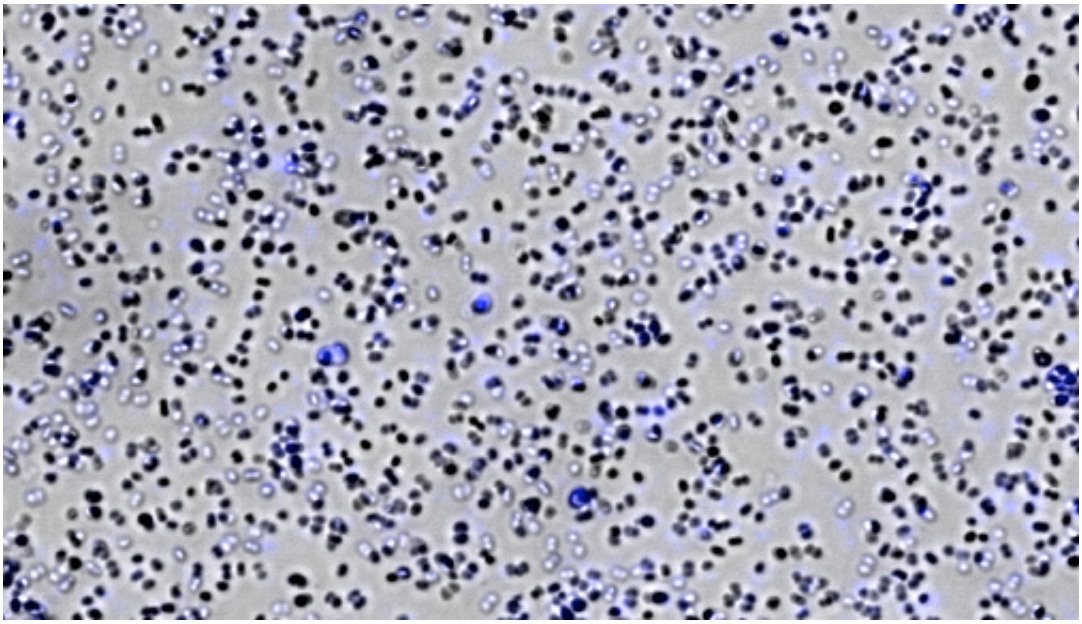

Figure 5.14. Fluorescence Stain of *D. radiodurans* sample following SFG laser irradiation. The live bacteria appear as black or white spheres ($\sim$ 1 μm in diameter). Lysed cells appear as larger blue, irregular, features.

Bacteria survivability tests showed no measurable change in SFG signal intensity over the timescale of the scanning (approximately 1.5 hours). Preliminary fluorescent microscopy images show a 90 % survivability rate (Figure 6.14). The staining method used here demonstrates that the cells are alive after 2 hours of laser irradiation. The stain is absorbed by cellular DNA only when cells are metabolically active, and is visible upon cellular lysis using fluorescence microscopy. Microscopy images also show that there is not significant cellular lysis.

5.6 Summary and Future Work

Characterization studies of bacteria cell surfaces using SFG vibrational spectroscopy demonstrate the feasibility of the technique with live bacteria. The CH_2/CH_3 stretching region of the SFG spectra is unique to each species of bacteria which is likely due to differences in surface protein composition and structure. We do not ex-

pect functional groups in the CH region (methyl and methylene) to interact directly with the actinides, but they may be sensitive to perturbations of other nearby surface groups due to actinide complexation (more so if there is a significant change of surface structure). These experiments have shown that SFG spectroscopy can be used to examine the cellular surface of multiple species of bacteria, where a non-invasive, non-destructive technique is required. A thorough survivability study is needed, but initial results suggest that both *D. radiodurans* and *B. sphaericus* survive SFG laser irradiation.

In the future we plan to carry out SHG/SFG studies directed towards understanding reactivity of heavy metals and radionuclides at the interface of these bacterial surfaces, as well as with oxides, soil organic matter. Future studies will focus on the adsorption of aqueous actinide species (such as UO_2^{2+}) on bacteria, model mineral oxide (SiO_2), and humic acid-coated surfaces. We will use SHG to confirm the adsorption of uranyl ions (via electronic resonances of the aqueous metal species), and SFG to investigate the type of interaction at the interface (physisorption versus chemisorption). The sub-monolayer sensitivity of this technique will allow us to study these interfacial reactions at trace concentrations. The effects of pH, temperature, concentration, ionic strength, etc. on sorption and reactions at these interfaces will also be investigated in situ. This work will complement previous bulk studies of UO_2^{2+} sorption (onto mineral and bacterial surfaces) done in the Nitsche laboratory using LIF and EXAFS measurements.[22; 13; 14]

A mechanistic and molecular-level understanding of the interfaces at which actinide binding occurs is necessary for designing remediation methods for nuclear waste. Previous research in our laboratory, as well as our preliminary work on characterizing bacterial surfaces, shows that SFG spectroscopy allows for in situ spectroscopic and structural studies directly on surfaces and at buried interfaces. SFG spectroscopy is the most promising technique for studies of biological and environmental surfaces

and interfaces in realistic environments, and will be highly effective when used in conjunction with other surface science techniques.

Bibliography

[1] Bioremediation of Metals and Radionuclides: What it is and how it works, Natural and Accelerated Bioremediation Research Program Report to the Department of Energy, **2003** LBNL-42595.

[2] Silva, R. J.; Nitsche, H. *Radiochimica Acta*, **1995**, *70*, 377.

[3] Bidoglio, G. *Radiochimica Acta*, **1992**, *58*, 191.

[4] Lovley, D. R.; Coates, J. D. *Curr. Opin. Bio-technol.*, **1997**, *8*, 285.

[5] Macaskie, L. E. *Crit. Rev. Biotechnol.*, **1991**, *11*, 41.

[6] Silva, R. J.; Nitsche, H.; Advances in Plutonium Chemistry, 1968-2000; Hoffman, D., editor, The American Nuclear Society: La Grange Park, IL, **2002**, 89.

[7] Lloyd, J. R.; Macaskie, L. E. Environmental Microbe-Metal Interactions, Lovley, D. E., editor, ASM Press, **2000**

[8] Choppin, G. R. *Radiochimica Acta*, **1992**, *58/59*, 113.

[9] Lister, T. E.; Pinhero, P. J. *Langmuir*, **2001**, *17*, 2624.

[10] Battista, J. R. *Annu. Rev. Microbiol.*, **1997**, *51*, 203.

[11] Fredrickson, J. K.; Kostandarithes, H. M.; Li, W.; Plymale, A. E.; Daly, M. J. *App. Envir. Microbiolog*, bf 2000, *66*, 2006.

[12] Haas, J. R.; *Chem. Geology*, **2001**, *180*, 33.

[13] Panak, P. J.; Nitsche, H. *Radiochimica Acta*, **2001**, *89*, 499.

[14] Panak, P. J.; Nitsche, H. *Radiochimica Acta*, **2002**, *90*, 1.

[15] Renninger, N.; Knopp, R.; Nitsche, H.; Clark, D. S.; Keasling, J. D. *Applied and Environmental Microbiology*, **2004**, *70*, 7404.

[16] Somorjai, G. A. *Introduction To Surface Chemistry And Catalysis, Chapter 1*; John Wiley & Sons, Inc.: New York, NY, **1994**.

[17] Shen, Y. R. *Pure and Applied Chemistry*, **2001**, *10*, 1589.

[18] Miranda, P. B.; Shen, Y. R. *J. Phys. Chem B*, **1999**, *103*, 3292.

[19] Eisenthal, K. B. *Chem. Reviews*, **1996**, *96*, 1343.

[20] Richmond, G. L. *Chem. Reviews*, **2002**, *102*, 2693.

[21] Sleytr, U. B.; Beveridge, T. *Trends in Microbiology*, **1999**, *7*, 253.

[22] Gong, C. M. S.; University of California, Berkeley, Ph.D. Thesis, **2004**

[23] Baumeister, W.; Karrenberg, F.; Rachel, R.; Enger, A.; Ten Heggeler, B.; Saxton, W. O. *Eur. J. Biochem.*, **1982**, *125*, 535.

[24] Egelseer, E. M.; Leitner, K.; Jarosch, M; Hotzy, C.; Zayni, S.; Sleytr, U. B.; Sara, M. *J. Bacteriology*, **1998**, *180*, 1488.

Appendix A

Solid Phase Peptide Synthesis

Solid phase peptide synthesis (SPPS), also known as Merrifield synthesis (after Bruce Merrifield who won the 1984 Nobel Prize in Chemistry for its development), is a method for synthesizing high purity and high yield peptides in a single reaction vessel via a stepwise iterative process. Peptides are synthesized on a solid support from the C (carboxy) terminus to the N (amino) terminus.

A.1 Solid Supports

The solid-phase supports used in SPPS consists of insoluble and chemically inert resins, often polystyrene polymer beads. In our synthesis we used a rink amide 4-methylbenzhydrylamine (MBHA) resin (amide groups used to cross link amino acids to the support), shown in Figure A.1. The first step in resin preparation is swelling the resin: soaking in n-methyl-2-pyrrolidone (NMP) causes the polymer to swell, increasing the accessibility of reagents to the functional groups on the support. The second step in the SPPS is to covalently link the first amino acid to the resin support, typically via an acid or base labile bond with a linker molecule. The carboxylic acid group of the protected amino acid must be activated prior to coupling to the resin. The amino acid is mixed with n-hydroxybenzotriazole (HOBT) for about 20 minutes to activate the carboxylic acid and then added to the resin. When using the Advanced ChemTech 396 (described in Chapter 3), this mixture is agitated overnight. This manual step is necessary to ensure complete coupling of the first amino acidthe overall yield is dependent upon the efficiency of the first coupling step, so this is very important. Pre-loading the first amino acid was not necessary when using the Advanced Biosystems instrument (used for synthesis of peptides described in Chapter 4), which typically uses longer coupling times.

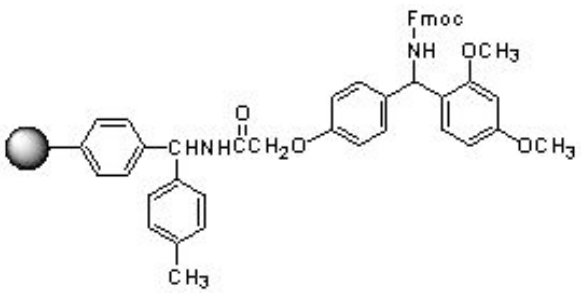

Figure A.1. Rink amide (MBHA) resin.

A.2 Protected Amino Acids

Some amino acids contain side chains with functional groups that are reactive and can interfere with formation of the peptide bond. These side chains are protected with a bulky group (usually a tert-butyl or a trityl functional group) which sterically hinders side-chain reactions. The alpha-amino group of each amino acid is protected with a 9-fluorenylmethyloxycarbonyl (FMOC) group, which is removed prior to couple, and ensures that the peptide bond forms at the unprotected C-terminal group. This method leads to head-to-tail peptide chain growth.

A.3 Peptide Chain Elongation

The peptide chain is constructed by an iterative process involving the removal of the FMOC group in a deprotection step, and the addition of an excess of the next amino acid (we use a 9 equivalents excess). The carboxy group of the new amino acid is activated for amide bond formation by a compound which chemically transforms it into an active ester (in our synthesis we use N,N-diisopropylcarbodiimide (DIC) in piperidine). The resin-bound dipeptide is washed and filtered to remove remaining uncoupled amino acid, and the process is repeated until the desired sequence is achieved.

A.4 Terminal Group Modification

A common modification that we used in our synthesis is to have the C-terminus of the peptide synthesized as an amide, rather than a free carboxylic acid, and similarly, to acetylate the N-terminus. These modifications eliminate the charged groups at the termini, and may allow the peptide to assume a conformation more closely resembling that of internal peptide segments, rather than the protein termini. The C-terminal amide is a product of the synthesis using rink amide resin. Acylation of the N-terminus

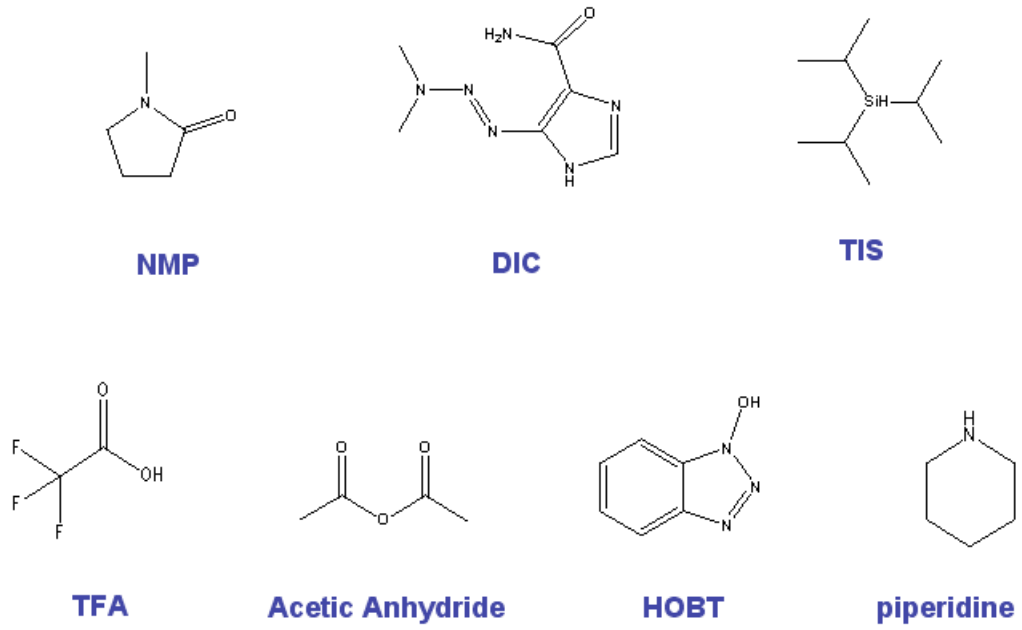

Figure A.2. Reagents used in FMOC solid phase peptide synthesis.

is accomplished by adding acetic anhydride (30% in pyridine) to the resin-bound peptide and agitating for 30 minutes.

A.5 Deprotection and Cleavage from Resin

Cleavage of the completed, deprotected peptide from the resin is the most difficult step in SPPS. A reagent that removes the protecting groups but does not alter the sequence of the synthetic peptide is needed. We use the methods of David King (Howard Hughes Medical Institute, and UC Berkeley MCB department). "Reagent K" solution, consisting of 95 % trifluoroacetic acid (TFA) in water, is used for both deprotection and cleavage. The dry resin-peptide is placed in a 15 mL conical glass centrifuge tube, and 2 mL of Reagent K is added per 100 mg of resin-bound peptide. The mixture is stirred every 15-30 minutes, for 2-4 hours depending on peptide sequence (deprotecting side chains such as lysine or arginine require longer cleavage times)–but never longer than 6 hours total. The TFA/peptide solution may contain a number of potentially reactive species that could react with the deprotected peptide. To minimize these unwanted reactions, a scavenger is often used, and in this case

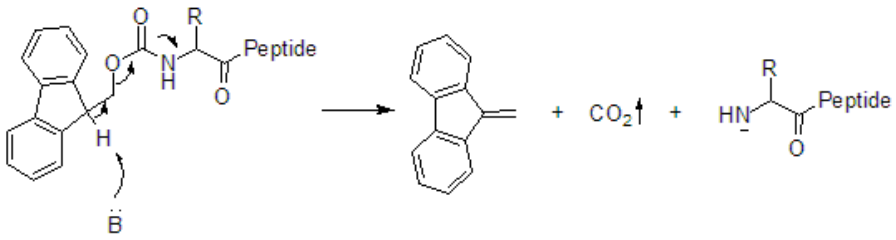

Figure A.3. FMOC chemistry scheme. Basic conditions are used to remove the FMOC group, where evolution of carbon dioxide drives the process thermodynamically.

consisted of 2.5 % triisopropylsilane in Reagent K. After cleavage and deprotection, the mixture is filtered into a 25 mL round bottom flask through a medium porosity glass frit. After rinsing the resin 2 to 3 times with 1-2 mL of TFA, the solution is evaporated to a syrup on a rotovap using warm water (until the peptide begins to crash out of solution). The remaining pepide syrup should be redissolved in a small amount (400 μL) of TFA, and squirted forcibly with a glass pipet into a 15 mL centrifuge tube containing 10-12 mL of t-butyl methyl ether (MTBE). The peptide forms an immediate precipitate, while the TFA, linker and scavenger-protecting group components are all ether soluble. The ether solution may need to be cooled on ice for several minutes. The tube is then placed in a centrifuge for two minutes, decanted, and another 10 mL of fresh ether added. This washing step should be repeated 4-6 times, until a fluffy white precipitate remains (the solid will be gummy if there is still TFA and protecting group present). Cover loosely with a chim wipe, and air dry the peptides in the tube overnight (in a fume hood). The crude peptides can be kept as is, or redissolved and lyophilized. The peptides should be stored dry, in a dark freezer.

A.6 Reversed Phase-HPLC Purification

Reversed-phase high pressure liquid chromatography (rp-HPLC) is used for peptide purification. We have used the procedure of David King . A 25 cm C-18 column (Vydac 300 A, 10 μm, 218TP1010) column and a Vydac cartridge guard column were used. Mobile phase of acetonitrile (MeCN) (B solvent) gradient in water (A solvent), both containing 0.1% trifluoroacetic acid (TFA) works for most peptides. A good starting point is a gradient of 15% B over 60 minutes at a flowrate of 2.3 mL/min (backpressure of $<$ 1000 psi). This should lead to a retention time of 20-25 min. Column are loaded at 5-10% MeCN, and raised to 15% in 60 min. If the peak elutes before 15 min, it is likely eluting isocratically and may contain polar impurities. Loading several smaller samples (20 mg/injection) will result in a better purification. UV detection at 230 nm (amide n to π^* transition) should be used (peptides do not absorb at 280 nm). The column should be rinsed with 50-60 % MeCN for 7 min between each run, and equilibrated with 5-10 % MeCN for 15 min. Peptides should be prepared

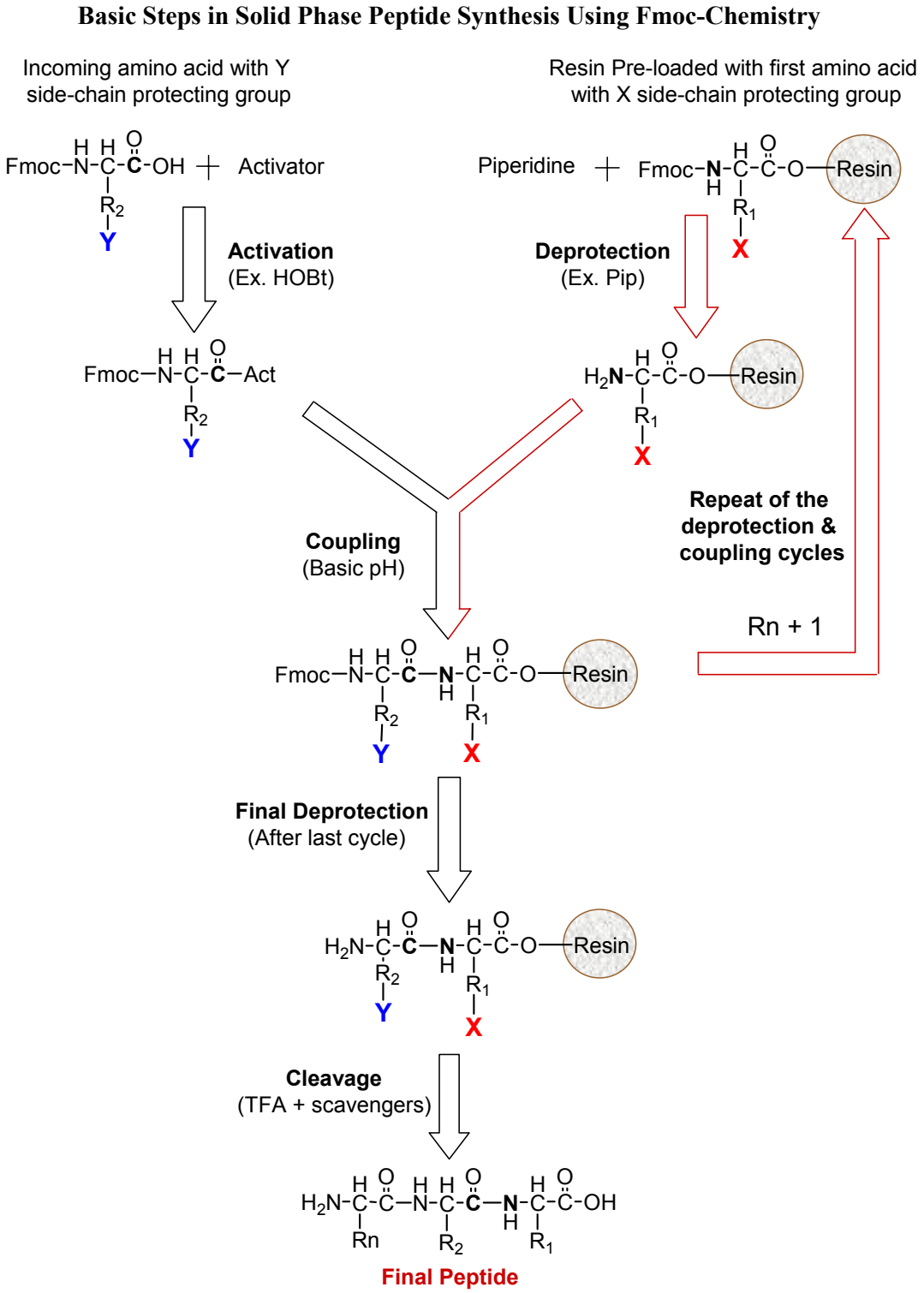

Figure A.4. FMOC synthetic scheme used in solid phase peptide synthesis. Figure from Sigma Aldrich.

in 5-10 % MeCN. Columns should be stored in 100% n-propanol. N-propanol should be run at about half of the normal flowrate (due to its high viscosity) to avoid high column backpressure.

A.7 Note on Synthesis of Hydrophobic and Hydrophilic Peptides

Typical problems with the SPPS method include incomplete activation of protected amino acids (often leading to aggregation), and incomplete deprotection of the final peptide. With these peptide sequences, we also observed incomplete coupling leading to deletions and truncations, which resulted in low yield of full length product (particularly for polylysine, polyalanine and polyleucine peptides). When synthesizing peptides with bulky side-chains, we often doubled the typical coupling time for the reaction, which significantly improved yields.

The hydrophobic characteristic and the low number of charged residues in our sequences resulted in product that is difficult to solubilize, characterize and purify. The shortness of the sequences mean the peptide is not retained well on the HPLC column. Very hydrophilic peptides (such as polylysine) are also difficult to lyophilize. The hydrophobic polyalanine and polyleucine peptides only had one charged group (the C-terminal amide group) following acetylation, so we were unable to properly characterize these peptides using electrospray ionization mass spectrometry (ESI-MS). For these samples, we used matrix assisted laser desorption (MALDI) mass spectrometry for characterization. We can estimate that for the amphiphilic peptides, the minimum purity synthesized was 70%. The hydrophobic peptides appeared to be of much lower quality, and most likely were not the full length. MALDI mass spectral data suggests an average chain length of 5 and 11 for polyleucine 7mer and 14mer, respectively. However, it is difficult to determine whether the MALDI peaks observed were M^{+2} (or higher) versus M^{+1} peaks of shorter fragments, since the MALDI ionization technique results in more fragmentation than electrospray ionization (where the most intense peak is usually the M^{+1} ion).